TARGETING METABOLIC DYSREGULATION IN METABOLIC DYSFUNCTION-ASSOCIATED STEATOTIC LIVER DISEASE

by

Christina Thabet Saed

A thesis submitted in partial fulfillment of the requirements for the degree of

Doctor of Philosophy

in

Pharmaceutical Sciences

Faculty of Pharmacy and Pharmaceutical Sciences
University of Alberta

Abstract

Metabolic dysfunction-associated steatotic liver disease (MASLD) is a condition characterized by the accumulation of fat in the liver of persons who do not consume alcohol, commonly associated with metabolic dysregulation. MASLD is rising globally, particularly in Canada, impacting more than 7 million people. MASLD is a serious condition that can elevate the likelihood of developing heart disease and type 2 diabetes (T2D). No medication has yet received approval to treat this serious illness. Recent research indicates that glucose metabolism is disrupted in MASLD, and the rate-limiting enzyme in glucose metabolism, pyruvate dehydrogenase (PDH, gene *Pdha1*), is suppressed. Thus, we posit that enhancing PDH activity to boost glucose metabolism in the liver could alleviate the impact of MASLD. Our laboratory has demonstrated that ranolazine, a medication prescribed for heart disease, can effectively treat MASLD in obese mice, which was correlated with elevated PDH activity. We aim to investigate whether ranolazine exhibits similar beneficial effects in T2D. We induced experimental T2D in male mice (15 weeks of high-fat diet along with a single low-dose injection of streptozotocin [75 mg/kg] at 4 weeks). The mice were administered either a vehicle control or ranolazine (50 mg/kg) once daily through oral gavage. We evaluated blood glucose levels by monitoring glucose tolerance, insulin tolerance, and pyruvate tolerance, while hepatic steatosis was evaluated by measuring triacylglycerols (TAGs) content. Ranolazine did not affect blood glucose levels in mice with experimental T2D or influence the amount of fat stored in the liver. Ranolazine's beneficial effects on MASLD may be restricted to obese persons and not extend to those who are obese with T2D.

MASLD raises the risk of developing insulin resistance and T2D associated with obesity. Recent research from our laboratory has shown that activating PDH may mitigate MASLD caused by obesity using the antianginal drug ranolazine. Our goal was to investigate if ranolazine's capacity to alleviate obesity-induced MASLD and hyperglycemia depends on the enhancement of hepatic PDH activity. Therefore, we generated hepatic PDH knockout mice (*Pdha1*$^{\text{Liver-/-}}$) and fed a high-fat diet for 12 weeks to promote obesity, while lean controls were given a low-fat diet. *Pdha1*$^{\text{Liver-/-}}$ mice and their Alb$^{\text{Cre}}$ littermates were randomly assigned to receive either a vehicle control or ranolazine (50 mg/kg) once daily through oral gavage for the last 5 weeks. Subsequently, we evaluated body composition, glucose tolerance, and pyruvate tolerance. Hepatic TAGs were measured using the Bligh and Dyer lipid extraction technique. *Pdha1*$^{\text{Liver-/-}}$ mice did not show any noticeable variations in physical characteristics (such as fat mass, body weight, and glucose tolerance) compared to their Alb$^{\text{Cre}}$ littermates, but a little tendency towards a modest deterioration in pyruvate tolerance was noted. Ranolazine therapy improved glucose tolerance and slightly reduced hepatic TAG concentration in obese Alb$^{\text{Cre}}$ mice but not in *Pdha1*$^{\text{Liver-/-}}$ obese mice. The former was not influenced by alterations in hepatic mRNA levels of genes that control lipogenesis. Ultimately, liver-specific PDH loss does not effectively induce an MASLD phenotype. However, hepatic PDH activity plays a role in the mechanism by which the antianginal drug ranolazine improves glucose tolerance and reduces hepatic steatosis in obesity.

We have shown that pimozide, an antipsychotic drug that typically inhibits dopamine 2 receptors (D2R), can effectively reduce glucose levels in mice with an experimental obesity/T2D model. The observations were linked to the unconventional effects of pimozide in binding and inhibiting succinyl-CoA:3-ketoacid CoA transferase (SCOT) in skeletal muscle. Additionally, the Similarity

Ensemble Approach (SEA) was utilized, identifying X-box binding protein 1 (XBP1) as a promising target for pimozide. Due to the significant role of XBP1 in the unfolded protein response (UPR) and its influence on endoplasmic reticulum (ER) stress regulation, we shifted our attention to inositol-requiring enzyme 1 (IRE1). We aimed to determine the extent of this connection using both in vitro and in vivo experiments. HepaRG cells were grown in Williams' Medium supplemented with 2 mM oleic acid and treated with either a vehicle or pimozide (12.5 nm) for 16 hours. We induced experimental T2D in 8-week-old male C57BL/6J mice by feeding them a high-fat/high-sucrose diet for 10 weeks. Additionally, a single dose of streptozotocin (STZ; 75 mg/kg) was given to the animals fed the high-fat diet at 4 weeks. After 8 weeks of the regimen, all mice were randomly assigned to receive either a vehicle control or pimozide (10 mg/kg) every other day via oral gavage until the study ended. Two weeks after administering pimozide, we evaluated glucose regulation using a glucose tolerance test and assessed hepatic steatosis by measuring TAG levels. HepaRG cells treated with pimozide showed a notable reduction in steatosis and increased levels of IRE1 and XBP1. Our data showed that pimozide enhanced glucose levels in mice with experimental T2D without affecting hepatic TAG content. These results indicate that pimozide may be beneficial in reducing hepatic steatosis, as shown by its significant influence on steatosis in HepaRG cells. The improvement in blood glucose levels without changing the amount of fat in the liver of mice with experimental T2D suggests that pimozide has a complex effect that warrants more investigation into its processes and potential use in treating metabolic diseases.

Preface

This thesis is an original work by Christina Thabet Saed. Ethics approval for the following research was received from the University of Alberta Animal Use and Care Committee under Animal Use Protocol #00001412.

Chapter 1 contains an excerpt from the following publication:

Christina T Saed, Seyed Amirhossein Tabatabaei Dakhili, and John R Ussher. Pyruvate Dehydrogenase as a Therapeutic Target for Nonalcoholic Fatty Liver Disease. *ACS Pharmacol Transl Sci*. 2021 Mar 3;4(2):582-588.

All authors listed have contributed substantially, directly, and intellectually to the work.

Chapter 2 has been published:

Christina T. Saed, Amanda A. Greenwell, Seyed Amirhossein Tabatabaei Dakhili, Keshav Gopal, Farah Eaton, and John R. Ussher. The anti-anginal ranolazine does not confer beneficial actions against hepatic steatosis in male mice subjected to high-fat diet and streptozotocin-induced type 2 diabetes. *Can J Physiol Pharmacol*. 2022 May;100(5):393-401.

C.T.S and J.R.U conceived and designed the research plan. C.T.S organized all experiments, completed molecular work (western blotting, real-time qPCR, TAGs assay, ALT, and AST assay) and in vivo experiments (management of treatment protocol, assessment of body composition, and glucose measurements), completed all data analysis and drafted the manuscript. A.A.G, K.G and S.A.T.D assisted with blood glucose

measurements, western blotting and real-time qPCR experiments, F.E assisted with the management of mouse care, J.R.U edited and revised the manuscript and approved the final version.

Chapter 3 has been published:

Christina T. Saed, Seyed Amirhossein Tabatabaei Dakhili, Amanda A. Greenwell, Jordan S.F. Chan, Kunyan Yang, Keshav Gopal, Farah Eaton, Rami Al Batran, and John R. Ussher. The antianginal ranolazine fails to improve glycaemia in obese liver-specific pyruvate dehydrogenase deficient male mice. *Basic Clin Pharmacol Toxicol*. 2023 Aug;133(2):194-201.

C.T.S and J.R.U conceived and designed the research plan. C.T.S organized all experiments, completed molecular work (western blotting, real-time qPCR, and TAGs assay) and in vivo experiments (management of treatment protocol, assessment of body composition, and glucose measurements), completed all data analysis and drafted the manuscript. S.A.T.D, A.A.G, J.S.F.C, K.Y, and K.G assisted with molecular work and in vivo experiments. F.E set up breeding pairs and genotyped the mouse pups, and R.A.B conducted western blot experiments to confirm the knockout mice's status. R.U edited and revised the manuscript and approved the final version.

Chapter 4 is under preparation for publication:

Christina T. Saed*, Seyed Amirhossein Tabatabaei Dakhili*, Amanda A. Greenwell, Kunyan Yang, Keshav Gopal, Jordan S.F. Chan, Tanin Shafaati, Indiresh A. Mangra-Bala, Magnus J. Stenlund,

Sally R. Ferrari, Kristil Almahfoud, Farah Eaton, and John R. Ussher. The antipsychotic agent pimozide alleviates steatosis in HepaRG cells by activating the IRE1/XBP1 pathway.

*Denotes equal contribution

C.T.S, S.A.T.D, and J.R.U conceived and designed the research plan. C.T.S organized all experiments, completed molecular work (western blotting, real-time qPCR, and TAGs assay) and in vivo experiments (management of treatment protocol, circulating insulin levels, assessment of body composition, and glucose measurements), and in vitro experiments (western blotting, real-time qPCR, and histology), completed all data analysis and drafted the manuscript. S.A.T.D conducted Similarity Ensemble Approach (SEA). K.Y measured circulating insulin levels. T.S and S.R.F assisted with in vitro experiments. S.A.T.D, A.A.G, K.Y, K.G, J.S.F.C, I.A.M, M.J.S, and K.A assisted with molecular work and in vivo experiments, F.E assisted with the management of mouse care and histology, J.R.U edited and revised the manuscript.

Acknowledgements

In the journey of my academic pursuit, there stands a figure whose presence has been more than just that of a mentor. Dr. John Ussher, with his unwavering support and patience, has been a guiding light throughout the completion of this thesis. His mentorship has not only shaped my academic endeavours but also played a pivotal role in defining the person I am today. As I stepped into the lab for the first time, I realised that while some of my skills needed refinement, Dr. Ussher saw potential in me. He provided me with numerous collaborative opportunities that not only polished my skills but also allowed me to excel. His dedication to the field of science and his exceptional mentorship have left an indelible mark on my journey. I am particularly grateful for Dr. Ussher's words of encouragement, constantly pushing me beyond my limits. His encouragement has inspired me to strive for excellence in all my endeavours.

I want to express my sincere gratitude to my committee members, Dr. Ayman El-Kadi and Dr. Arno Siraki, for their invaluable support, feedback, and guidance throughout this thesis. Their expertise and dedication have been instrumental in shaping my research. I am also grateful to them for writing my reference letters, as their support has been crucial in my academic journey. Dr. El-Kadi and Dr. Siraki are not just professors but mentors who consistently guide and support students. Their willingness to go above and beyond for students has created a supportive environment where we can thrive. They have truly impacted my academic and personal life, and I am fortunate to have them guiding me through my educational journey.

To my lab mates, Dr. Seyed Amirhossein Tabatabaei Dakhili, my last project would not have existed without your help. Kunyan Yang (Martin) and Jordan Chan, thank you for your continual support and for fostering such a positive work environment. To Dr. Keshav Gopal and Farah Eaton for their guidance and support during my journey. Having you as a resource for assistance gives me great comfort. To my best friend, Dr. Amanda Greenwell, I am genuinely grateful and consider myself incredibly lucky to have you as a colleague and my closest friend. Your friendship means the world to me; no words can express my gratitude for all you do. Thank you for always being there for me. To the newest members of the Ussher lab family, Sally Ferrari, Linyue Dong, Magnus Stenlund, Akil Mangra-Bala, and Tanin Shafaati, it has been a pleasure working with you and having you as part of our team. The Ussher lab is more than simply a workplace; it's like a second home where I feel safe and supported. My lab mates are more than merely coworkers; they are family to me, and I am grateful for each of you. Thank you for all you do to make our lab such a pleasant and welcoming environment.

Finally, I would like to express my deepest gratitude to my family: my mom, my dad, my two sisters, Marina and Engy, and my brothers-in-law, Michael ElKiess Mena and Bay Bakin Abdelmaseeh. Leaving them to move to a foreign country was one of my hardest decisions, but their support never wavered. They kept in touch late and early, reassuring me that I was never alone. They are my everything, and their love and dedication make me successful. I would also like to thank my little nieces, Mera and Jonista, and nephews, Mark and Jonathan. Your presence in my life gives me great joy and comfort. Playing games and conversing with you has provided both relaxation and delight. Your unconditional devotion, encouragement, and support have been an anchor of strength for me during this journey.

Table of Contents

List of Tables

List of Figures

List of Abbreviations

ACC	Acetyl CoA carboxylase
AAAs	Aromatic amino acids
AcAc	Acetoacetate
Acaca	Acetyl-CoA carboxylase alpha
ACAT	Acetyl coenzyme A acetyltransferase
Acta2	Alpha-smooth muscle actin
Akt	Protein kinase B
ALT	Alanine aminotransferase
AMPK	AMP-activated protein kinase
ANOVA	Analysis of variance
AST	Aspartate aminotransferase
ATF6	Activating transcription factor 6
ATP	Adenosine 5′-triphosphate
AUC	Area under the curve
BCAAs	Branched-chain amino acids
BCKA	Branched chain ketoacid dehydrogenase

BCKDK	Branched chain ketoacid dehydrogenase Kinase
BiP	Binding immunoglobulin protein
BMI	Body mass index
Bp	Base pair
BSA	Bovine serum albumin
βHAD	β-hydroxyacyl CoA dehydrogenase
βOHB	β-hydroxybutyrate
BT2	3,6-dichlorobenzo[b]thiophene-2-carboxylic acid
CACNA1G	Calcium voltage-gated channel subunit alpha1 G
Ccn2	Cellular communication network factor 2
CD36	Cluster of differentiation 36
CHOP	C/EBP homologous protein
ChREBP	Carbohydrate response element-binding protein 1
CO_2	Carbon dioxide
Col1a1	Collagen type I alpha 1
Col1a2	Collagen type I alpha 2
CPT	Carnitine palmitoyl transferase
D2R	Dopamine 2 receptors

DAG	Diacylglycerol
DCA	Dichloroacetate
DDIT3	DNA damage-inducible transcript 3
DGAT	Diacylglycerol acyltransferase
DIO	Diet-induced obesity
DNAJB9	DNAJ homolog subfamily B member 9
DNL	De novo lipogenesis
eIF2α	Eukaryotic initiation factor 2 alpha
ER	Endoplasmic reticulum
FAS	Fatty acid synthase
G1P	Glucose-1-phosphate
G6P	Glucose-6-phosphate
G6PD	Glucose-6-phosphate dehydrogenase
GAPDH	Glyceraldehyde 3-phosphate dehydrogenase
GLUT2	Glucose transporter 2
GTT	Glucose tolerance test
HCC	Hepatocellular carcinoma
HDL	High-density lipoprotein

HFD	High-fat diet
HIR	Hepatic insulin resistance
HMG- CoA	3-hydroxy-3-methylglutaryl-coenzyme A
HMGCS2	3-hydroxy-3-methylglutaryl-coenzyme A synthase 2
HNF4α	hepatocyte nuclear factor 4-alpha
HOMA-IR	Homeostatic model assessment of insulin resistance
Hsp90	Heat shock protein-90
IL1β	Interleukin-1 beta
IL2	Interleukin-2
IL6	Interleukin-6
INSIG2	Insulin-induced gene-2
IRE1	Inositol-requiring enzyme 1
LCAD	Long-chain acyl CoA dehydrogenase
LDL	Low-density lipoprotein
LFD	Low-fat diet
MASH	Metabolic dysfunction-associated steatohepatitis
MASLD	Metabolic dysfunction-associated steatotic liver disease
MetS	Metabolic syndrome

MRI	Magnetic resonance imaging
NADH	Nicotinamide adenine dinucleotide
NADPH	Nicotinamide adenine dinucleotide phosphate
NAFLD	Non-alcoholic fatty liver
NASH	Non-alcoholic steatohepatitis
NF-κB	Nuclear factor-kappa B
PC	Pyruvate carboxylase
PCK1	Phosphoenolpyruvate carboxykinase 1
PCR	Polymerase chain reaction
PDC	Pyruvate dehydrogenase complex
PDH	Pyruvate dehydrogenase
PDHK	Pyruvate dehydrogenase kinase
PDHP	Pyruvate dehydrogenase phosphatase
PERK	Protein kinase RNA-like ER kinase
PPARα	Peroxisome proliferator-activated receptor-alpha
PPARγ	Peroxisome proliferator-activated receptor-gamma
Ppia	Cyclophilin A
PPP	Pentose phosphate pathway

PPP1R15A	Protein phosphatase 1 regulatory subunit 15A
PS10	2-[(2,4-dihydroxyphenyl) sulfonyl] isoindoline-4,6-diol
R5P	Ribose 5-phosphate
RIDD	Regulated IRE1-dependent decay
SCD	Stearoyl-CoA desaturase
SCOT	Succinyl-CoA:3-ketoacid CoA transferase
SREBF1	Sterol regulatory element-binding transcription factor 1
SREBP1c	Sterol regulatory element binding protein 1c
STAT	Signal transducer and activator of transcription
STZ	Streptozotocin
T2D	Type 2 diabetes
TAG	Triacylglycerol
TCA	Tricarboxylic acid cycle
Timp	Tissue inhibitors of metalloproteinase
TNF-α	Tumor necrosis factor-alpha
UDP	Uridine diphosphate
UPR	Unfolded protein response
VC	Vehicle control

VLDL	Very low-density lipoprotein
XBP1	X-box binding protein

Chapter 1: Introduction

1.1 Comprehending Metabolic Dysfunction-Associated Steatotic Liver Disease

1.1.1 Overview of Metabolic Dysfunction-Associated Steatotic Liver Disease

Metabolic dysfunction-associated steatotic liver disease (MASLD), previously referred to as non-alcoholic fatty liver disease (NAFLD)/hepatic steatosis, is a condition in which excess fat (triacylglycerols [TAGs]) accumulates (>5% within hepatocytes, primarily in the form of lipid droplets, in the liver of an individual in the absence of alcohol abuse or other attributable causes such as hepatitis C infection (1, 2). MASLD replaces NAFLD as the comprehensive name to include hepatic steatosis in patients with at least one of five cardiometabolic risk factors (3, 4). Non-alcoholic steatohepatitis (NASH) is now referred to as metabolic dysfunction-associated steatohepatitis (MASH), highlighting the metabolic aspects of liver inflammation. The new phrases aim to offer a more thorough explanation of the metabolic factors linked to fat accumulation in the liver. The terminology change is necessary due to the absence of sufficient nomenclature since the initial description of the ailment. The term ‘NAFLD’ was coined in 1986; however, the significant increase in NAFLD publications began prominently in 2000 (5, 6). A recent study has revealed that most disorders categorized as NAFLD are linked to metabolic variables such as obesity, insulin resistance, and elevated cholesterol or lipids. The American Association for the Study of Liver Diseases has proposed a change to reduce stigma by deleting the words ‘fatty’ and ‘alcohol’. It is crucial to have a name that indicates the underlying reasons for the ailment. Understanding the source of liver illness is crucial as addressing it can aid in the liver’s recovery.

Chapters 2 and 3 were published before the terminology update. We will continue using the current language, incorporating new terms as needed to maintain awareness of this severe liver condition.

Unfortunately, MASLD is increasing exponentially and has become one of the leading causes of morbidity worldwide, where it is estimated to affect nearly one-third of the adult population in Western nations (7-9). The excess lipid/TAG storage in MASLD does not necessarily worsen liver function. Still, in the presence of inflammation, it may progress to a more advanced form referred to as MASH, which can also increase the risk for hepatocellular carcinoma (1). The liver clinicopathologic entity is increasingly recognized as a major health burden in developed countries. Within this estimate, liver cancer accounts for 600,000 to 900,000 deaths (10). Currently, liver disease is the eleventh-leading cause of death, accounting for over two million deaths annually (1 out of every 25 deaths); in the last three decades, the prevalence of MASLD has increased globally by more than 50%, rising from 25.3% in 1990–2006 to 38.0% in 2016–2019 (11).

While MASLD can often be relatively benign, the progression of MASLD is tightly correlated with systemic insulin resistance and can also increase the risk for type 2 diabetes (T2D) and cardiovascular disease (1, 12). One of the primary drivers of MASLD is underlying obesity. Thus, there has been extensive interrogation into understanding the mechanisms contributing to the pathology and natural progression of MASLD, as this may lead to novel therapies for preventing insulin resistance and/or T2D. Whether MASLD is necessarily causal toward insulin resistance and/or T2D is a complex issue and a topic of ongoing study, as clear dissociations between hepatic

steatosis and insulin resistance have also been reported, whereas insulin resistance may also cause MASLD (13).

Obesity is strongly associated with MASLD, and it is more common in individuals with higher body mass index (BMI) (14), rising from 26.2% in those with a BMI < 24 kg/m^2 to 72.4% in individuals with a BMI over 30 kg/m^2 (15). Global studies indicate that the occurrence of MASLD in obese people ranges from 60% to 95%, emphasizing the significant connection between obesity and the accumulation of fat in the liver (16, 17). Obesity also plays a role in metabolic syndrome (MetS), which includes abdominal obesity, hypertension, dyslipidemia, and inadequate glucose regulation, further raising the risk of MASLD. Fat distribution, especially in the abdomen, plays a crucial role in developing MASLD, highlighting the significance of fat accumulation on liver health. Obesity, along with insulin resistance and dyslipidemia, contributes to the development of MASLD by increasing the release of free fatty acids from adipose tissue, leading to liver fat accumulation and metabolic dysfunction. Excessive fat in obese persons leads to increased levels of TAG in the liver, causing an accumulation of fat in the liver and metabolic disturbances.

The primary objective of this thesis is to examine the dysregulation of energy metabolism in the pathophysiology of MASLD and its consequential impact on the progression of the disease. This thesis aims to explore the intricate correlation between metabolic irregularities caused by obesity and the development of MASLD to identify novel therapeutic approaches for mitigating this growing health concern.

1.1.2 Key Physiological Pathways Underlying Metabolic Dysfunction-Associated Steatotic Liver Disease

The mechanisms underlying the development of MASLD are multifaceted and involve intricate interactions between MetS, inflammation, and oxidative stress pathways (**Figure 1.1**). The strong link between MASLD and MetS, which includes obesity, hyperglycemia, dyslipidemia, and systemic hypertension, is central to its etiology. MetS not only raises the risk of MASLD, but it also exacerbates a number of the disease's symptoms and complications (18, 19). Lipotoxicity, defined by the negative consequences of lipid accumulation in extra-adipose tissues such as the liver, is another critical mechanism through which MASLD occurs, contributing to its development and progression (20). Sustained abnormalities in lipid metabolism in MASLD alter the delicate balance between oxidants and antioxidants, resulting in cellular lipotoxicity, lipid peroxidation, chronic endoplasmic reticulum (ER) stress, and mitochondrial dysfunction. Hepatocyte exposure to high quantities of free fatty acids causes lipotoxicity, disrupting cellular homeostasis and inducing inflammatory responses and cell death. This cascade is aggravated by increased oxidative stress, which worsens liver damage and accelerates disease progression. Lipotoxicity activates stress pathways, causing inflammatory processes and fibrogenesis, which accelerates the progression from benign steatosis to more severe symptoms such as MASH. The complex interplay of altered lipid metabolism, oxidative stress, and lipotoxicity highlights the diverse pathophysiology of MASLD, highlighting the significant potential of interventions that aim to target these pathways for treating this common hepatic condition (21-23).

Oxidative stress is a key component in developing MASLD, primarily via activating the redox-sensitive transcription nuclear factor kappa-light-chain-enhancer of B cells (NF-κB) (22).

Excessive buildup of fatty acids in MASLD causes problems with the functioning of mitochondria and an increase in β-oxidation, resulting in excess of the reactive oxygen species, which are generated by both endoplasmic reticulum stress and activated NADPH oxidases, surpass the cellular antioxidant defences, leading to the occurrence of oxidative stress (24). Stress initiates signalling pathways that activate the IκB kinase complex, resulting in the phosphorylation of IκB and its subsequent destruction. Consequently, NF-κB is released and moves to the nucleus, which attaches to DNA and triggers the transcription of genes that stimulate inflammation, cell survival, and other stress responses. The inflammatory reaction, characterized by releasing cytokines and other inflammatory mediators, worsens liver damage and advances the disease from simple steatosis to more severe steatohepatitis. Effectively controlling MASH requires targeting the relationship between oxidative stress and NF-κB activation. Moreover, mitochondrial dysfunction and oxidative stress play important roles in connecting saturated fat consumption to the development and advancement of MASLD, emphasizing the significance of mitochondrial oxidative damage in this mechanism. The nuclear factor erythroid 2-related factor 2 and antioxidant response element pathway is an important regulator of antioxidant response that helps reduce damage caused by oxidative stress (25). It has the ability to restore normal lipid metabolism and can be targeted therapeutically to prevent the formation and progression of MASLD (26-28). Oxidative stress is critical in developing MASLD by altering lipid metabolism, promoting inflammation, and causing cellular damage (29). It is crucial to target oxidative stress pathways to manage this common liver disorder effectively.

Along with liver damage and metabolic imbalance, mitochondrial dysfunction plays a key role in the pathophysiology of MASLD. Impaired mitochondrial fatty acid oxidation and decreased

mitochondrial quality are key aspects in the evolution of MASLD, leading to the accumulation of lipids in the liver and the development of inflammation and fibrosis (30). Research has shown that mitochondrial dysfunction in MASLD is caused by mitochondrial oxidative damage, abnormalities in the electron transport chain, and oxidative phosphorylation, all of which worsen liver damage and disease progression (31). The connection between mitochondrial dysfunction and MASLD is supported by molecular, biochemical, and biophysical studies showing mitochondrial abnormalities in afflicted people (30). Therapeutically focusing on mitochondria and adjusting their activity show potential for new treatments for MASLD/MASH, highlighting the importance of addressing mitochondrial abnormalities in controlling this common liver illness (32). Understanding the impact of mitochondrial dysfunction on MASLD improves our knowledge of its disease-causing processes and identifies prospective treatment targets to improve clinical results.

Ceramides, diacylglycerols (DAGs), and de novo lipogenesis (DNL) are crucial components in the complicated development of MASLD, coordinating a series of molecular processes that result in liver fat accumulation, insulin resistance, and impaired mitochondrial function. Ceramides and DAGs, important lipid compounds, interfere with cellular signalling pathways and metabolic balance (33). Dysregulated DNL worsens lipid accumulation in liver cells, altogether leading to the advancement of MASLD. Increased DAG levels activate protein kinase C, disrupting insulin signalling and enhancing hepatic glucose synthesis, leading to fat accumulation in the liver (19). Ceramides hinder insulin signalling, leading to metabolic dysfunction and promoting the accumulation of lipids in the liver (23, 34). Furthermore, uncontrolled DNL increases the production of fatty acids and TAGs in the liver, worsening lipid accumulation and causing hepatic

steatosis (35). Ceramides worsen liver damage and inflammation in MASLD by promoting inflammation and cell death, therefore increasing disease severity. The complex disturbance of lipid regulation, particularly involving DAGs, ceramides, and DNL, leads to an imbalance in cell stability and triggers hepatic steatosis, a key characteristic of MASLD. Abnormal ceramide production in liver cells leads to ongoing mitochondrial malfunction by inhibiting specific components of the electron transport chain, which hinders mitochondrial respiration and energy production (36), leading to increased cellular stress and plays a role in causing liver damage in MASLD. Pharmaceutical strategies that prevent ceramide production by blocking enzymes like ceramide synthases or dihydroceramide desaturase 1 have demonstrated effectiveness in early studies for decreasing liver fat accumulation and enhancing the body's response to insulin. These approaches present promising treatment options for MASLD and alleviate its associated effects (36, 37).

To conclude, MASLD is a multifaceted disorder impacted by various mechanisms, such as dysregulation of lipids, oxidative stress, and mitochondria dysfunction. Exploring these fundamental physiological pathways has the potential to develop efficacious therapeutic interventions for MASLD. Comprehending the complex interaction among these pathways will be of utmost importance in furthering our understanding of the pathophysiology of MASLD and in developing novel therapies to enhance patient outcomes.

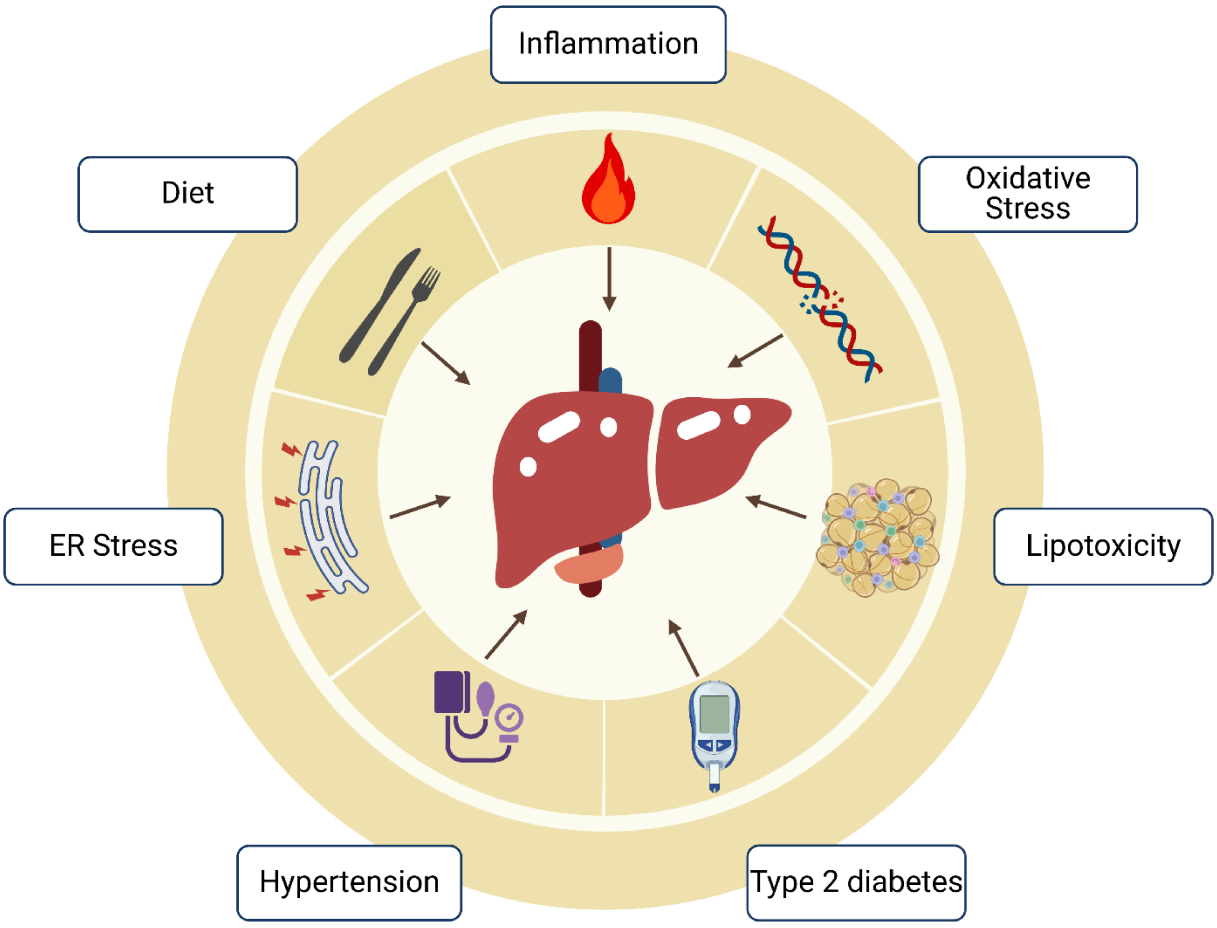
Inflammation
Oxidative Stress
Lipotoxicity
Type 2 diabetes
Hypertension
ER Stress
Diet

Figure 1.1 *Pathophysiological Factors of Metabolic Dysfunction-Associated Steatotic Liver Disease.* This illustration shows the interrelated pathophysiological factors contributing to MASLD development. Metabolic Syndrome (MetS) comprises illnesses such as hypertension and type 2 diabetes. Lipotoxicity is the harmful effects of excessive fat accumulation in non-adipose tissues, as lipid droplets depict. Chronic inflammation can cause a variety of metabolic disruptions. Ceramides can lead to insulin resistance and cellular damage when present in high amounts. Oxidative stress is represented by a stylized DNA helix with superimposed sparks, indicating damage from an imbalance of free radicals and antioxidants. Endoplasmic Reticulum (ER) stress occurs when unfolded proteins overload the ER; ER stress contributes to liver inflammation, cellular damage, and the progression of MASLD to more severe stages. Type 2 Diabetes is symbolized by a drop of blood containing a sugar cube, denoting high blood glucose levels. **Created with BioRender.com**.

1.1.3 Intermediary Energy Metabolism in the Healthy Liver and Metabolic Dysfunction-Associated Steatotic Liver Disease

Healthy liver energy metabolism is essential for preserving metabolic equilibrium and general well-being. The liver is critical in maintaining glucose and lipid balance, which is crucial for insulin sensitivity and overall metabolic well-being (38, 39). Studies have indicated that changes in liver energy metabolism are prevalent in individuals with acute and chronic liver conditions, as well as in mouse models of obesity, T2D, and fatty liver disorders (40, 41). The changes underscore the significance of comprehending metabolic shifts in liver diseases and their influence on liver function. Liver function and energy metabolism are crucial factors to consider in patients with hepatocellular carcinoma arising from hepatitis B-related cirrhosis, particularly when accompanied by comorbidities such as thyroid disease, kidney disease, and mental instability (42). Comprehending the complexities of hepatic energy metabolism, such as fatty acid metabolism and mitochondrial activity, is crucial for properly managing metabolic diseases and their related problems. MASLD is a disorder closely associated with disrupted metabolic processes affecting glucose and lipid metabolism, amino acid balance, and systemic metabolism (43). MASLD commonly displays characteristics of MetS, such as disrupted glucose and lipid metabolism, indicating the widespread effects of metabolic imbalances in this liver disorder (44). Studies have demonstrated that MASLD development is characterized by specific metabolic patterns, and analyzing metabolites in the bloodstream might offer helpful knowledge about metabolic alterations as the illness advances. The progression from MASLD to MASH is influenced by several variables, highlighting the diverse character of changes in systemic metabolism during MASLD advancement (45). Dysregulated lipid metabolism in MASLD affects liver health and is associated with an increased risk of cardiovascular disease (46). Changes in how the liver

processes fats and cholesterol have a significant role in the higher risk of cardiovascular disease seen in people with MASLD, emphasizing the widespread effects of disturbed lipid metabolism in this liver disorder (47). Impaired glucose metabolism in MASLD underscores the broader metabolic disturbances associated with this condition, highlighting the significant influence of dietary factors such as excessive consumption of high-calorie, nutritionally unbalanced foods on the metabolic dysfunction related to this liver disorder (48).

This thesis will focus on exploring strategies to enhance the perturbed energy metabolism in MASLD and identify effective therapeutic targets for managing and treating this condition.

1.1.4 Histopathologic Features of Metabolic Dysfunction-Associated Steatotic Liver Disease

Hepatic steatosis is defined as the accumulation of lipids, primarily TAGs, in the cytoplasm of hepatocytes, as previously mentioned. Hepatocytes with a low fat content are considered normal; however, if this fat content exceeds 5%, it leads to the development of MASLD (49). The 5% threshold is derived from preliminary biochemical research, indicating that lipids comprise roughly 5% of the average liver weight (50). The asymptomatic nature of MASLD often necessitates diagnosis through incidental discoveries of abnormal liver enzymes or the presence of steatosis in imaging studies. Notably, liver function tests, particularly transaminases such as alanine transaminase (ALT), aspartate transaminase (AST), and gamma-glutamyl transferase, serve as key indicators when aberrant (51). Elevated transaminase levels, notably ALT, are frequently observed; however, it is noteworthy that up to 80% of patients may present with within-normal-range ALT values (40 IU/L for males and 31 IU/L for females). Moreover, ALT levels

may decrease, while AST levels may rise, with the progression of fibrosis to cirrhosis. Critically, ALT readings lack a direct correlation with histological findings, rendering them ineffective for diagnosing MASLD and assessing disease severity. Regrettably, an overreliance on abnormal liver tests by clinicians may lead to an oversight of substantial liver disease in patients, potentially resulting in missed opportunities for timely intervention and treatment options (52). As such, a more nuanced and comprehensive approach to diagnosing and monitoring MASLD is imperative to ensure an accurate assessment of disease status and guide appropriate therapeutic interventions.

Liver biopsy is the gold standard diagnostic tool for determining the proper diagnosis, recording the grading of necroinflammation and staging of fibrosis, and predicting the prognosis for patients exhibiting radiologic or clinical signs of MASLD. Liver biopsy is now limited to a small number of MASLD patients due to its invasive nature, discomfort during the procedure, high cost, and the possibility of uncommon but real consequences. Patients with MASLD who have established risk factors for developing steatohepatitis with severe fibrosis, such as advanced age (>40 years), obesity, and/or T2D, may benefit from liver biopsy (53). As an alternative, methods for quantifying fatty liver that are more objective and accurate have been developed, primarily using digital image analysis. Recent research indicates that using guideline pictures may improve the precision of microscopical fat measurement (54). Although widely used, conventional non-invasive imaging modalities like computed tomography, magnetic resonance imaging (MRI), or ultrasound lack the sensitivity required to discern subtle levels of hepatic fat (below 30% hepatocytes). In contrast, advanced imaging techniques such as 1H-magnetic resonance spectroscopy, MRI-estimated proton density fat fraction, and ultrasound-based controlled attenuation parameter exhibit robust correlations with histologically confirmed steatosis, offering heightened diagnostic accuracy

across both adult and pediatric MASLD cases (55, 56). A recent addition to this landscape is the controlled attenuation parameter, employing ultrasound-based transient elastography to assess steatosis and estimate liver stiffness concurrently (40). This innovative method represents a promising step towards overcoming the limitations of traditional diagnostic approaches, providing a comprehensive evaluation of hepatic steatosis and liver health in a non-invasive and more patient-friendly manner.

1.2 Introduction to Energy Metabolism in the Liver

1.2.1 Glucose Metabolism in the Liver

The liver plays a crucial role in maintaining the body's glucose balance by regulating its metabolism in a highly dynamic and closely controlled manner. The liver is a vital organ in glucose metabolism, acting as a pivotal hub for the intake, storage, synthesis, and release of glucose into the bloodstream (**Figure 1.2**). The liver maintains glucose levels in the bloodstream within a restricted range through complex metabolic pathways. This process is crucial for supplying energy to different tissues and organs, especially during fasting or increased energy requirements. Gaining a comprehensive understanding of the complex mechanisms that regulate glucose metabolism in the liver is essential for uncovering the underlying causes of metabolic disorders such as diabetes and for creating specific and effective treatments.

The extent to which the liver contributes to glucose consumption compared to other tissues varies in different studies, ranging from one-third to 50-60% of the consumed glucose. The remaining portion of total glucose elimination after meals is attributed to peripheral glucose absorption,

which encompasses skeletal muscle and non-insulin-sensitive tissues, namely the brain (57). Glucose is predominantly taken up by human hepatocytes through glucose transporters, with glucose transporter-2 (GLUT2 or solute carrier family 2, member A2, *SLC2A2*) being the main transporter in humans. GLUT2 is present in multiple tissues, such as the liver, kidney, pancreatic β-cells, and small intestine (58). Hepatic glucose absorption is independent of insulin in contrast to other tissues. Instead, it is predominantly controlled by blood glucose levels, with hyperglycemia being the primary stimulus for glucose transportation into hepatocytes. Upon entering the cells, unbound glucose is enzymatically phosphorylated by glucokinase (also named hexokinase IV) to generate glucose 6-phosphate (G6P). In rodent studies, the absence of GLUT2 in the kidney has been linked to enhanced glucose tolerance and notable glucosuria (59). However, the enhancement in regulating blood glucose levels was abolished when GLUT2 was deleted in both the liver and kidneys, suggesting that the improvement is attributable to the lack of renal GLUT2 (59). The livers lacking GLUT2 showed hyperplasia, as indicated by a 40% rise in liver mass and a 30% rise in liver DNA content (60). GLUT2 whole-body knockout mice displayed hyperglycemia, reduced insulin levels, significantly increased glucagon levels in the blood, severe glycosuria, and frequently experienced mortality during the weaning period. This result is probably because glucose generation before weaning heavily depends on gluconeogenesis (61). These findings underscore the critical role of renal GLUT2 in glucose metabolism and highlight the complex interplay between glucose transporters in different tissues.

G6P is a pivotal point for glucose metabolism due to its numerous potential outcomes within the cells. Following isomerization, it triggers three significant metabolic pathways: glycogen synthesis, glycolysis, and the pentose phosphate pathway (PPP). Overnutrition causes the liver to

undergo de novo lipogenesis, which turns excess G6P into fatty acids. Furthermore, it is crucial to save glucose during fasting to provide the necessary building blocks for sustaining biomass, particularly for cell regeneration (62). Following a meal, a significant proportion of the excessive amount of carbohydrates is stored as glycogen in the liver, specifically inside the hepatocytes, as well as in the muscles through glycogenesis. Hepatic glycogen typically accounts for approximately 5% of the liver's total weight in healthy individuals (63). G6P is isomerized into glucose-1-phosphate (G1P) and transformed into uridine diphosphate (UDP) glucose to start glycogen synthesis. Uridine triphosphate is used by glucose-1-phosphate uridyltransferase to convert G1P to UDP glucose. The phosphate group of G1P combines with the alpha phosphate of uridine triphosphate to produce pyrophosphate, which speeds up the reaction (64). Glycogen synthase then forms an alpha-1,4 glycosidic link between UDP-glucose and a glycogen chain.

During feeding periods, glucose undergoes oxidation to produce carbon dioxide (CO_2) through a sequence of metabolic pathways. These pathways include glycolysis in the cytosol, the tricarboxylic acid cycle and the respiratory chain in the mitochondria. The initial stage of glycolysis involves the conversion of G6P into fructose-6 phosphate, which leads to the production of triose-phosphate. This process ultimately generates 2 pyruvate molecules and a small quantity of adenosine 5'-triphosphate (ATP) (2 ATP molecules) (65). Following entry into the mitochondria, pyruvate is converted to acetyl-CoA by the enzyme pyruvate dehydrogenase (PDH), establishing a connection between glycolysis and the tricarboxylic acid cycle (TCA). This step is essential for the subsequent generation of ATP in cellular respiration. (*A detailed discussion of the impact of PDH on obesity will be provided in a subsequent section of this chapter*).

The PPP, also called the pentose phosphate shunt or phosphogluconate pathway, is an important component of glucose metabolism. It uses G6P to generate fructose 6-phosphate and glyceraldehyde 3-phosphate through oxidative and non-oxidative pathways. Contrary to glycolysis, the PPP does not produce ATP to fulfil cellular energy needs. Instead, it makes two essential metabolites: ribose 5-phosphate (R5P) and NADPH (66). R5P functions as a crucial constituent in the process of nucleic acid production, whereas NADPH serves as the necessary reducing agent for the synthesis of fatty acids and the regeneration of reduced glutathione from its oxidized form glutathione disulfide, also known as oxidized glutathione by the enzyme glutathione reductase. It is noteworthy that juvenile animals show increased activity in the PPP in tandem with the synthesis of TAGs (67). Nevertheless, the extended occurrence of fatty liver disease in obese Zucker diabetic rats is associated with reduced activity of the PPP, suggesting that this mechanism is mainly used for synthesizing molecules rather than defending against oxidative stress (67). Notably, mice with G6P deficiency show lower levels of free fatty acids in their blood and improved insulin signaling in the liver (68). Nevertheless, these mice do not display reduced fat accumulation or significant changes in MASLD compared to wild-type mice. The mechanisms that cause the G6P deficiency that do not affect adiposity or lipid metabolism are still not fully understood (68).

During fasting, the liver controls glycogenolysis, which is the breakdown of glycogen, to release glucose into the bloodstream in order to meet the body's metabolic needs; glycogen stores yield around 190 grams of glucose, above the daily need of 160 grams (43, 69). At the same time, skeletal muscle glycogen helps to supply immediate energy for muscular contractions (70). As fasting continues and the liver's glycogen stores decrease, the liver switches to gluconeogenesis, a critical

step for creating glucose from non-glucose molecules such as glycerol, glycogen-forming amino acids, and lactic acid (71). This process involves enzymatic conversions: pyruvate carboxylase transforms pyruvate into oxaloacetate, phosphoenolpyruvate carboxykinase 1 (PCK1) catalyzes the conversion of oxaloacetate to phosphoenolpyruvate, fructose 1,6-bisphosphatase converts fructose 1,6-bisphosphate to fructose 6-phosphate, and ultimately, glucose 6-phosphatase mediates the conversion of glucose 6-phosphate to glucose, facilitating its release into the bloodstream (72, 73). Gluconeogenesis accounts for 54% of glucose synthesis during a 14-hour period of fasting, which rises to 64% after 22 hours and peaks at 84% after 42 hours (74). Insulin is pivotal in regulating various metabolic pathways in the liver, including gluconeogenesis. Hepatic insulin resistance (HIR) disrupts this regulation, leading to gluconeogenesis and lipid synthesis dysregulation. HIR facilitates excessive gluconeogenesis, contributing to the onset of (pre) diabetes while also stimulating DNL, resulting in hepatic steatosis. Moreover, the dyslipidemia associated with HIR promotes the release of very low-density lipoprotein (VLDL), increasing the risk of MASLD (75). Increased plasma insulin stimulates lipogenesis through sterol regulatory element binding protein 1c (SREBP1c), and increased plasma glucose levels resulting from excessive indulgence in gluconeogenesis stimulate lipogenesis through carbohydrate response element binding protein (ChREBP). Hence, the simultaneous occurrence of high levels of insulin and glucose greatly increases DNL, which is responsible for as much as 38% of the deposition of fatty acids in MASLD.

Studies in mice have demonstrated that inhibiting PCK1, a critical enzyme that controls the rate of gluconeogenesis, speeds up the development of hepatocellular carcinoma (76). However, PCK1 has diverse functions beyond maintaining glucose balance, including regulating lipogenesis by

activating SREBP1c (77). Individuals with hypoglycemia and hyperlactatemia also show diffuse hepatic macrosteatosis due to impaired PCK1 activity. Similarly, mice with reduced *Pck1* expression exhibit insulin resistance, low glucose levels, and fatty liver disease, highlighting the crucial importance of PCK1 (78). Furthermore, liver-specific PCK1 deficient animals displayed significantly worsened hepatic steatosis, fibrosis, and inflammation in mouse models fed a high fat/high fructose diet. This further highlights the crucial importance of PCK1 in maintaining liver health (79).

In summary, the liver plays a complex function in glucose metabolism, encompassing the control of glycogen storage, gluconeogenesis, and lipid synthesis. Gaining a comprehensive understanding of the complex equilibrium of these systems is crucial for effectively managing metabolic illnesses such as diabetes and MASLD. In addition, it is crucial to highlight the significance of specific treatments in managing liver health and disease progression, as evidenced by the influence of critical enzymes and transporters, including GLUT2 and PCK1.

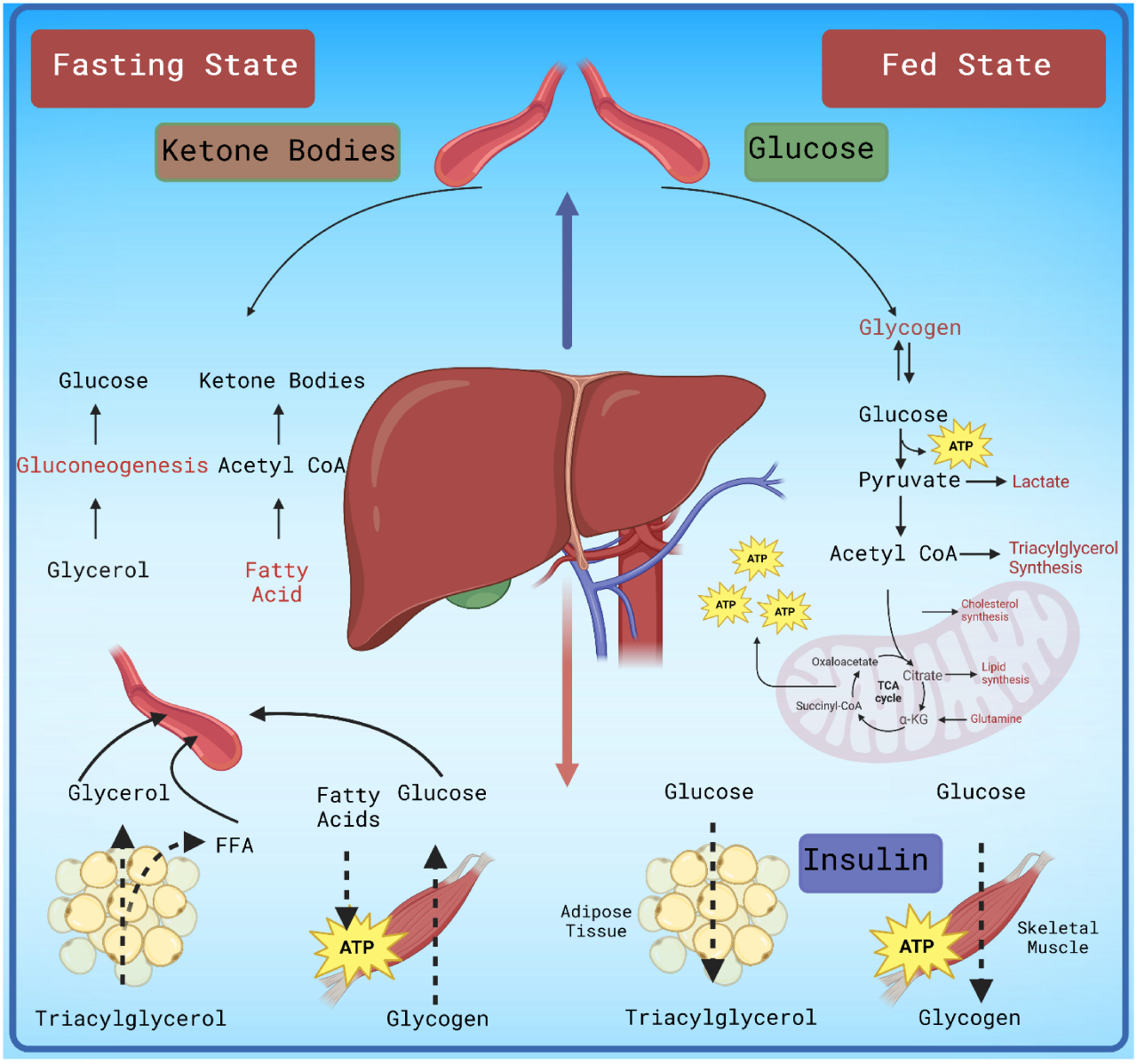
Fasting State
Fed State
Ketone Bodies
Glucose
Glycogen
Glucose
Ketone Bodies
Gluconeogenesis
Acetyl CoA
Glycerol
Fatty Acid
Glucose
ATP
Pyruvate
Lactate
Acetyl CoA
Triacylglycerol Synthesis
ATP
ATP
ATP
Cholesterol synthesis
Oxaloacetate
Citrate
Lipid synthesis
TCA cycle
Succinyl-CoA
α-KG
Glutamine
Glycerol
FFA
Fatty Acids
Glucose
Glucose
Glucose
Insulin
Adipose Tissue
ATP
ATP
Skeletal Muscle
Triacylglycerol
Glycogen
Triacylglycerol
Glycogen

Figure 1.2 *Metabolic Pathways in the Liver During Fasting and Fed State During Fasting*. The liver regulates blood glucose levels by producing glucose through gluconeogenesis, using non-carbohydrate sources like glycerol and fatty acids. During fasting (Left Side), fatty acid oxidation increases as hepatic glycogen stores are utilized, producing acetyl-CoA. This compound is then transformed into ketone bodies, which serve as an alternate energy source in extended periods of fasting. In the fed state (Right Side), the liver responds to insulin by absorbing glucose and converting it to pyruvate through glycolysis, producing ATP and precursor molecules for other metabolic pathways. Extra glucose is stored as glycogen, while acetyl-CoA synthesises new lipids, producing triacylglycerol and cholesterol. The relationship between the liver and peripheral tissues is emphasized, where insulin encourages the storage of glucose as glycogen in muscle tissue and produces triacylglycerol in adipose tissue. This picture highlights the liver's crucial function in regulating energy balance by managing the use and storage of nutrients based on the body's metabolic needs. **Created with BioRender.com**.

1.2.2 Fatty Acid Metabolism in the Liver

The liver plays a crucial role in controlling lipid metabolism inside the body. It has a pivotal function in producing and breaking down fatty acids. Fatty acids within the liver arise from dietary or endogenous sources (80). During fasting, non-esterified fatty acids are released from subcutaneous and visceral adipose tissue TAGs and are transported to the liver by the hepatic artery. The fatty acids can be utilized for two purposes: to produce TAGs to synthesise VLDL or to be oxidized for energy by β-oxidation. The liver primarily esterifies excess fatty acids to produce TAGs stored in lipid droplets (81). During the postprandial state, bile acids emulsify dietary TAGs in the intestinal lumen after they are hydrolysed mainly by pancreatic lipase. Subsequently, these TAGs are assimilated into chylomicrons within the gastrointestinal tract, facilitating the transportation of fatty acids to other tissues (82). The liver has the ability to convert dietary carbohydrates into new fat through a process called DNL (83). After a meal, higher insulin levels inhibit the breakdown of TAGs in adipose tissue and promote the synthesis of new fatty acids, leading to their storage rather than their use for energy production. The regulation of DNL mainly occurs at the transcriptional level. Plasma insulin stimulates the activation of the endoplasmic reticulum membrane-bound transcription factor SREBP1c, which transfers to the nucleus and enhances the expression of genes involved in the biosynthesis of fatty acids (84). The liver's intake of excessive plasma glucose also induces the expression of ChREBP. This transcription factor promotes the transcription of most genes involved in fatty acid biosynthesis and pyruvate kinase (85). Cluster of differentiation 36 (CD36), commonly referred to as fatty acid translocase, has a vital function in controlling fatty acid metabolism by facilitating the absorption of long-chain fatty acids into cells (86, 87) (**Figure 1.3**). A recent study has discovered that CD36 has a new role in fat resynthesis that extends beyond its recognized function as a transporter of free fatty acids.

CD36 facilitates the maintenance of balanced levels of lipids in the liver by controlling the processing of SREBP1c (88). SREBP1 is translocated from the ER to the Golgi for processing, ultimately stimulating lipogenesis. This is achieved by CD36 working in tandem with insulin-induced gene-2 (INSIG2) to break down the association between INSIG2 and the SREBP cleavage-activating protein-SREBP complex (88). The process of CD36-mediated DNL in hepatocytes is recognized as a crucial factor in the development of MASLD. Recent research has shown that curcumin, a natural polyphenol found in turmeric, helps reduce fatty liver and lower cholesterol and TAG levels in both animal and human studies (89, 90). The data show that curcumin can effectively treat dyslipidemia and MASLD. However, its quick systemic clearance and low bioavailability limit its therapeutic efficacy. Enhancing the drug's stability and water solubility by including two polyethylene glycols (mPEG454) can significantly reduce serum TAG levels and alleviate hepatic steatosis. This is achieved by blocking hepatic-specific peroxisome proliferator-activated receptor-gamma (PPAR-γ) and CD36 (91). Despite the absence of clinical evidence on this improved formulation, these findings highlight its potential as a promising therapeutic strategy for managing MASLD.

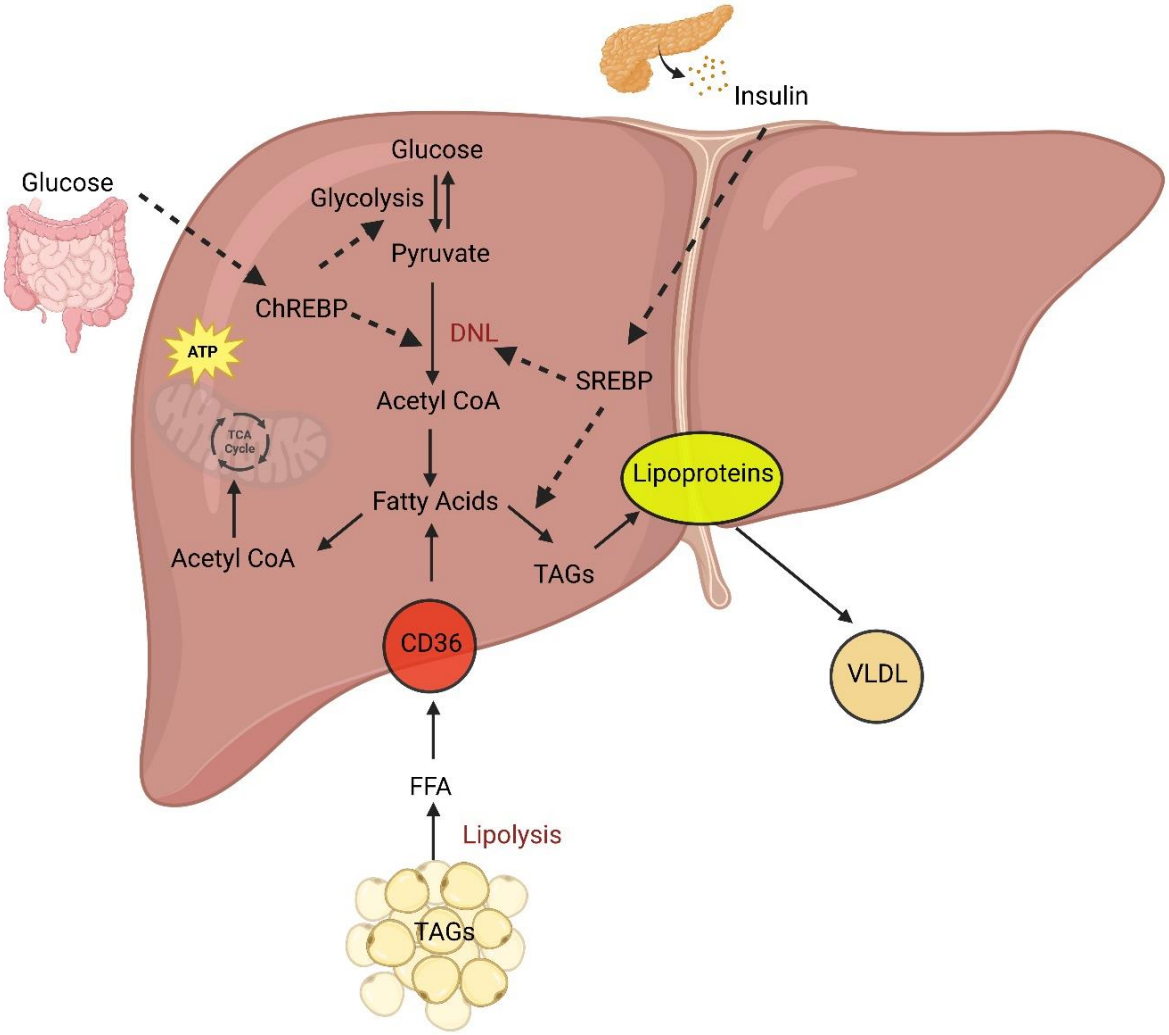
Insulin
Glucose
Glucose
Glycolysis
Pyruvate
ChREBP
DNL
ATP
SREBP
Acetyl CoA
TCA Cycle
Lipoproteins
Fatty Acids
Acetyl CoA
TAGs
CD36
VLDL
FFA
Lipolysis
TAGs

Figure 1.3 *Summary of Hepatic Fatty Acid Metabolism.* The graphic illustrates the processes of hepatic lipid metabolism in detail. Glucose can be broken down through glycolysis in hepatocytes to produce pyruvate, which then enters the TCA cycle, ultimately leading to the generation of adenosine triphosphate (ATP). Excess glucose can be directed towards de novo lipogenesis (DNL), a metabolic process facilitated by enzymes such as carbohydrate-responsive element-binding protein (ChREBP) and sterol regulatory element-binding protein (SREBP), resulting in the production of fatty acids. The produced fatty acids are converted into triacylglycerols (TAGs), which are either stored inside cells or transported as part of very low-density lipoproteins (VLDL) for export from the liver. Simultaneously, free fatty acids (FFAs) from the bloodstream enter liver cells through the cluster of differentiation 36 (CD36) transporter and can either undergo mitochondrial β-oxidation for energy production or be converted back into TAGs. Insulin regulates fatty acid esterification and storage by increasing it and reducing lipolytic activity, which helps store energy when abundant nutrients are available. **Created with BioRender.com**. Adapted from Vacca *et al*. (2015) (92).

1.2.3 Protein and Amino Acid Metabolism in the Liver

The liver synthesizes around 85-90% of the total protein in circulation, with albumin being the most abundant, constituting approximately 55% of plasma protein content (93) (**Figure 1.4**). While earlier studies mainly focused on glucose and fat metabolism, recent research has emphasised the function of dietary protein and the disruption of amino acid metabolism. Since the liver plays a critical role in protein and amino acid metabolism, altering circulating amino acid levels is often seen in chronic liver diseases. These processes include glutathione synthesis, inflammation, oxidative stress, and pathways like the TCA cycle and β-oxidation. There is extensive evidence indicating that patients with MASLD and T2D regularly exhibit high levels of branched-chain amino acids (BCAAs) and aromatic amino acids (AAAs) (94-96). Moreover, a recent study has found high relationships between circulating amino acids, more precisely, certain crucial amino acids such as BCAAs, AAAs, L-proline, L-valine, L-isoleucine, L-leucine, and L-phenylalanine directly affect insulin levels and homeostatic model assessment of insulin resistance (HOMA-IR) (97, 98). In addition, L-methionine directly affects insulin levels, while L-tyrosine positively affects HOMA-IR. ALT levels are linked to AAAs, L-phenylalanine, and L-tryptophan (99). The function of the branched-chain ketoacid dehydrogenase (BCKDH) enzyme, which is essential in breaking down BCAAs, is controlled after the process of translation by BCKDH kinase, which phosphorylates the BCKDH enzyme, leading to its deactivation. The phosphorylation process, facilitated by BCKDH kinase, is a crucial mechanism for regulating BCKDH activity. In the heart, the small chemical BT2, also known as 3,6-dichlorobenzo[b]thiophene-2-carboxylic acid, was deliberately made to mimic branched-chain keto acids (BCKA) and precisely target branched-chain ketoacid dehydrogenase kinase (BCKDK) (100). BT2 exerts cardioprotective effects against heart failure models by allosterically binding to BCKDK and successfully reducing cardiac levels

of BCAAs and BCKAs. In numerous rodent models of cardiometabolic disease, BT2 has been shown to reduce BCAA and BCKA circulation levels, improve glucose tolerance and insulin sensitivity, and reduce DNL (101-105). Similarly, administering BT2 decreases BCAA levels and improves glucose tolerance while reducing MASLD in obese mice (102, 104). However, surprisingly, genetically knocking down BCKDH kinase in the liver using shRNA-AAV did not result in any observable changes in glycemia or steatosis (104). This suggests that reducing BCKDH kinase in the liver alone may not be sufficient to improve metabolism.

The liver plays a pivotal role in the metabolism of proteins and amino acids, as it generates most proteins in the bloodstream and controls the levels of amino acids. Liver illnesses such as MASLD and T2D frequently exhibit disturbances in amino acid metabolism, characterised explicitly by heightened concentrations of branched-chain and aromatic amino acids. Directing efforts towards certain enzymes implicated in the breakdown of amino acids, such as BCKDK, exhibits the potential to enhance metabolic results.

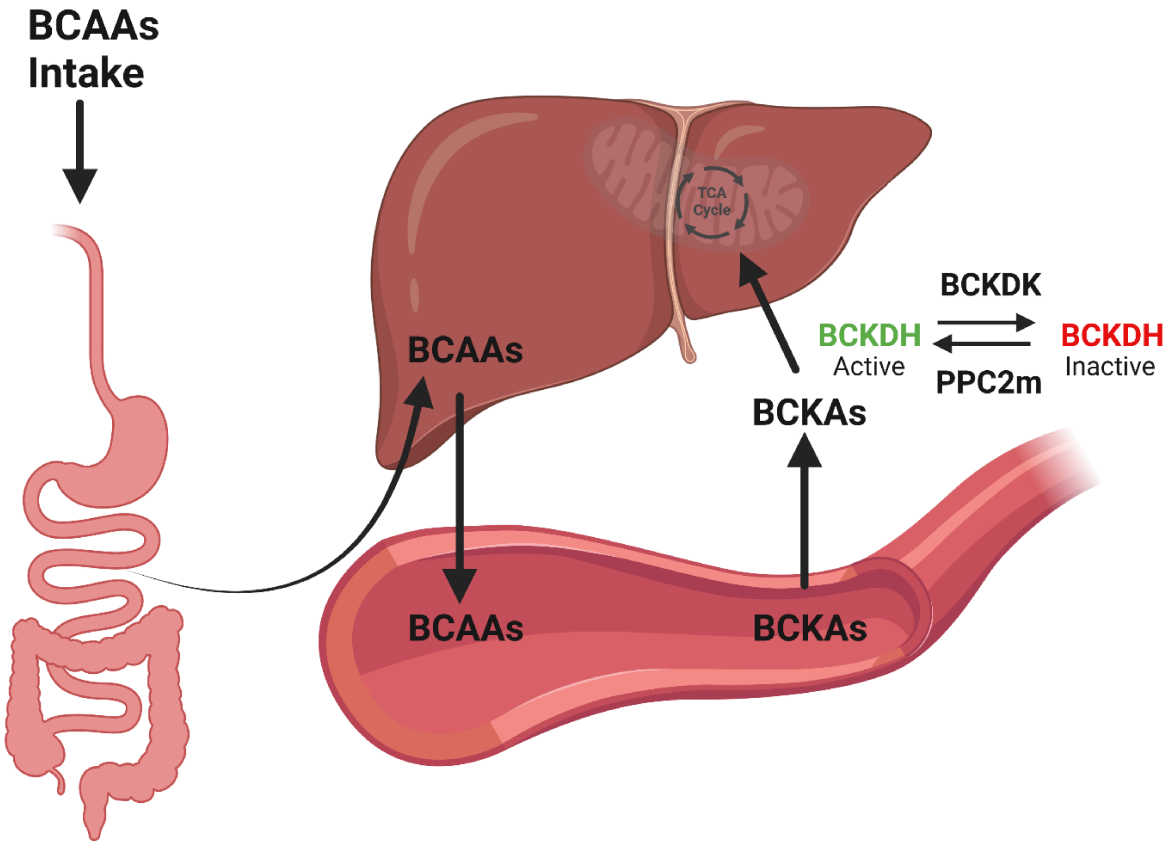
BCAAs
Intake
TCA
Cycle
BCKDK
BCKDH
Active
BCKDH
Inactive
PPC2m
BCAAs
BCKAs
BCAAs
BCKAs

Figure 1.4 *Branched-Chain Amino Acids Metabolism in the Liver.* This diagram illustrates the metabolic breakdown of branched-chain amino acids (BCAAs) in the liver, from ingestion to their several metabolic outcomes. BCAAs are absorbed from the gastrointestinal system after being consumed and delivered to the liver through circulation. Upon entering the liver, BCAAs undergo metabolism via many routes. Some branched-chain amino acids (BCAAs) are utilized in the liver's tricarboxylic acid (TCA) cycle to aid energy generation. BCAAs are deaminated by branched-chain amino acid transaminase to produce branched-chain keto acids (BCKAs). The BCKDH enzyme complex facilitates the degradation of BCKAs, a crucial process in BCAA metabolism. BCKDH complex activity is controlled by branched-chain ketoacid dehydrogenase kinase (BCKDK), which phosphorylates the complex, causing it to become inactive. Protein Phosphatase, Mg^2+/Mn^2+ dependent 2m (PPC2m) dephosphorylates the BCKDH complex to enhance active BCKDH and stimulate BCKA catabolism. Dephosphorylation increases BCKDH activity, promoting the breakdown of BCKAs. **Created with BioRender.com**. Adapted from Lo *et al*. (2022) (106).

1.2.4 Ketone Metabolism in the Liver

Ketone bodies make up 5–20% of the overall energy metabolism in a normal physiological state. Numerous physiological stimuli, including calorie restriction, exercise, and nutritional deprivation, affect the body's production and utilization of ketones (9). Under pathological conditions, such as uncontrolled diabetes and alcoholic ketoacidosis, wherein ketone body concentrations may elevate to 20 mM, ketogenesis is initiated through the hydrolysis of fatty acids, resulting in the production of acetone, acetoacetate (AcAc), and beta-hydroxybutyrate (βOHB) (10). These lipid molecules, collectively referred to as ketones, exhibit water solubility, negating the need for liposomal transport. AcAc and βOHB demonstrate heightened acidity with respective pKa values of 3.6 and 4.7 (107, 108). Despite being the primary site of ketogenesis within liver cell mitochondria, it is intriguing that the liver does not utilize ketone bodies due to the absence of the enzyme succinyl-CoA:3-ketoacid CoA transferase (SCOT) (gene name *OXCT1*) (11).

Carnitine palmitoyltransferase-1 (CPT1) facilitates the transport of fatty acids into the mitochondria, where subsequent beta-oxidation processes lead to the production of acetyl CoA. Thiolase, also known as acetyl coenzyme A acetyltransferase, catalyzes the conversion of two acetyl-CoA molecules into acetoacetyl-CoA. The enzyme 3-hydroxy-3-methylglutaryl-coenzyme A (HMG-CoA) synthase transforms acetoacetyl-CoA into HMG-CoA, which is further converted into AcAc by HMG-CoA lyase. AcAc can transform into acetone or βOHB through non-enzymatic decarboxylation or βOHB dehydrogenase. Significantly, βOHB and AcAc are the predominant ketone bodies utilized by vital organs such as the heart and brain for energy (109).

Upon reaching extrahepatic tissues, βOHB is converted to AcAc by the enzymes beta-hydroxybutyrate dehydrogenase and beta-ketoacyl-CoA transferase, subsequently reverting to acetyl-CoA. Following the citric acid cycle and oxidative phosphorylation yields 22 ATP per molecule (110-113). Since acetone cannot be converted back to acetyl-CoA, it must be inhaled or eliminated through urine. The ketone bodies—AcAc, acetone, and βOHB—are small metabolites generated from lipids and are an alternative energy source for all living organisms. Notably, there are higher concentrations of ketone bodies, AcAc and βOHB, than acetone.

When there is a shortage of glucose in the body, ketone bodies are produced as an alternative fuel source and operate as a metabolic signal that controls several cellular processes. The liver produces them during the breakdown of fats. Ketogenesis is a metabolic process that yields ketone bodies, which offer the body an alternate energy source. Because 3-hydroxy-3-methylglutaryl-coenzyme A synthase 2 (HMGCS2) is highly expressed in hepatocytes, the liver largely takes place ketogenesis in mammals (13). It is worth noting that hepatocytes lack the expression of succinyl-CoA:3-oxo-acid CoA-transferase (SCOT), a ketolytic mitochondrial enzyme (114). Hepatocytes can thus only produce ketone bodies; they cannot undergo oxidation. Intestinal epithelial cells have the second-highest expression of HMGCS2. A recent study demonstrated intestinal stem cells' capacity to differentiate and regenerate is impaired when HMGCS2 is lost (115). Research indicates that some DNL-related genes, including *Srebp1*, carbohydrate response element-binding protein 1 (*Chrebp1*), and stearoyl-CoA desaturase 2 (*Scd2*), are expressed more when there is insufficient ketogenesis (14).

1.3 Potential Therapeutic Approaches Targeting Metabolic Dysfunction-Associated Steatotic Liver Disease in Obesity and Type 2 Diabetes

1.3.1 Pyruvate Dehydrogenase and Hepatic Glucose Oxidation

The liver plays a major role in whole-body glucose homeostasis, with glucose transporter 2 serving as the primary transporter for hepatic glucose uptake (116). Following transport into the liver, glucose is phosphorylated by glucokinase to G6P and has a variety of metabolic fates. This includes (1) undergoing glycogenesis for storage as glycogen, (2) shuttling into the pentose phosphate pathway to generate reduced nicotinamide adenine dinucleotide phosphate for supporting DNL and the production of reduced glutathione, and (3) undergoing glycolysis to support small amounts of energy (ATP) production with the eventual generation of pyruvate (**Figure 1.5**).

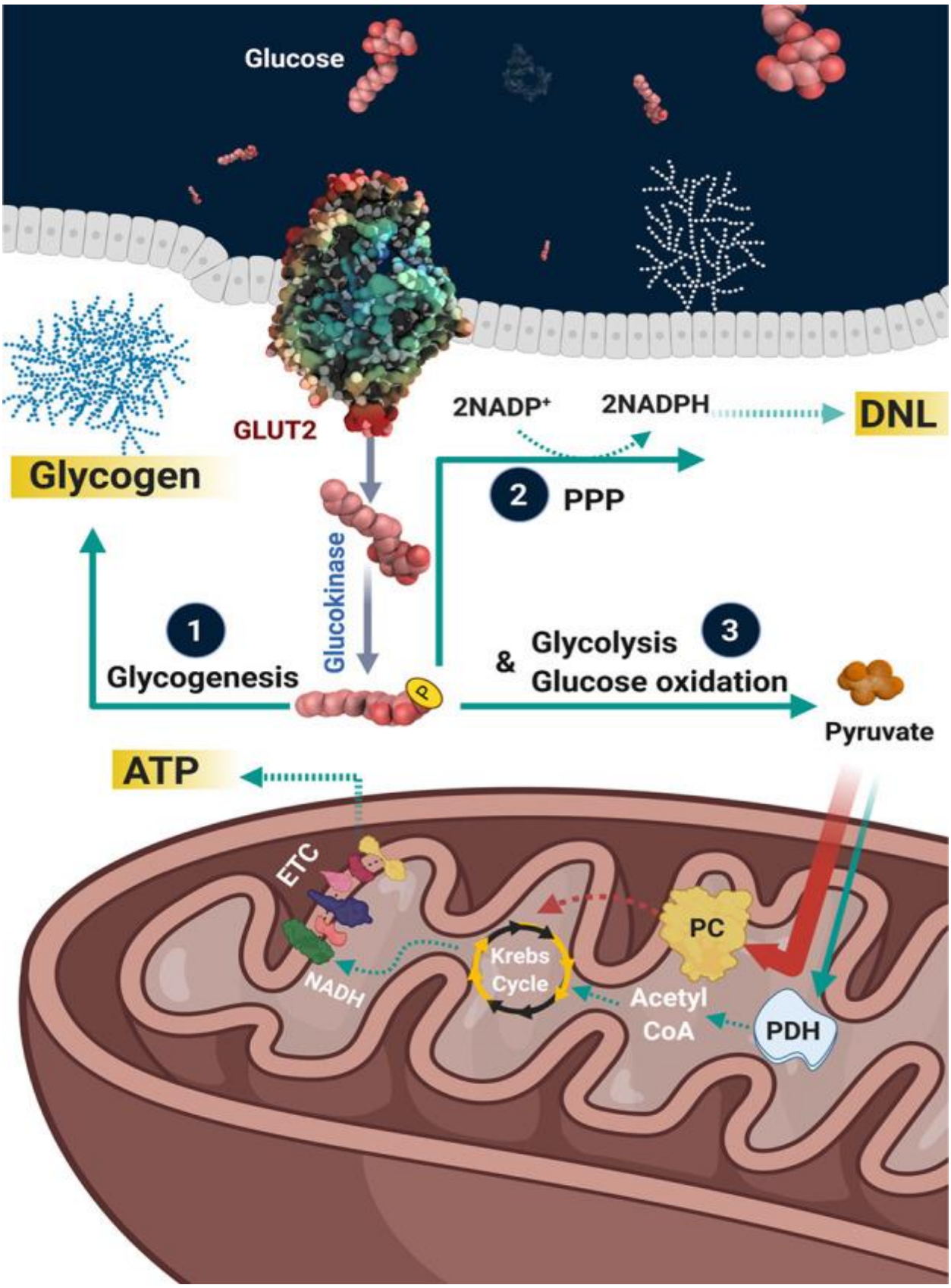
Glucose
GLUT2
Glycogen
2NADP+
2NADPH
DNL
2
PPP
Glucokinase
1
Glycogenesis
&
Glycolysis
3
Glucose oxidation
Pyruvate
ATP
ETC
NADH
Krebs
Cycle
PC
Acetyl
CoA
PDH

Figure 1.5 *Hepatic Glucose Metabolism*. Upon glucose transporter 2 (GLUT2) mediated entry into the hepatocyte, glucokinase phosphorylates glucose into glucose-6-phosphate, which subsequently undergoes 3 major metabolic fates. This includes (1) storage as glycogen via glycogenesis, (2) the PPP to generate important cofactors (NADPH) to support DNL and the production of reduced glutathione, and (3) to generate small amounts of energy (ATP) via aerobic glycolysis, which results in the formation of pyruvate as an end-product. This pyruvate may be transported into the mitochondria via the mitochondrial pyruvate carrier, following which the majority is carboxylated into oxaloacetate via PC, whereas a much smaller fraction is decarboxylated into acetyl CoA via PDH. Published in Saed *et al*. 2021 (117).

In order to maximize ATP production during glucose metabolism, glycolytically derived pyruvate is transported into the mitochondria via the mitochondrial pyruvate carrier, following which pyruvate is decarboxylated into acetyl CoA via the pyruvate dehydrogenase (PDH) complex (PDC) (**Figure 1.6**). It should be noted though that pyruvate oxidation only accounts for a minor fraction of glucose/pyruvate metabolism in the liver, even in the post-prandial state, as the vast majority of mitochondrial pyruvate is carboxylated into oxaloacetate via pyruvate carboxylase (PC), which contributes to supporting DNL (118).

The PDC is a fundamental enzyme involved in cellular energy metabolism and the rate-limiting enzyme of glucose oxidation. The PDC is composed of three enzymes with distinct activities that act in a sequential fashion; PDH (or enzyme 1 [E1]), dihydrolipoyl acetyltransferase (DLAT or E2), and dihydrolipoyl dehydrogenase (DLD or E3) (for extensive review of the PDC please refer to refs (119, 120), which ultimately result in the formation of acetyl-CoA, CO_2, and reduced nicotinamide adenine dinucleotide (NADH) (**Figure 1.6**). PDC generated acetyl-CoA feeds into the Krebs Cycle, subsequently resulting in formation of the reducing equivalents NADH and reduced flavin adenine dinucleotide, which acts as electron donors to fuel oxidative phosphorylation in the mitochondrial electron transport chain for ATP production.

The oxidation of pyruvate through the PDH component of the PDC is tightly regulated by a variety of post-translational modifications, with phosphorylation/dephosphorylation of specific serine residues of PDH being the most extensively characterized to date (119, 120). Two tightly bound regulatory enzymes, pyruvate dehydrogenase kinase (PDHK), of which there are four isoforms, and pyruvate dehydrogenase phosphatase (PDHP), of which there are two isoforms, catalyze the

deactivating phosphorylation and activating dephosphorylation of PDH, respectively (**Figure 1.6**). Moreover, PDC-derived metabolic byproducts and byproduct ratios, including acetyl CoA/free CoA and the NADH/NAD^+, can regulate PDH activity secondary to regulating the activity of PDHK and PDHP. Recent studies have also identified that PDH can be regulated by both acetylation (121, 122) and glutathionylation (123, 124), both of which inhibit PDH activity and subsequent glucose oxidation.

In the liver, PDH activity is stimulated post-prandially, whereby PDH-derived acetyl CoA is used not only to support ATP production but also to support DNL (125). In contrast, during fasting or prolonged starvation, PDH activity is decreased as a consequence of elevated fatty acid oxidation rates and corresponding increases in the acetyl CoA/free CoA and the NADH/NAD^+ ratios. In addition, increases in the acetyl CoA/free CoA ratio also stimulate the activity of PC, which converts pyruvate into oxaloacetate. This is an essential metabolic adaptation from a physiological homeostasis standpoint during fasting/starvation, as this allows pyruvate to be used as a substrate for gluconeogenesis, thereby allowing the body to maintain normoglycemia.

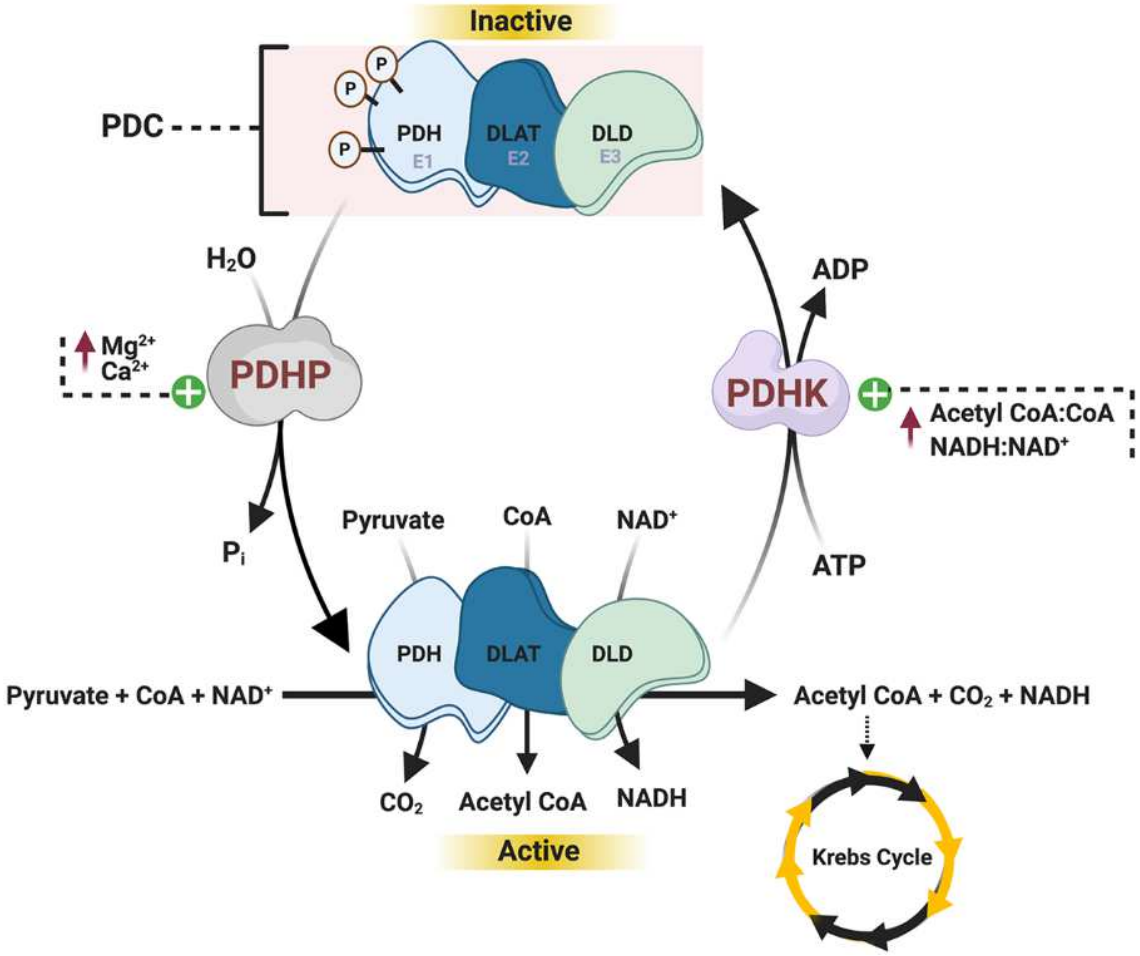
Inactive
PDC
P
P
P
PDH
E1
DLAT
E2
DLD
E3
H2O
Mg2+
Ca2+
PDHP
ADP
PDHK
Acetyl CoA:CoA
NADH:NAD+
Pi
Pyruvate
CoA
NAD+
ATP
PDH
DLAT
DLD
Pyruvate + CoA + NAD+
Acetyl CoA + CO2 + NADH
CO2
Acetyl CoA
NADH
Active
Krebs Cycle

Figure 1.6 *Enzymatic Regulation of the PDH Complex*. The PDH complex is a multienzyme complex comprising three major enzymes, including PDH (enzyme 1 [E1]), dihydrolipoyl acetyltransferase (DLAT or E2), and dihydrolipoyl dehydrogenase (DLD or E3). PDH is responsible for the decarboxylation of pyruvate and is tightly controlled by phosphorylation, whereby 4 isoforms of PDHK phosphorylate/deactivate PDH, and 2 isoforms of PDHP dephosphorylate/activate PDH. PDHK is positively regulated by increased acetyl CoA/CoA and NADH/NAD+ ratios, whereas increases in pyruvate inhibit PDHK but stimulate PDHP. In addition, increases in mitochondrial calcium and magnesium concentrations can also stimulate PDHP. Published in Saed *et al*. (2021) (117).

1.3.2 Pyruvate Dehydrogenase Activity in Obesity

Pivotal studies by Jeoung and Harris demonstrated that targeting PDH activity might have therapeutic value in obesity, as they observed that mice harboring a whole-body deletion of PDHK4 were protected against insulin resistance when fed a high-fat diet (HFD; 59.5% kcal from lard) for 18 weeks (126). Reasons for this protection have primarily been attributed to actions in skeletal muscle, as experimental obesity increases muscle PDHK4 expression, thereby impairing muscle PDH activity and subsequent glucose oxidation rates. Moreover, a multitude of studies have now demonstrated that increasing muscle PDH activity and glucose oxidation imparts a potent glucose-lowering response in obesity. For example, provision of mangiferin (a primary constituent of mango tree extract) in the diet increases soleus muscle PDH activity and glucose oxidation rates, likely due to a significant reduction in PDHK4 expression, ultimately improving glucose tolerance and insulin sensitivity in obese mice (127). In addition, it has also been demonstrated that increases in muscle PDH activity are key mechanisms by which either increasing muscle carnitine acetyltransferase activity or decreasing muscle ketone body oxidation rates result in an overall improvement in glucose homeostasis in experimental obesity (128, 129). Illustrating the clinical relevance of PDH as a target, supplementation for 6 months with l-carnitine (2 g/day) increased vastus lateralis muscle PDH activity (secondary to reductions in the acetyl CoA/free CoA ratio (130) and lowered both circulating glucose and insulin levels in overweight/obese, insulin-resistant human subjects (129).

1.3.3 Hepatic Pyruvate Dehydrogenase Activity in Metabolic Dysfunction-Associated Steatotic Liver Disease

While the previous section alluded to increases in muscle glucose oxidation representing the mechanism by which stimulating PDH activity imparts beneficial actions in obesity, the majority of these studies have not considered whether increases in PDH activity/glucose oxidation in other organs could be responsible. Reasons for hepatic PDH activity not being considered likely involve the minimal contribution that pyruvate oxidation has in terms of overall pyruvate metabolism in the liver (118). Furthermore, liver-specific PDH deficient mice exhibit robust reductions in hepatic glucose production and an improvement in whole-body insulin sensitivity (125), which would raise concern with regard to stimulating hepatic PDH activity in the setting of MASLD. However, these studies were not performed in the context of HFD supplementation and obesity.

The prototypical pan-PDHK inhibitor is dichloroacetate (131), but this agent is limited by a short half-life, and thus a series of novel PDHK inhibitors were recently developed by the Chuang laboratory, with the strongest candidate being 2-[(2,4-dihydroxyphenyl)sulfonyl]isoindoline-4,6-diol (PS10) (132). While acute treatment of mice with PS10 appears to stimulate PDH activity in multiple organs, prolonged PS10 treatment appears to harbor selectivity toward increasing hepatic PDH activity (132). Moreover, treatment of male C57BL/6J mice fed an HFD (60% kcal from lard) for 14 weeks with PS10 (70 mg/kg once daily) during the final 4 weeks improved glucose tolerance, which was associated with a robust reduction in hepatic steatosis as indicated by decreased Oil Red O staining (132, 133). As MASLD is a major risk factor for insulin resistance/T2D, this suggests that systemic activation of PDH to increase glucose oxidation rates may also improve glucose homeostasis via reductions in hepatic steatosis. Indeed, despite

mangiferin treatment increasing muscle PDH activity/glucose oxidation in obese mice, it also caused marked reductions in adiposity (127), suggesting that reductions in hepatic steatosis may have been present. Observations from Go *et al*. engendered further interest along this perspective, as mice with a whole-body PDHK2 deficiency demonstrated protection against insulin resistance when subjected to experimental obesity via chronic HFD (60% kcal from lard) supplementation, which they specifically attributed to a reduction in hepatic steatosis (134). Furthermore, they observed that experimental obesity increased hepatic PDHK2 mRNA/protein expression, thereby decreasing hepatic PDH activity, whereas obese PDHK2 deficient mice exhibited normal hepatic PDH activity, which was associated with decreased liver weights and hepatic steatosis compared to their obese wild-type littermates. Because PDHK2 deficient mice also demonstrated reductions in adiposity in response to experimental obesity, the reductions in hepatic steatosis could once again be secondary to weight loss. However, liver-specific knockdown of PDHK2 via tail vein injection of an adenovirus also lowered hepatic TAGs content and improved glucose tolerance, alluding to effects in the liver being a major driver of the phenotype observed in PDHK2 deficient mice.

Additional support for increasing hepatic PDH activity and subsequent glucose oxidation rates to mitigate obesity-related MASLD have been observed with ranolazine, a second-line therapy used for the treatment of angina. While ranolazine's mechanism of action for improving angina stems from its ability to inhibit the late inward sodium current by blocking the voltage-gated sodium channel subunit 1.5 (135), ranolazine has also been demonstrated to increase glucose oxidation rates in both isolated working heart and muscle preparations (136, 137). Accordingly, male C57BL/6J mice fed an HFD (60% kcal from lard) for 10 weeks were subsequently treated with

ranolazine (50 mg/kg daily) for 30 days while remaining on the HFD, which led to marked reductions in the liver weight/body weight ratio and hepatic TAGs content, as well as an overall improvement in glycemia (138). The ranolazine mediated improvement in hepatic steatosis was associated with decreased hepatic PDH phosphorylation (indicative of increased PDH activity), which may involve a direct effect, as ranolazine treatment of HepG2 cells also decreased PDHK4 mRNA expression and subsequent PDH phosphorylation. Importantly, reductions in hepatic steatosis are necessary for the glucose-lowering actions of ranolazine, as a single treatment of obese male C57BL/6J mice with ranolazine failed to lower hepatic TAGs content and glucose levels during a pyruvate tolerance test. Conversely, a 1-week treatment of obese male C57BL/6J mice with ranolazine was sufficient to lower hepatic TAGs content, which was now associated with improved glycemia during a pyruvate tolerance test. As obese individuals are often at risk for angina/ischemic heart disease, it may prove worthwhile for future studies to assess the prevalence of MASLD in subjects treated with ranolazine in this patient population.

1.3.4 Potential Mechanisms by Which Increasing Hepatic Pyruvate Dehydrogenase Activity Attenuates Metabolic Dysfunction-Associated Steatotic Liver Disease

Although a number of studies support the premise that increases in hepatic PDH activity and glucose oxidation protect against obesity-related MASLD, the specific mechanisms involved remain to be elucidated. It has been proposed that the mechanism by which PDHK2 deficiency in the liver protects against hepatic steatosis is an increased rate of hepatic ketogenesis (134). Ketogenesis is the physiological process by which fatty acids are metabolized and converted into the ketone bodies AcAc and βOHB, which primarily take place in the liver and can dispose of

approximately two-thirds of hepatic fatty acid uptake (139, 140). Increases in hepatic PDH activity divert pyruvate away from supporting anaplerosis through PC mediated entry into the Krebs Cycle, thereby lowering Krebs Cycle intermediates and promoting ketogenesis, all of which was observed in obese PDHK2 deficient mice (134). Furthermore, hepatic mRNA expression of 3-hydroxymethyl-3-methylglutaryl CoA synthase 2, the fate-committing enzyme of ketogenesis, was also increased in obese PDHK2 deficient mice, while hepatocytes isolated from these mice demonstrated decreased formation of $^{14}CO_2$ from [$^{14}C_1$]-octanoate and an increased rate of βOHB formation. These findings are compatible with studies in liver-specific PC deficient mice, whereby these animals also demonstrated robust increases in hepatic ketogenesis, though only macrovesicular and not microvesicular steatosis were improved in their livers when fed an HFD (141). In contrast, pharmacological PDHK inhibition with PS10 did not influence hepatic Krebs Cycle flux or increase circulating ketone bodies in obese C57BL/6J mice (133). Instead, it may decrease hepatic steatosis by decreasing nuclear levels of carbohydrate-responsive element binding protein, thereby decreasing hepatic DNL. Such observations, however, are incompatible with findings in liver-specific PDH deficient mice, demonstrating that PDH-derived acetyl CoA plays an important role in supporting hepatic DNL (125, 142). Such observations support the notion that diverting pyruvate away from PC may be more important than increasing its flux through PDH in the liver, though hepatic TAGs content was not decreased in these animals.

As previously mentioned, increases in glucose oxidation often result in a corresponding reduction of fatty acid oxidation via the glucose-fatty acid cycle described by Randle *et al* (143). Thus, on the surface, one might predict that stimulating hepatic PDH activity and glucose oxidation would inhibit fatty acid oxidation through Randle's glucose-fatty acid cycle, thereby shuttling fatty acids

toward lipogenic pathways and increasing hepatic TAGs accumulation. Observations in obese PDHK2 deficient mice or obese mice treated with either PS10 or ranolazine clearly indicate that this is not the case, even though ranolazine has also been shown to decrease fatty acid oxidation rates in both cardiac and skeletal muscle (136, 137). Of interest, it has been suggested that the glucose-fatty acid cycle is most relevant to cardiac and skeletal muscle, while being less applicable in the liver (144), which may explain why stimulating hepatic PDH activity does not promote hepatic steatosis and can surprisingly mitigate obesity-related MASLD (133, 134, 138). It is also possible that since flux through PDH accounts for only a minor fraction of overall pyruvate metabolism in the liver, any increase in hepatic glucose oxidation offset by a decrease in fatty acid oxidation is minimal. On the contrary, if the glucose-fatty acid cycle is relevant in the liver and increasing hepatic PDH activity does result in a corresponding and significant reduction in hepatic fatty acid oxidation, it is possible this may induce an energy deficit that stimulates the energy sensor, AMP activated protein kinase (AMPK). Indeed, decreasing fatty acid oxidation can stimulate AMPK activity (145), and increased AMPK phosphorylation (indicative of increased AMPK activity (146)) was observed in obese male C57BL/6J mice treated with PS10 (133). Moreover, numerous studies have demonstrated that augmenting AMPK activity can prevent and/or reverse hepatic steatosis and the progression of MASLD (147).

Taken together, several proposed mechanisms, including increases in hepatic ketogenesis or AMPK activity and decreases in hepatic DNL or flux through PC may explain how stimulating PDH activity and glucose oxidation confers benefit against obesity-related MASLD (**Figure 1.7**). Nonetheless, it remains to be conclusively determined whether these mechanisms are truly

required for the salutary actions against MASLD in response to hepatic PDH activation, which will need to be addressed in future preclinical studies.

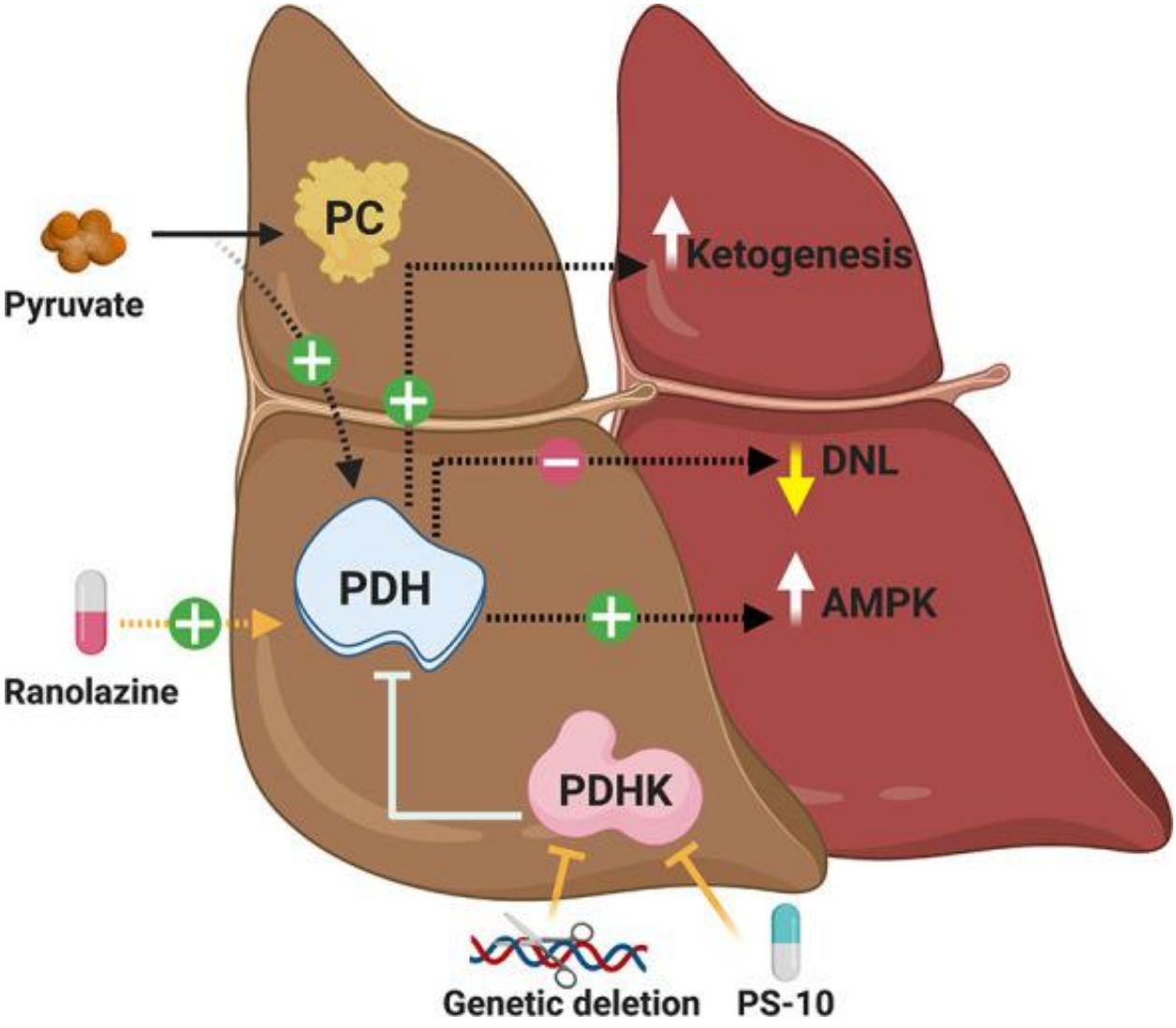

Figure 1.7 *Proposed Mechanisms Explaining How Increased Hepatic PDH Activity Ameliorates MASLD*. Increases in hepatic PDH activity and subsequent glucose oxidation rates may reduce hepatic steatosis and the progression of MASLD by possibly increasing hepatic ketogenesis, decreasing hepatic DNL, stimulating AMPK activity, or diverting pyruvate away from PC. Published Saed *et al*. 2021 (117).

1.3.5 Inositol-Requiring Enzyme 1 Activity and Hepatic Lipid Metabolism

When misfolded or unfolded proteins accumulate in the lumen of the cellular ER, the ER experiences stress. The unfolded protein response (UPR) is activated in response to this condition, leading to a coordinated cellular response. The UPR involves the initiation of distinct signal transduction pathways, such as those facilitated by inositol-requiring enzyme 1 (IRE1), double-stranded RNA-dependent protein kinase (PKR)-like ER kinase (PERK), and activating transcription factor-6 (ATF6) (148, 149). These pathways are activated in response to ER stress and coordinate alterations in protein synthesis and gene expression programs. The UPR is a cellular process that tries to restore equilibrium by resolving the difficulties caused by the buildup of unfolded proteins within the ER. This process emphasizes the complex methods that cells use to ensure the quality control of proteins. Although UPR is a protective mechanism cells use to regain ER equilibrium, extreme or protracted ER stress causes tissue damage and cell death (**Figure 1.8**). Growing evidence links ER stress to illnesses such as inflammation, cardiovascular diseases, and metabolic disorders (150).

The liver plays a crucial role in regulating nutrition and lipid metabolism, with the ER as a central location for lipid processing. Numerous enzymes and regulatory proteins are dedicated to managing lipid metabolism within the ER. However, disturbances in ER function can lead to hepatic steatosis, inflammation, and insulin resistance, highlighting the significance of maintaining ER homeostasis for overall liver health (151). IRE1α is linked to heat shock protein 5 (Hspa5/BiP/Grp78, or GRP78) and is kept repressed in an environment without stress. During ER stress, the separation of BiP enables the activation of IRE1α through dimerization and trans-autophosphorylation. IRE1α, when activated, exhibits site-specific endoribonuclease (RNase)

activity at the carboxyl end of its cytoplasmic domain. This activity removes 26 nucleotides from the mRNA that encodes X-box-binding protein 1 (*Xbp1*). This atypical, unconventional splicing event takes place extranuclear, leading to a translational frameshift and the production of a 371 amino-acid isoform, XBP1s (XBP1 spliced) (152). The XBP1s protein operates by relocating to the nucleus to activate transcriptional programs that increase the expression of a wide range of UPR-associated genes involved in protein entry into the ER, protein folding and ER biogenesis. The IRE1-XBP1 pathway is one of the three primary branches of the UPR and has been recognized as a crucial controller of hepatic lipid metabolism. Hepatocyte-specific IRE1 knockout mice exhibit significant hepatic fat accumulation and decreased insulin sensitivity on a high-fat diet (45% kcal fat) (153). Additionally, these mice show reduced levels of circulating TAG, cholesterol, low-density lipoprotein (LDL), and high-density lipoprotein (HDL). These results suggest that IRE1α deletion leads to severe hepatic steatosis accompanied by hypolipidemia. In line with the impact of IRE1α deletion on hepatic lipid metabolism, a different study involving the removal of hepatic IRE1 and induction of ER stress with tunicamycin revealed intriguing findings (154). Subject to a 24-hour tunicamycin injection, control mice displayed moderate macrovesicular steatosis, while liver-specific IRE1 knockout animals exhibited significant microvesicular steatosis. After 72 hours, control mice showed complete resolution of hepatic steatosis, whereas IRE1 knockout mice continued to display fatty deposits, underscoring the crucial role of IRE1 in preventing and recovering from ER stress-induced fatty liver disease. Notably, IRE1 knockout mice exhibited macrovesicular steatosis after 72 hours, indicating a delayed formation of larger lipid droplets in response to ER stress. These observations highlight the dynamic influence of IRE1 on the development and resolution of hepatic steatosis under ER stress.

In parallel, the repercussions of XBP1 deletion in specific cell types consistently result in adverse outcomes, hindering the maturation of β-cells into plasma cells when removed from lymphoid precursors (155); its absence in intestinal epithelia heightens susceptibility to inflammatory bowel disease (156), and depletion in central nervous system neurons promotes leptin resistance and obesity (157). In these scenarios, deliberate XBP1 depletion increases ER stress in affected cells, potentially leading to cellular demise and subsequent inflammation. Mice deficient in XBP1 in the liver at birth exhibited average body weight and liver mass, no discernible physical abnormalities, and no signs of liver injury as assessed by histological examination and blood ALT levels (158). Mice lacking hepatic XBP1 exhibit a significant decrease in plasma TAGs, cholesterol, and free fatty acids, while hepatic TAG levels are unaltered (159). Additionally, the absence of XBP1 leads to the continuous activation of its upstream activator, IRE1. The key genes involved in the production of fat, such as stearyl CoA desaturase 1 (*Scd1*), diacylglycerol acetyltransferase 2 (*Dgat2*), and acetyl CoA carboxylase 2 (*Acc2*), are noticeably suppressed in hepatic XBP1 knockout mice. In parallel findings, mice with hepatic XBP1 knockout, when subjected to a high-fat diet (fructose), displayed no alterations in mRNA levels of lipogenic genes such as fatty acid synthase (*Fasn*), *Scd1*, *Acc1*, and *Acc2*. Intriguingly, there was a modest reduction in SREBP-1c expression in XBP1-deficient liver compared to wild-type liver under high fructose diet conditions, potentially contributing to the decreased expression of lipogenic genes (159).

The effect of XBP1 deletion on lipogenesis observed in previous studies was not replicated in liver IRE1 knockout mice after a 12-week period of high-fat diet feeding. Insulin signaling was comparable in both groups of mice, but the livers of animals lacking IRE1 showed considerably elevated levels of steatosis compared to the control mice (160). However, there was no discernible

variation in the expression of critical genes implicated in the processes of fatty acid oxidation. These findings indicate that the decreased ability of IRE1 mutant mice livers to process higher levels of hepatic fatty acids after extended fasting or high-fat diet feeding may not be caused by defective fatty acid oxidation but rather by a malfunction in the export of TAGs from the liver. Analysis of hepatic VLDL secretion demonstrated a notable decline in plasma TAG accumulation and rates of hepatic VLDL-TAG secretion in IRE1 knockout mice compared to control mice. This suggests a decrease in TAG content in apoB-containing lipoprotein particles released from the livers of IRE1 knockout mice. These data indicate that the deletion of IRE1 does not have an impact on the production of fat. Still, it may influence the export of TAGs from the liver and the assembly of VLDL in the endoplasmic reticulum (160). The results emphasize the complex involvement of XBP1 and IRE1 in liver lipid metabolism and identify prospective targets for treating metabolic diseases related to disrupted lipid balance.

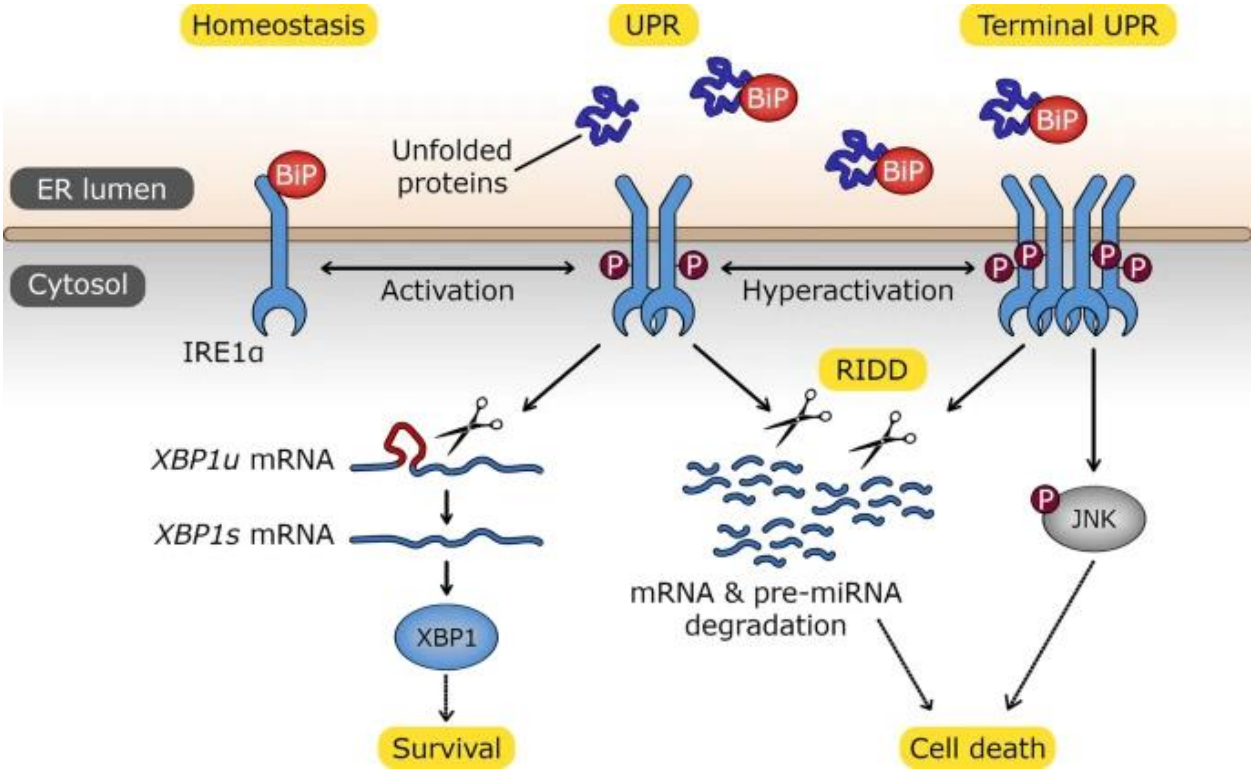
Homeostasis
UPR
Terminal UPR
BiP
BiP
BiP
Unfolded proteins
ER lumen
Cytosol
Activation
Hyperactivation
IRE1α
RIDD
XBP1u mRNA
XBP1s mRNA
JNK
mRNA & pre-miRNA degradation
XBP1
Survival
Cell death

Figure 1.8 *Schematic Representation Illustrates the Downstream Effects of Endoplasmic Reticulum Stress-Induced Inositol-Requiring Enzyme 1 (IRE1) Activation*. These consequences encompass proadaptive X-box binding protein 1 (XBP1s)-dependent transcriptional signaling, as well as apoptotic RNA degradation (RIDD) and c-Jun N-terminal kinase (JNK) pathway activation. Adapted from Bartoszewska *et al*. (2023) (161).

1.3.6 Inositol-Requiring Enzyme 1 Activity in Type 2 Diabetes

The UPR is a focal point in T2D research, as it plays a pivotal role in insulin secretion and the pathogenesis of T2D. This underscores the intricate relationship between ER disruption, UPR activation, and the onset of T2D. Interestingly, the effect of IRE1 knockout varies across different tissues. Pancreatic β-cells-specific IRE1 knockout models have demonstrated a diabetic phenotype characterized by sustained elevation in blood glucose levels and markedly reduced serum insulin levels without alterations in pancreatic islet size or number (162). In MIN6 pancreatic β-cells, knockdown of IRE1 impaired proinsulin, insulin content, and secretion. However, restoring the IRE1-XBP1 pathway led to the recovery of proinsulin and insulin levels and secretion (162). In myeloid-specific IRE1 deletion mice, HFD-induced obesity was prevented by decreased body weight and adiposity without impacting lean mass. These mice also showed superior blood glucose regulation, reduced hyperinsulinemia, and enhanced insulin sensitivity (163). Additionally, loss of IRE1 in myeloid cells led to increased energy expenditure, as evidenced by significantly higher oxygen consumption and elevated core body temperatures in HFD-fed mice (163).

A complete lack of XBP1 leads to the death of embryos early on in development (164). A study revealed that progressive hyperinsulinemia developed as early as 4 weeks in BALB/c genetic background mice with a null mutation in one XBP1 allele ($XBP1^{+/-}$), fed an HFD, and continued throughout the experiment compared to their littermate. When $XBP1^{+/-}$ animals were compared to wild-type controls, C-peptide levels were likewise noticeably higher in these animals. When HFD was administered to $XBP1^{+/-}$ mice, blood glucose levels rose in both the fed and fasting states, resulting in a marked increase in glucose intolerance. Deleting one XBP1 allele predisposes mice

to diet-induced peripheral insulin resistance and T2D, even when islet morphology and function are equivalent across genotypes (165).

Deletion of XBP1 in β-cells led to a minor increase in blood glucose levels compared to wild-type littermates, accompanied by a modest decrease in serum insulin levels, suggesting inadequate insulin production to sustain normal glucose levels (166). In contrast to the mice with IRE1 β-cell knockout mice, the animals with β-cells XBP1 knockout mice showed reduced size of the islet and lower insulin levels in the pancreas. Additionally, they displayed structural defects, including disorderly islet structure. Although there are similarities, the phenotypes of IRE1α and XBP1 knockout mice exhibited distinct differences, indicating that each gene has specific functions. Nevertheless, it is still uncertain to what degree these actions of IRE1, which do not rely on XBP1, contribute to the survival of β-cells and insulin secretion. The cleavage of proinsulin-processing enzyme mRNAs significantly necessitates more significant IRE1 activity than XBP1 splicing, indicating that this phenomenon exclusively occurs in hyperactivated IRE1α circumstances (167). Therefore, the phenotypes of IRE1 and XBP1 knockout mice are not identical, suggesting the presence of unique functions specific to each gene. However, it is unclear to what extent these XBP1-independent functions of IRE1 contribute to the viability and insulin secretory function of β-cells. It is important to note that the cleavage of proinsulin-processing enzyme mRNAs requires higher IRE1 activity than XBP1 splicing, suggesting that the former would occur only when IRE1α is hyperactivated. Another study showed the role of XBP1 in hepatocyte nuclear factor 4-alpha (HNF4α) β-cells knockout mice; HNF4α is a conserved transcription factor that plays a crucial role in regulating the initial development and long-term functioning of various adult organs. HNF4α is critical for the proper functioning of β-cells, as demonstrated by human mutations that

lead to Mature-Onset Diabetes of the Young 1 (MODYI). This condition is characterized by decreased glucose-stimulated insulin secretion in the pancreatic β-cells (168). Malfunctions in HNF4α can hinder the functioning of β-cells by disrupting XBP1 control and causing dysfunction in ER. Eliminating HNF4α in preexisting islets led to a substantial reduction in the expression of XBP1 in the islets (169). The forced induction of either un-spliced or spliced XBP1 was enough to restore impaired insulin production. XBP1 also has a role in preserving the specialized characteristics of β-cells, therefore contributing to the regulation of β-cells function. Dedifferentiation, which refers to the loss of mature β-cell phenotypic and cellular identity, has been identified as a major factor contributing to β-cells failure in T2D. Both animal and human research provide evidence that mature β-cells can undergo a transition to transform into various types of islet cells in the context of T2D (170). In XBP1 β-cells knockout mice, the expression of the GLUT2 was significantly decreased compared to control mice (166). In addition, the arrangement of islet cells in mice with a genetic knockout of the XBP1 gene in β-cells frequently showed changes, with α-cells scattered across the islets. Surprisingly, the mass of α-cells was about quadrupled in mice with a deletion of the XBP1 gene in β-cells compared to their control mice (166). This highlights the complex interaction between transcription factors such as XBP1 and the regulation of insulin release in pancreatic β-cells, providing insights into possible treatment targets for diabetes.

1.3.7 Potential Mechanisms by Which Increasing Inositol-Requiring Enzyme 1 Activity Attenuates Metabolic Dysfunction-Associated Steatotic Liver Disease

Activation of IRE1 is essential for modulating insulin production in pancreatic β-cells. IRE1 signalling is linked to insulin production when triggered in response to short-term exposure to elevated glucose levels (171). Deletion of IRE1, specifically in β-cells of mice, decreased proinsulin translation, reduced levels of pancreatic proinsulin and insulin content, and decreased insulin secretion after a meal. This deletion also caused a reduction in mRNA levels of proteins involved in recruiting ribosomes to the endoplasmic reticulum and processing mRNA (172). similarly, the deletion of β-cells *Xbp1* resulted in elevated glucose levels in the blood due to a significant reduction in the amount of insulin in the pancreas (167). Inhibiting IRE1 phosphorylation impedes insulin production (171). Nevertheless, prolonged exposure of β-cells to elevated glucose levels can cause ER stress and excessive activation of IRE1, inhibiting insulin gene production. Hence, the effect of IRE1 activation on insulin production in pancreatic β-cells relies on the length and strength of the stimulus, emphasizing the complex function of IRE1 signalling in controlling this crucial process (173).

IRE1/XBP1s have been linked to cardiovascular disease (174); increasing the expression of IRE1 has been demonstrated to enhance heart function by protecting pathological remodelling in the heart caused by pressure overload (175). Overexpressing IRE1α, specifically in the heart, results in maintained function, decreased area of fibrosis, enhanced adaptive UPR signalling, and reduced expression of inflammatory and pathogenic genes (176). Moreover, the activation of IRE1 has been associated with promoting myocardial angiogenesis and protecting the heart from reperfusion injury during ischemia/reperfusion (177).

While several research studies point to the idea that elevated IRE1-XBP1 activity and ER protect against MASLD, the precise mechanisms are unknown. Studies have demonstrated that increasing the expression of XBP1 in mice with obesity may protect against MASLD by controlling the transcription of fibroblast growth factor 21 (178) while also decreasing the levels of TAGs and DAGs in the liver (179). In addition, XBP1 exerts direct control on a specific group of genes involved in lipid metabolism, such as farnesyl diphosphate synthase and hydroxysteroid 17-beta dehydrogenase 7 (180). Nevertheless, it is essential to mention that XBP1 does not directly control the expression of specific crucial genes involved in lipid synthesis, such as *Dgat2*. In the setting of obesity and MASLD, there is typically an association between dysregulated lipid metabolism and abnormalities in the secretion of VLDL. Moreover, the NF-κB and inflammasome pathways are essential for regulating lipid metabolism. A study was conducted on male Sprague-Dawley rats who were fed with HFD. The rats were treated with a flavonoid polyphenol, quercetin, which resulted in higher expression of XBP1 and greater levels of VLDL (181). This indicates a possible mechanism by which XBP1 could improve the condition of MASLD. Although quercetin has demonstrated favourable outcomes in laboratory experiments conducted on cells and animals with MASLD, its practical use in MASLD treatment is restricted due to the absence of clinical trials and difficulties in its administration, such as low solubility, limited absorption into the body, and instability. Thus, the appropriateness of using it as a treatment choice for individuals with MASFLD is still unclear.

Pimozide, a diphenylbutylpiperidine class medication, was initially developed by Janssen Pharmaceutical Company in 1963 as a first-generation antipsychotic. It is primarily used to manage Tourett's Disorder, a neurological disorder characterized by recurrent twitches and erratic

movements referred to as ‘tics’. Recent research from our laboratory has unveiled pimozide’s potential as an antihyperglycemic agent, demonstrating its ability to improve blood glucose levels and insulin sensitivity in obese mice (128). These actions were attributed to pimozide binding ability to SCOT enzyme in the D-oxyanion pocket. Our new study reveals that pimozide can also increase IRE1 (**Chapter 3, data not published**), and pimozide was able to decrease steatosis in HepaRG without affecting the critical lipogenesis markers (e.g., *ACC1*, *ACC2*, *SREBF1*, *FAS*). These findings underscore the multifaceted therapeutic potential of pimozide in metabolic disorders.

1.4 Statement of Hypotheses and Aims

MASLD/hepatic steatosis is a significant risk factor for the development of steatohepatitis and liver cirrhosis. In addition, it is a major contributor to obesity-related insulin resistance and T2D. Thus, it is imperative that we discover new agents that can treat this devastating condition. Recent studies have suggested activating PDH, the rate-limiting enzyme of glucose oxidation, maybe a novel approach to reverse obesity-induced MASLD. We recently demonstrated that treatment with the antianginal therapy, ranolazine, reverses MASLD in an experimental mouse model of high-fat diet-induced obesity (DIO). Moreover, previous studies have demonstrated that ranolazine directly increases glucose oxidation in the muscle and heart, and we have previously confirmed that ranolazine also increases PDH activity in the liver (138, 182). We, therefore, aim to investigate the impact of ranolazine on MASLD associated with T2D, aiming to extend the favourable actions observed in obesity-related MASLD. Our second aim is to elucidate the role of hepatic PDH

activity in mediating ranolazine's effects on MASLD, utilizing a newly developed hepatocyte-specific PDH knockout mouse model.

Our focus is on discovering novel therapeutic approaches, explicitly emphasising computational models. Previously, we showed that pimozide binds to SCOT (128). This discovery led us to conduct a recent investigation, which demonstrated that pimozide also has a strong affinity for IRE1. These interactions indicate possible ways in which pimozide could be used for therapeutic purposes. MASLD is frequently linked to obesity, is a worldwide health issue and is a significant contributor to the risk of developing T2D. Pimozide, a psychotropic drug, demonstrates potential in controlling glucose levels. Our research suggests that pimozide's interaction with SCOT in skeletal muscle decreases glucose levels. Additional investigation reveals that pimozide has an affinity for IRE1, which plays a critical role in ER stress. We hypothesize that pimozide could be a viable treatment for MASLD/T2D through its interactions with IRE1.

The objectives of each study, which focused on distinct aspects of the overarching hypotheses, are outlined below according to chapter:

Chapter 2: We hypothesized that ranolazine, an anti-anginal medication, may exert favourable effects on MASLD associated with T2D. Our objectives are to

1. Determine whether ranolazine, a second-line anti-anginal therapy, has similar effects on MASLD associated with T2D as it does on obesity-induced MASLD.

2. Investigate the impact of ranolazine treatment on glycemia in a mouse model of experimental T2D.

3. Compare the outcomes of ranolazine treatment between individuals with obesity and those who are obese with T2D in terms of its salutary actions against MASLD.

Chapter 3: We hypothesized that ranolazine improves MASLD associated with obesity through increasing pyruvate dehydrogenase (PDH) in the liver, the key enzyme in glucose metabolism to produce energy. Our objectives are to

1. Investigate whether the ability of ranolazine to mitigate obesity-induced MASLD and hyperglycemia requires increases in hepatic PDH activity, the rate-limiting enzyme of glucose oxidation.

2. Generate liver-specific PDH-deficient ($Pdha1^{Liver-/-}$) mice and use it as a model for studying the role of hepatic PDH in MASLD and hyperglycemia associated with obesity.

3. Assess the phenotypic differences between $Pdha1^{Liver-/-}$ mice and their (Alb^{Cre}) littermates, including adiposity and glucose tolerance.

4. Evaluate the impact of ranolazine treatment on glucose tolerance and hepatic triacylglycerol content in obese $Pdha1^{Liver-/-}$ and Alb^{Cre} mice.

Chapter 4: We hypothesized that pimozide, an antipsychotic agent, may alleviate fatty liver by activating the IRE1/XBP1 Pathway (ongoing work). Our objectives are to

1. Validate the interaction between pimozide and XBP1 through in vitro and in vivo experiments.
2. Investigate the potential of pimozide, an antipsychotic drug, as a therapy for MASLD associated with T2D.
3. Explore the mechanisms underlying the effects of pimozide on glucose metabolism, including its interaction with XBP1.
4. Evaluate the potential of pimozide as a treatment for T2D-associated other metabolic disorders.

Chapter 2: The Anti-Anginal Ranolazine Does Not Confer Beneficial Actions Against Hepatic Steatosis in Male Mice Subjected to High-Fat Diet and Streptozotocin-Induced Type 2 Diabetes

Christina T. Saed[1,2,3], Amanda A. Greenwell[1,2,3], Seyed Amirhossein Tabatabaei Dakhili[1,2,3], Keshav Gopal[1,2,3], Farah Eaton[1,2,3], and John R. Ussher[1,2,3]

[1]Faculty of Pharmacy and Pharmaceutical Sciences, University of Alberta, Edmonton, AB Canada

[2]Alberta Diabetes Institute, University of Alberta, Edmonton, AB Canada

[3]Cardiovascular Research Centre, University of Alberta, Edmonton, AB Canada

PUBLISHED: Christina T. Saed, Amanda A. Greenwell, Seyed Amirhossein Tabatabaei Dakhili, Keshav Gopal, Farah Eaton, and John R. Ussher. The anti-anginal ranolazine does not confer beneficial actions against hepatic steatosis in male mice subjected to high-fat diet and streptozotocin-induced type 2 diabetes. *Can J Physiol Pharmacol*. 2022 May;100(5):393-401.

2.1 Abstract

Non-alcoholic fatty liver disease (NAFLD) is characterized by the accumulation of excess fat in the liver in the absence of alcohol and increases one's risk for both diabetes and cardiovascular disease (e.g., angina). We have shown that the second-line anti-anginal therapy, ranolazine, mitigates obesity-induced NAFLD, and our aim was to determine whether these actions of ranolazine also extend to NAFLD associated with type 2 diabetes (T2D). Eight-week-old male C57BL/6J mice were fed either a low-fat diet or a high-fat diet for 15 weeks, with a single dose of streptozotocin (STZ; 75 mg/kg) administered in the high-fat diet-fed mice at 4 weeks to induce experimental T2D. Mice were treated with either vehicle control or ranolazine during the final 7 weeks (50 mg/kg once daily). We assessed glycemia via monitoring glucose tolerance, insulin tolerance, and pyruvate tolerance, whereas hepatic steatosis was assessed via quantifying triacylglycerol content. We observed that ranolazine did not improve glycemia in mice with experimental T2D, while also having no impact on hepatic triacylglycerol content. Therefore, the salutary actions of ranolazine against NAFLD may be limited to obese individuals but not those who are obese with T2D.

2.2 Introduction

Non-alcoholic fatty liver disease (NAFLD) is a condition characterized by excess fat accumulation (>5% in hepatocytes) in the absence of excessive alcohol consumption or other conditions known to promote hepatic steatosis (e.g., hepatitis C infection) (2, 183). Although simple steatosis in the

liver is often benign, if left unchecked in the long-term, NAFLD can transition to much more serious non-alcoholic steatohepatitis or hepatocellular carcinoma, while severe cases result in the requirement of liver transplantation (184). Furthermore, insulin resistance is frequently associated with NAFLD, regardless of whether the individual is lean or obese, and both are major risk factors for the future development of type 2 diabetes (T2D). Of clinical relevance, obesity, NAFLD, and T2D all increase the risk for cardiovascular diseases, including hypertension, atherosclerosis, and angina (1). Thus, many patients with cardiovascular diseases such as angina are also comorbid for these other metabolic diseases, and it is imperative that we identify therapies that can simultaneously alleviate their multiple pathologies.

One such therapeutic agent that may be of particular interest regarding this question is the piperazine derivative ranolazine, which inhibits the late inward sodium current (I_{Na}) during cardiac repolarization and is a second-line therapy used in the management of angina (135, 185). Preclinical and clinical studies have demonstrated that ranolazine elicits glucose lowering properties (186-188), which may stem from direct actions to inhibit the I_{Na} in islet α-cells (186). On the contrary, previous studies have also demonstrated that ranolazine at clinically relevant concentrations stimulates glucose oxidation rates in the isolated working rat heart and isolated rat epitrochlear is muscle (136, 137). In addition, studies in mice subjected to high-fat diet (HFD) – induced obesity demonstrate that the hepatic activity of pyruvate dehydrogenase (PDH), the rate-limiting enzyme in glucose oxidation, is impaired and contributes to the pathology of obesity-induced NAFLD (133, 134). Intriguingly, treatment of male mice subjected to HFD-induced obesity with ranolazine reverses hepatic steatosis (decreased triacylglycerols (TAGs) content) and

improves glycemia, observations that were associated with a marked increase in hepatic PDH activity (138).

Taken together, ranolazine appears to have multiple beneficial actions in obesity that stem from both its ability to inhibit the I Na and to increase glucose oxidation, which may suggest it to be an ideal anti-anginal therapy to prescribe in individuals who have angina and are also obese with NAFLD. Nonetheless, whether ranolazine also has salutary actions against hepatic steatosis and subsequent progression of NAFLD associated with T2D remains unexplored. Herein, we investigated whether ranolazine treatment has similar favourable actions in NAFLD associated with T2D, given the potential role of PDH as a target for ranolazine's action.

2.3 Methods

2.3.1 Animal Care and Experimentation

All animal procedures were approved by the University of Alberta Health Sciences Animal Welfare Committee, Alberta, Canada, and performed according to the regulations and guidelines of the Canadian Council on Animal Care. Animals were housed in a temperature-controlled unit under a 12-h light/dark cycle with free access to drinking water and food. Eight-week-old male C57BL/6J (The Jackson Laboratory) mice were initially allowed a 1-week period to acclimatize to our animal facility upon arrival, following which they were provided either a low-fat diet (LFD; 10% kcal from lard, Research Diets D12450J) or an HFD (60% kcal from lard, Research Diets D12492) for a 15-week period. At 4 weeks into the dietary protocol, all HFD-fed mice received a single administration of streptozotocin (STZ; 75 mg/kg) (S0130-1G, Sigma–Aldrich) dissolved in 0.1 M

sodium citrate (pH 5.0) via intraperitoneal (i.p.) injection to induce experimental T2D (123, 189). All LFD-fed mice received a single administration of vehicle control at 4 weeks into the dietary protocol. At 4 weeks post-STZ administration, mice were randomized to receive once daily treatment with either vehicle control (sterile Milli-Q water) or ranolazine (50 mg/kg) (S1425, Selleck Chemicals) via oral gavage for 7 weeks. Upon study completion all mice were euthanized using i.p. injection of sodium pentobarbital (12 mg) (00141704, Bimeda-MTC) following a 16-h fast and 4-h refed. All mice subsequently had their livers extracted, washed once with phosphate-buffered saline (PBS) and separated into four lobes that were immediately snap-frozen in liquid N_2 using Wollenberger tongs and stored at –80 °C.

2.3.2 Body Composition

Conscious lean and T2D mice were placed in an EchoMRI™ (4in1/700) body composition analyzer to assess lean and fat mass. Body fat is the total mass of fat molecules in the body, measured in terms of the weight of canola oil. Lean mass refers to the total muscular tissue in the body that contains water, omitting fat, bone minerals, and non-contributing components like hair and claws.

2.3.3 Assessment of Glucose Homeostasis

Mice were transferred to clean static cages with all cage enrichments and fasted for either 6, 16, or 24 h with free access to drinking water before undergoing an i.p. glucose tolerance test (2 g/kg for lean mice, 1 g/kg for T2D mice) (DX0145, Sigma–Aldrich), i.p. insulin tolerance test (0.5 U/kg for lean mice, 0.7 U/kg for T2D mice) (02024233, Novo Nordisk Canada), or i.p. pyruvate tolerance test (2 g/kg) (P2256, Sigma–Aldrich), respectively. Samples were collected from tail

whole blood at 0, 15, 30, 60, 90, and 120 min post insulin, glucose, or pyruvate administration, using the Contour Next blood glucose monitoring system (Bayer, NJ, USA).

2.3.4 Assessment of Circulating Insulin Levels

Samples were collected from mouse tail whole-blood (~5 µL) during the glucose tolerance test immediately prior to injecting glucose (0 min) and at 15-min post glucose administration. Plasma insulin was measured using a commercially available enzyme-linked immunosorbent assay kit (ELISA kit, ALPCO Diagnostics). In brief, samples were placed in a 96-well microplate with 75 µL working strength conjugation buffer. Next, the plate was incubated in an orbital microplate shaker for 2 h at room temperature, following which the microplate was washed six times with a provided working strength wash buffer. The reaction was subsequently initiated by adding 100 µL tetramethyl benzidine to each well for 30 min, following which the reaction was terminated by adding 100 µL of stop solution. The optical density of each sample was then determined at 450 nm (Synergy H1 Hybrid Reader; BioTek) and used to calculate the plasma insulin levels (128).

2.3.5 Western Blotting

Powdered frozen mouse liver samples (~20 mg) were homogenized in buffer containing 50 mM Tris HCl (pH 8 at 4 °C), 1 mM ethylenediaminetetraacetic acid (EDTA), 10% glycerol (w/v), 0.02% Brij-35 (w/v), 1 mM dithiothreitol, and protease and phosphatase inhibitors (Sigma–Aldrich). The homogenate was centrifuged at 4 °C for 20 min at maximum speed (21 000g) and the supernatant was collected into new tubes. Following extraction, protein was quantified using a Bradford protein assay kit (Bio-Rad Laboratories). Protein samples (15 µg or 40 µg) were then denatured and subjected to Western blotting via 10% sodium dodecyl sulfate polyacrylamide gel electrophoresis. Proteins traversed the stacking gel for 15 min at 100 V, following which the

voltage was increased to 120 V as the proteins traversed the separating gel for 1 h. Thereafter, the proteins were transferred via electrophoresis to nitrocellulose membranes (1620115; Bio-Rad Laboratories) for 2 h at 100 V. Following transfer, all membranes were blocked with 5% skim milk in tris-buffered saline Tween-20 (TBS-T; P7949, Sigma–Aldrich) for 40 min. The membranes were further incubated overnight with primary antibody at 4 °C. The following day, immunodetection was performed using a secondary anti body (1:2000) in 5% skim milk in TBS-T and incubated for 90 min with shaking at room temperature. The membranes were washed three times with TBS-T for 10 min each. Finally, protein bands were visualized using enhanced chemiluminescence (PI34580; Thermo Fisher Scientific). Membranes were probed with the following antibodies; long-chain acylCoA dehydrogenase (LCAD; ab129711, Abcam), β-hydroxyacyl CoA dehydrogenase (β HAD; ab37673, Abcam), protein kinase B (Akt; 9272 S, Cell Signaling), phospho-Akt (4060 S, Cell Signaling), PDH kinase 4 (PDHK4; ab214938, Abcam), PDH (3205 S, Cell Signaling), phospho-PDH serine 293 (ABS204; Millipore Sigma), phospho-PDH serine 300 (AP1064; Millipore Sigma), phospho-PDH serine 232 (AP1063; Millipore Sigma), fatty acid synthase (FAS; 3180 S, Cell Signaling), diacylglycerol acyltransferase-1 (DGAT1; ab189994, Abcam), and heat shock protein-90 (610418; BD Biosciences). All antibodies were prepared in a 1:1000 dilution in 3% bovine serum albumin with the exception of LCAD (1:2000), βHAD (1:2000), and DGAT1 (1:333).

2.3.6 Real-Time Quantitative PCR Analysis

RNA was extracted from powdered liver samples (~20 mg) using TRIzol (15596018, Thermo Fisher Scientific). In brief, samples were homogenized with 500 µL of TRIzol. Next, 100 µL chloroform was added to each sample, which were kept at 4 °C for 10 min, followed by centrifugation at 14 000g for 10 min at 4 °C. The resulting supernatants were transferred to new

tubes and 250 µL isopropanol was added while being kept at room temperature for 5 min. Last, the samples were centrifuged at 4 °C at 14 000g for 10 min and washed twice with 1 mL 75% ethanol in RNase-free water. The samples were subsequently air dried before adding 30 µL RNase-free water, and RNA was quantified by measuring absorbance at 260 nm using a NanoDrop™ 2000 spectrophotometer (Thermo Fisher Scientific). First-strand cDNA synthesis was carried out using the iScript Reverse Transcription Supermix (Bio-Rad Laboratories), followed by real-time PCR which was carried out with a CFX Connect Real-Time PCR machine (Bio-Rad Laboratories) using SYBR Green (KK4601; Kapa Viosystems). Cyclophilin A (Ppia) was used as an internal house-keeping gene to quantify relative mRNA transcript levels of various genes (**Table 2.1)** using the $2^{-\Delta\Delta Ct}$ method to determine relative gene expression levels. The 2-ΔΔCt approach assesses gene expression changes by comparing target gene cycle threshold (CT) values to an internal reference gene, allowing for consistent quantification across experimental circumstances. This method calculates ΔCt values for each sample by subtracting internal control CT values from target gene CT values and then comparing them to a reference sample to determine ΔΔCt values. Finally, the formula 2^-(ΔΔCt) is used to calculate fold change in gene expression, enabling relative expression quantification (190).

2.3.7 Assessment of TAG Content

TAGs were extracted from powdered frozen liver (~20 mg) samples via homogenization with a 2:1 chloroform:methanol solution. In brief, after sample homogenization, 0.2 volumes of methanol were added to each sample and samples were kept on ice for 10 min, following which they were centrifuged at 3500g for 10 min. To allow the mixture to separate into two phases, 0.2 volumes of 0.04% (w/v) CaCl2 was added, followed by centrifugation at 2400g for 20 min. The supernatant was discarded, and the remaining TAG extract was washed twice with 150 µL of pure solvent

upper phase. Finally, 50 μL methanol was added to produce a singular phase. The samples were subsequently dried under N_2 gas at 60 °C, and the remaining TAG containing pellets were dissolved in 50 μL of 3:2 tert-butyl alcohol X-100 methyl alcohol (1:1). The samples were stored overnight at 4 °C, and the following day all samples were quantified for TAG content using a commercially available enzymatic colorimetric assay kit (Wako Pure Chemical Industries) (128).

2.3.8 Assessment of Circulating Alanine Aminotransferase (ALT) and Aspartate Aminotransferase (AST) Levels

Blood samples were collected from mice during euthanasia into 1.7 mL Eppendorf tubes coated with 0.5 M EDTA. The blood samples were centrifuged at 4 °C at 2000g for 10 min. The resulting supernatants were transferred to new Eppendorf tubes and stored at –80 °C until use. Circulating ALT and AST levels were subsequently measured in these blood samples via use of commercial kits (REF 10205-4 and REF 10206-4) purchased from Cypress Diagnostics Inc. (Campbellville, ON, Canada) and ran on the EasyRA Analyzer (Bedford, MA, USA) (128).

2.3.9 Statistical Analysis

All values are presented as means 6 standard error of the mean. The significance of differences was assessed using either a two-tailed, unpaired Student's t test, or a two-way ANOVA followed by a Bonferroni post hoc analysis. Differences were considered significant when $P < 0.05$. All data analysis was performed using GraphPad Prism version 9.0 software.

Table 2.1 *Primer Sequences*.

Gene	Forward Primer	Reverse Primer
Ppia	GCTGGACCAAACACAAACG	ATGCCTTCTTTCACCTTCCC
Fasn	GGTTACACTGTGCTAGGTGTTG	TCCAGGCGCATGAGGCTCAGC
Acaca	TAATGGGCTTCTGTGACTC	CTCAATATCGCCATCAGTCTTG
Srebf1	GGAGCCATGGATTGCACATT	GGCCCGGGAAGTCACTGT
G6pd	ACACCGACTACTACAGCAACAG	CCTCGAAAGATAGCAAGAGTAG
Chrebp	GAGTGCTTGAGCCTGGCTTACA	GCTCTCCAGATGGCGTTGTTCA

2.4 Results

2.4.1 Ranolazine Treatment Does Not Decrease Fat Mass or Improve Glycemia in Male Mice Subjected to Experimental T2D

To determine whether our findings that treatment with ranolazine can mitigate hepatic steatosis and improve glycemia in obese mice (138) are translatable to experimental T2D, we first induced T2D in mice via combination of HFD supplementation for 15 weeks, with a single dose of STZ (75 mg/kg) administered at the 4-week time point. We also performed similar experiments in lean mice fed an LFD for an equivalent time frame. Mice were subsequently randomized to vehicle control or ranolazine (50 mg/kg) treatment at 4-weeks post STZ (or at 8-weeks post LFD supplementation) for 7 weeks. Ranolazine treatment had no impact on body weight or fat mass in lean mice, and in contrast to our observations in obese mice, ranolazine treatment did not decrease body weight or fat mass in mice with experimental T2D **(Table 2.2)**. Moreover, ranolazine treatment did not affect lean mass or random fed blood glucose levels in both lean mice and mice with experimental T2D **(Table 2.2)**.

Table 2.2 *Impact of Ranolazine Treatment of Body Weight and Body Composition*

	Lean VC		Lean Ranolazine		T2D VC		T2D Ranolazine	
	Pre-Tx	Post-Tx	Pre-Tx	Post-Tx	Pre-Tx	Post-Tx	Pre-Tx	Post-Tx
Body weight (g)	30.3 ± 0.7	30.1 ± 1.0	30.5 ± 0.6	29.2 ± 0.6	38.7 ± 1.2*	37.8 ± 1.6*	38.8 ± 1.6*	37.7 ± 1.0*
Fat mass (g)	3.8 ± 0.3	4.1 ± 0.6	4.4 ± 0.6	3.6 ± 0.3	12.6 ± 0.9*	12.3 ± 1.0*	12.5 ± 1.7*	11.8 ± 1.2*
Fat mass (%)	12.6 ± 0.9	13.0 ± 1.4	14.6 ± 2.1	11.9 ± 1.3	32.5 ± 1.4*	33.8 ±1.7*	31.9 ± 3.1*	33.1 ± 2.1*
Lean mass (g)	24.3 ± 0.5	24.2 ± 0.5	23.7 ± 1.0	24.3 ± 0.7	23.6 ± 0.5	23.1 ± 0.6	24.1 ± 0.4	23.3 ± 0.4
Lean mass (%)	79.9 ± 0.7	78.8 ± 1.4	78.1 ± 2.3	80.6 ± 1.3	61.3 ± 1.4*	60.8 ± 1.6*	63.1 ± 3.3*	62.0 ± 2.4*
Glucose (mM)	9.2 ± 0.6	8.3 ± 0.5	9.6 ± 2.3	7.8 ± 0.4	11.0 ± 0.7	10.2 ± 0.3*	11.4 ± 0.9	10.0 ± 0.5*

Note: Body weight, fat mass, lean mass, and ad libitum blood glucose levels were measured at baseline and following 7 weeks of treatment (Tx) with ranolazine or vehicle control (VC) (n = 5–7 mice). Values represent mean ± standard error of the mean. Differences were determined using a two-way ANOVA followed by a Bonferroni post hoc analysis and considered significant if $P < 0.05$. *Significantly different from lean counterpart. T2D, type 2 diabetes.

As we expected, in lean mice ranolazine treatment also had no effect on i.p. glucose tolerance, i.p. insulin tolerance, and hepatic insulin signaling as determined by Akt phosphorylation at serine 473, a major regulatory node of insulin signaling **(Figure 2.1)**.

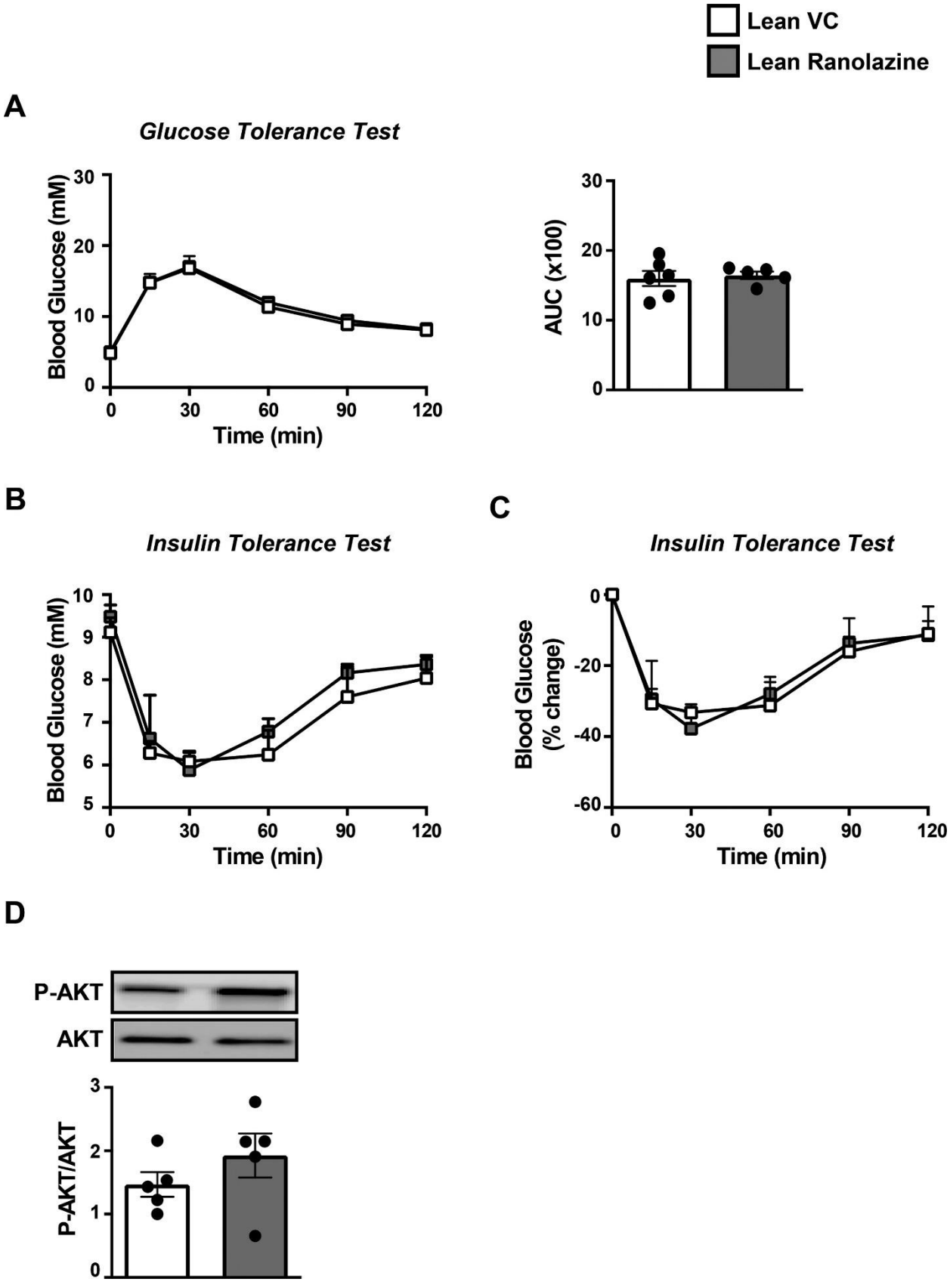
Lean VC
Lean Ranolazine
A
Glucose Tolerance Test
Blood Glucose (mM)
Time (min)
AUC (x100)
B
Insulin Tolerance Test
Blood Glucose (mM)
Time (min)
C
Insulin Tolerance Test
Blood Glucose (% change)
Time (min)
D
P-AKT
AKT
P-AKT/AKT

Figure 2.1 *Ranolazine Treatment Does Not Affect Glucose Homeostasis in Lean Male Mice*. **(A)** Glucose tolerance test and associated area under the curve (AUC), **(B and C)** insulin tolerance test, and **(D)** liver protein kinase B (Akt) phosphorylation (P-Akt) at serine 473 in lean mice treated with either vehicle (VC) or ranolazine (n = 5–6 mice). Values represent means ± standard error of the mean. Differences were determined using an unpaired two-tailed Student's t test, or a two-way ANOVA followed by a Bonferroni post-hoc analysis.

Following 2 weeks of treatment with ranolazine, we observed no improvement in i.p. glucose tolerance in ranolazine treated mice with experimental T2D, nor did we observe changes in circulating insulin levels at the 0- and 15-min time points of the glucose tolerance test **(Figure 2.2, A and B)**. After 4 weeks of treatment with ranolazine, we next performed an i.p. insulin tolerance test, whereby ranolazine treatment once again had no impact on insulin sensitivity in mice with experimental T2D **(Figure 2.2, C and D)**. Further supporting the premise that ranolazine did not improve insulin sensitivity, Akt phosphorylation at serine 473 was also similar in livers of mice with experimental T2D **(Figure 2.2E)**.

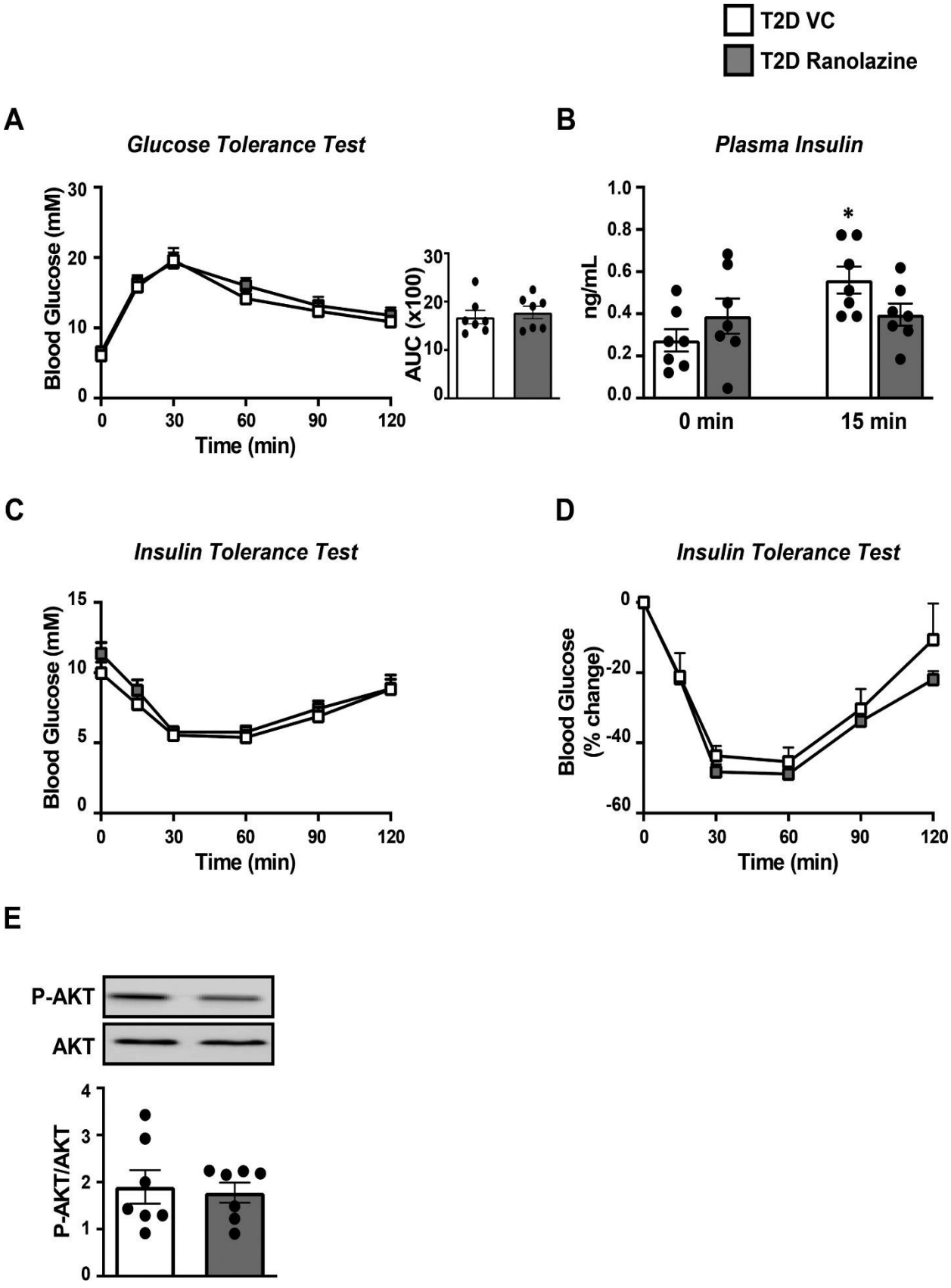
T2D VC
T2D Ranolazine
A
Glucose Tolerance Test
Blood Glucose (mM)
Time (min)
AUC (x100)
B
Plasma Insulin
ng/mL
0 min
15 min
*
C
Insulin Tolerance Test
Blood Glucose (mM)
Time (min)
D
Insulin Tolerance Test
Blood Glucose (% change)
Time (min)
E
P-AKT
AKT
P-AKT/AKT

Figure 2.2 *Ranolazine Treatment Does Not Affect Glucose Homeostasis in Male Mice Subjected to Experimental T2D*. **(A)** Glucose tolerance test and associated area under the curve (AUC), **(B)** plasma insulin levels during the glucose tolerance test, **(C and D)** insulin tolerance test, and **(E)** liver protein kinase B (Akt) phosphorylation (P-Akt) at serine 473 in mice subjected to experimental T2D treated with either vehicle control (VC) or ranolazine (n = 7 mice). Values represent means ± standard error of the mean. Differences were determined using an unpaired two-tailed Student's t test, or a two-way ANOVA followed by a Bonferroni post hoc analysis. *P < 0.05, significantly different from 0-min counterpart.

As an indirect measure of hepatic glucose production, we also assessed i.p. pyruvate tolerance at 5-weeks post treatment, which once again remained similar in ranolazine treated mice with experimental T2D **(Figure 2.3)**.

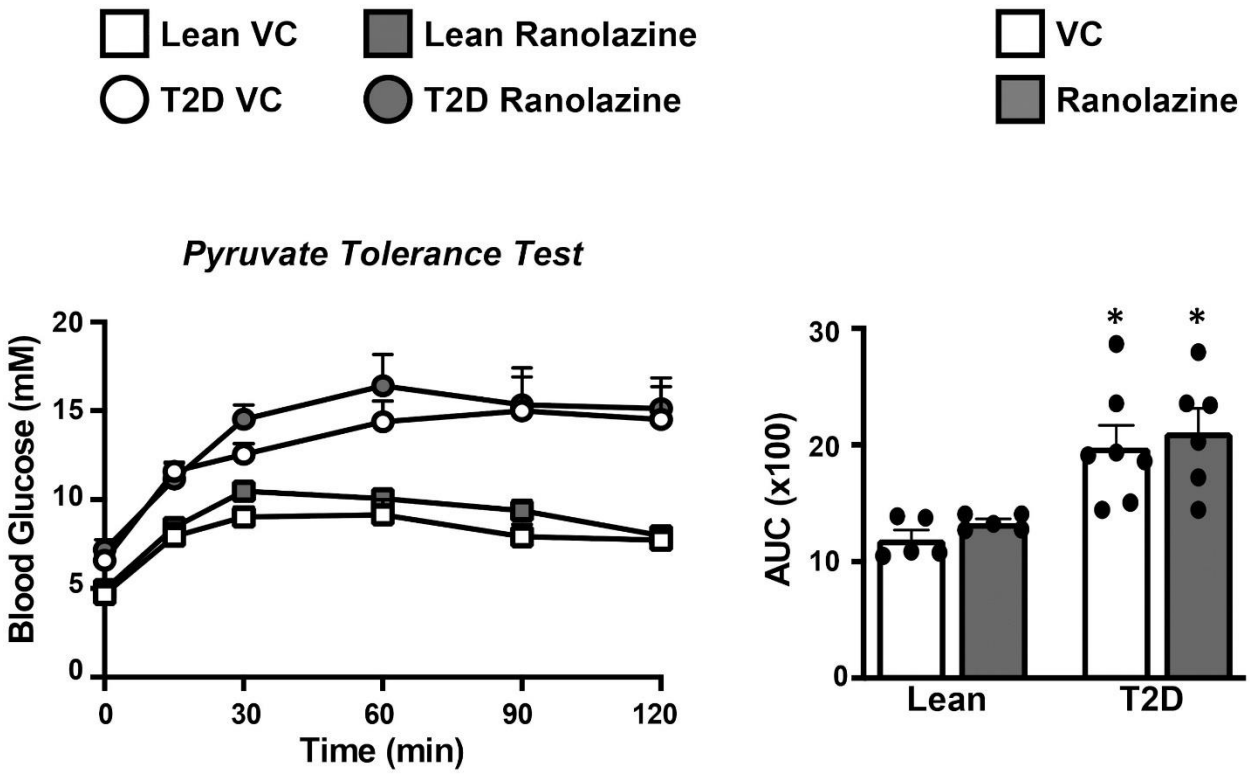

Figure 2.3 *Ranolazine Treatment Does Not Lower Hepatic Glucose Production in Male Mice Subjected to Experimental T2D*. Pyruvate tolerance test and associated area under the curve (AUC) in lean mice and mice subjected to experimental T2D treated with either vehicle control (VC) or ranolazine (n = 5–7 mice). Values represent means ± standard error of the mean. Differences were determined using a two-way ANOVA followed by a Bonferroni post hoc analysis. **P* < 0.05, significantly different from lean counterpart.

2.4.2 Ranolazine Treatment Does Not Mitigate Hepatic Steatosis in Male Mice Subjected to Experimental T2D

As our previous findings demonstrated that the ranolazine mediated improvement in glycemia was dependent on reductions in hepatic steatosis in obese mice, we next measured hepatic TAG content. Consistent with the lack of improvement in glycemia, mice with experimental T2D treated with ranolazine did not exhibit a reduction in hepatic TAG content **(Figure 2.4A)**. As a further index of liver dysfunction in mice with experimental T2D, we measured circulating levels of ALT and AST, which were also unaffected by ranolazine treatment **(Figure 2.4, B and C)**.

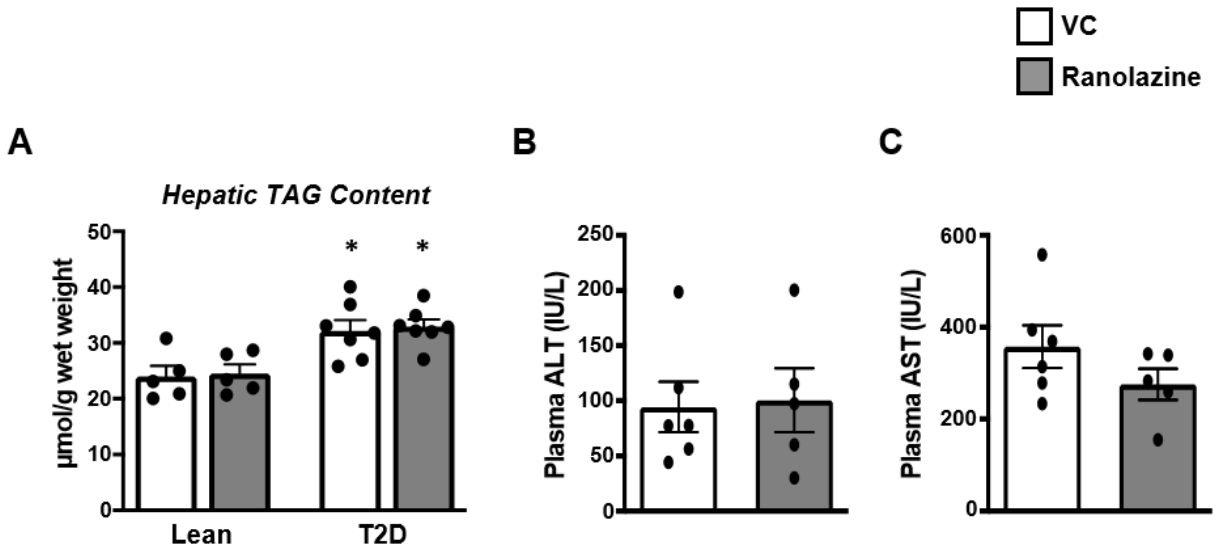

Figure 2.4 *Ranolazine Treatment Does Not Reduce Hepatic Steatosis in Male Mice Subjected to Experimental T2D*. **(A)** Liver triacylglycerol (TAG) content in lean mice and mice subjected to experimental T2D treated with either vehicle control (VC) or ranolazine (n = 5–7 mice). Circulating **(B)** alanine aminotransferase (ALT) and **(C)** aspartate aminotransferase (AST) levels in mice subjected to experimental T2D treated with either VC or ranolazine (n = 5–6 mice). Values represent means ± standard error of the mean. Differences were determined using an unpaired two-tailed Student's t test, or a two-way ANOVA followed by a Bonferroni post hoc analysis. *$P <$ 0.05, significantly different from lean counterpart.

Treatment with ranolazine also did not influence gene expression of key regulators of lipogenesis in mice with experimental T2D. Hepatic mRNA expression levels of FAS (*Fasn*), acetyl CoA carboxylase 1 (*Acaca*), sterol regulatory element binding protein 1c (*Srebf1*), glucose-6-phosphate dehydrogenase (*G6pd*), and carbohydrate response element binding protein (*Chrebp*) were all unaffected by ranolazine treatment **(Figure 2.5A)**. Furthermore, hepatic protein expression of FAS and DGAT1 also remained similar in ranolazine-treated mice with experimental T2D **(Figure 2.5, B and C)**. Hepatic TAG content is not only controlled by fatty acid uptake but also fatty acid oxidation rates in the mitochondria. Thus, we also assessed protein expression of key regulators of fatty acid oxidation, though ranolazine once more had no effect on both hepatic LCAD and βHAD expression **(Figure 2.5, D and E)**.

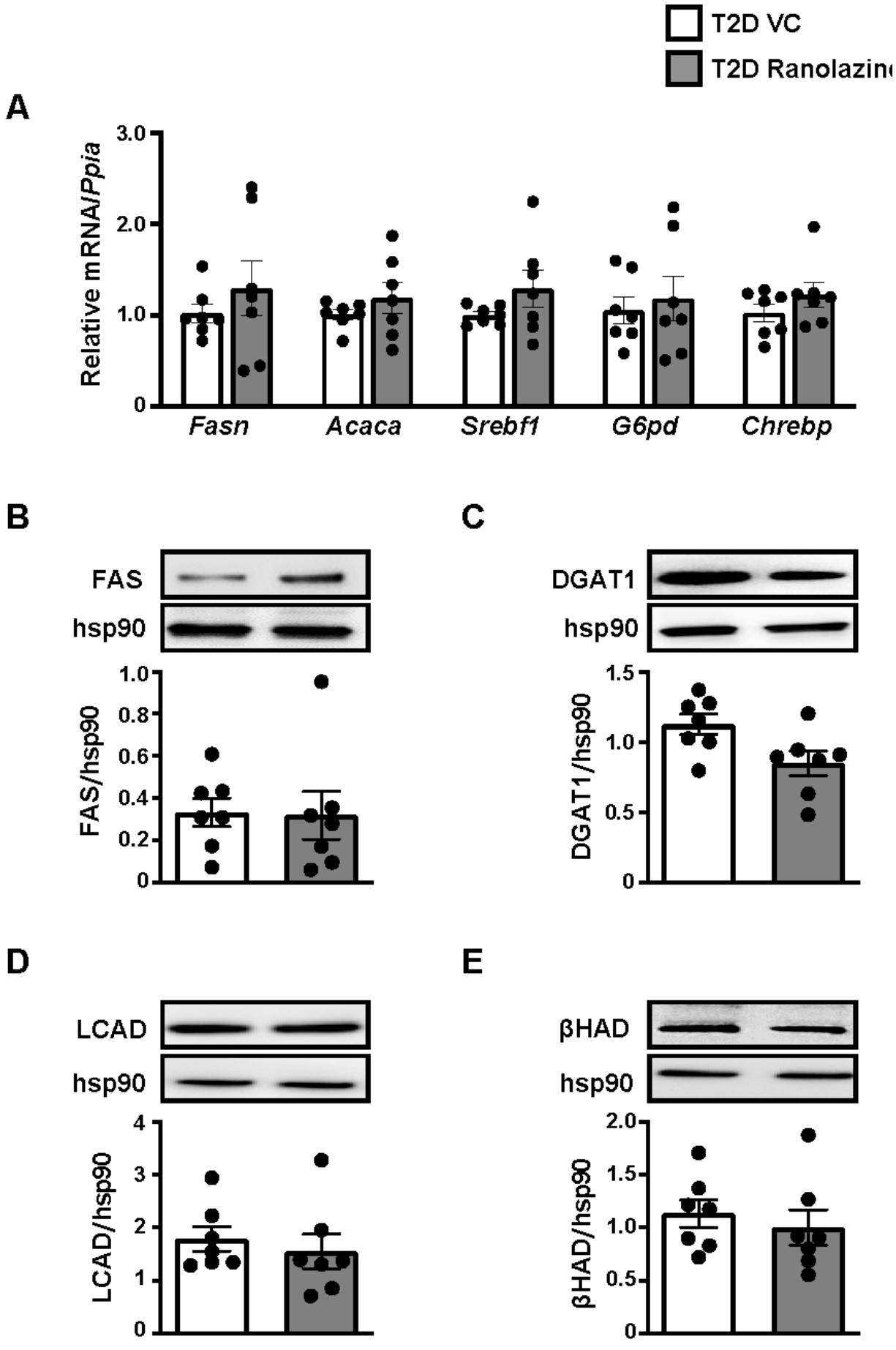
T2D VC
T2D Ranolazine
A
Relative mRNA/Ppia
3.0
2.0
1.0
0
Fasn
Acaca
Srebf1
G6pd
Chrebp
B
FAS
hsp90
FAS/hsp90
1.0
0.8
0.6
0.4
0.2
0
C
DGAT1
hsp90
DGAT1/hsp90
1.5
1.0
0.5
0
D
LCAD
hsp90
LCAD/hsp90
4
3
2
1
0
E
βHAD
hsp90
βHAD/hsp90
2.0
1.5
1.0
0.5
0

Figure 2.5 *Ranolazine Treatment Does Not Influence Expression of Regulators of Lipogenesis and Fatty Acid Oxidation in Male Mice Subjected to T2D*. **(A)** mRNA expression of genes involved in regulating lipogenesis (*Fasn*, *Acaca*, *Srebf1*, *G6pd*, and *Chrebp*), **(B–D)** protein expression of key regulators of lipogenesis including (B) fatty acid synthase (FAS) and **(C)** diacylglycerol acyltransferase-1 (DGAT1), as well as key regulators of fatty acid b-oxidation enzymes including **(D)** long-chain acylCoA dehydrogenase (LCAD), and **(E)**,) in livers from male mice subjected to experimental T2D treated with either vehicle control (VC) or ranolazine (n = 7 mice). Values represent means ± standard error of the mean. Differences were determined using an unpaired two-tailed Student's t test.

2.4.3 Ranolazine Treatment Does Not Improve Hepatic PDH Status in Male Mice Subjected to Experimental T2D

Previous studies have alluded to the importance of PDH activity in regulating hepatic steatosis, whereby augmenting hepatic PDH activity has been demonstrated to alleviate the progression of obesity-induced NAFLD (117, 134, 138). Of interest, we demonstrated that ranolazine's actions to decrease hepatic TAG content in obese mice were associated with increased hepatic PDH activity, consistent with past studies demonstrating that ranolazine increases glucose oxidation rates in both the isolated heart and skeletal muscle (136, 137). Ranolazine treatment of mice with experimental T2D, however, did not decrease hepatic PDH phosphorylation (indicative of increased PDH activity) at its three major regulatory sites, nor did it decrease protein expression of PDHK4, one of the primary kinases inhibiting PDH activity **(Figure 2.6)**.

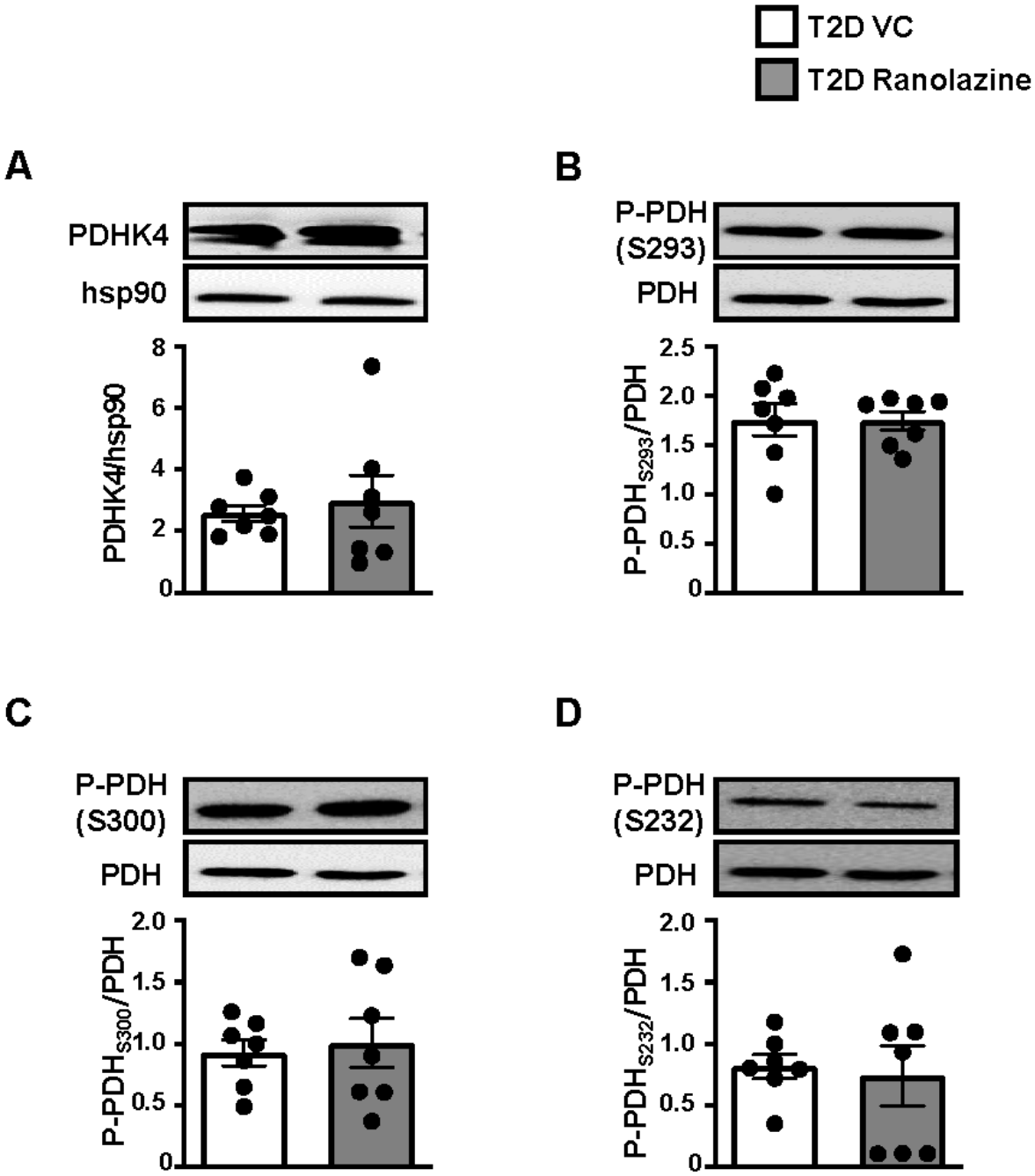
T2D VC
T2D Ranolazine
A
PDHK4
hsp90
PDHK4/hsp90
0
2
4
6
8
B
P-PDH
(S293)
PDH
P-PDHS293/PDH
0
0.5
1.0
1.5
2.0
2.5
C
P-PDH
(S300)
PDH
P-PDHS300/PDH
0
0.5
1.0
1.5
2.0
D
P-PDH
(S232)
PDH
P-PDHS232/PDH
0
0.5
1.0
1.5
2.0

Figure 2.6 *Ranolazine Treatment Does Not Improve Hepatic Pyruvate Dehydrogenase (PDH) Activity in Male Mice Subjected to Experimental T2D*. **(A)** PDH kinase 4 (PDHK4) expression, **(B)** PDH phosphorylation at serine 293, **(C)** serine 300, and **(D)** serine 232 in livers from male mice subjected to T2D treated with either vehicle control (VC) or ranolazine (n = 7). Values represent means ± standard error of the mean. Differences were determined using an unpaired two-tailed Student's t test.

2.5 Discussion

Ranolazine is a second-line anti-anginal agent that inhibits the I_{Na} (135, 185), though we previously reported that its ability to increase glucose oxidation may account for its secondary actions to alleviate hepatic steatosis and hyperglycemia in obese mice (138), suggesting it may also have clinical utility for NAFLD. Unfortunately, those observations do not appear to translate to NAFLD associated with T2D, as ranolazine treatment failed to improve glycemia and decrease hepatic TAG content in mice with experimental T2D.

These unexpected findings were surprising, as the only difference between our experimental model of T2D versus our previous findings in obese mice involves the use of low-dose STZ at the 4-week time point of the 15-weeks HFD supplementation protocol, which eliminates vulnerable β-cells. STZ, however, does have limitations that involve hepatic genotoxicity (191), and it can also directly induce myopathy (192). It has also been reported that STZ can induce cytotoxic actions in HepG2 human hepatoma cells secondary to oxidative stress and mitochondrial dysfunction (193). As PDH is susceptible to oxidative stress–mediated inhibition by glutathionylation (124, 194), it is possible that these actions of STZ may have prevented ranolazine from stimulating hepatic PDH activity as we have previously observed in obese mice. Thus, despite the combination HFD/STZ model accurately mimicking various important aspects of the T2D pathology such as its slow pathogenesis from glucose intolerance to insulin resistance and partial β-cell death (195), it may be worthwhile to repeat our studies in other models of T2D such as *db*/*db* mice.

In contrast, it may also be possible that stimulating hepatic PDH activity in the context of T2D is more challenging than in the insulin-resistant or prediabetic state. Indeed, PDH activity is a key component of substrate selection in metabolic flexibility, and there is growing recognition that metabolic inflexibility is a key feature of the pathology of T2D (196, 197). Thus, it remains possible that at least in the liver, the ability to restore metabolic flexibility is lost during the transition from insulin resistance and (or) prediabetes to a true T2D phenotype. As ranolazine failed to decrease PDH phosphorylation in livers from mice with experimental T2D, it would be of interest to determine whether direct inhibition of PDHK can mitigate T2D-related hepatic steatosis. Previous studies have demonstrated that treatment with the pan-PDHK inhibitor, dichloroacetate, and genetic deletion of PDHK2 both protect against obesity-induced NAFLD, but whether this remains true in the setting of overt T2D remains to be determined.

Because ranolazine did not improve hepatic PDH activity in mice with experimental T2D, in retrospect it is not surprising that we observed no improvements in both hepatic steatosis and glucose homeostasis. Our previous work in obese mice demonstrated that ranolazine treatment increased hepatic PDH activity, though these actions required ~1 week before it translated into a reduction in hepatic TAG content, and no improvement in glucose or pyruvate tolerance was observed until hepatic TAG levels decreased. Therefore, our findings do not negate PDH being a valid target to treat NAFLD, but rather suggest that caution be exercised in those that stand to benefit the most from this form of metabolic therapy. Based on current preclinical evidence it does appear that only obese nondiabetics would benefit from ranolazine's salutary actions against hepatic steatosis and subsequent improvements in glycemia. Importantly, recent studies in humans with coronary artery disease and NAFLD demonstrate that ranolazine treatment for 6 months

alleviates liver dysfunction as determined by decreased serum ALT and AST levels (198), suggesting that our preclinical observations may translate to the clinic. However, changes in glycemia and hepatic lipid accumulation (e.g., TAG content) were not assessed in this clinical study.

A limitation of our study is that our only assessment of hepatic steatosis involved measuring tissue TAG content following a chloroform:methanol extraction based on the Bligh and Dyer method (199). It will be important in future studies to reaffirm our findings using histological methods (e.g., Oil Red O) and more sophisticated methods (e.g., mass spectrometry) to quantify TAG content, the latter of which would also allow us to measure numerous other lipid metabolites implicated in mediating hepatic dysfunction (e.g., diacylglycerol, ceramide) (200).

Taken together, despite the promising findings demonstrating that the anti-anginal therapy ranolazine has novel actions to counteract NAFLD associated with obesity, the same promise does not appear to hold true for NAFLD associated with T2D. While ranolazine has been reported to improve glycemia in humans with T2D (187), other studies have reported no such benefit (201). , and it would be of interest to determine whether hepatic steatosis was improved in subjects from either of these studies. Because ranolazine failed to stimulate hepatic PDH activity in mice with experimental T2D, however, it may suggest that other strategies to promote PDH activity and glucose oxidation in the liver may be more desirable than ranolazine. Moreover, further research is required to understand the regulation of PDH activity in the liver during the progression of obesity towards an overt T2D state.

Acknowledgements & Grants

This study was supported by an Operating Grant from the Canadian Liver Foundation to JRU, and JRU is a Tier 2 Canada Research Chair (Pharmacotherapy of Energy Metabolism in Obesity).

Conflict of interest statement

The authors have no conflicts to declare.

Chapter 3: The Antianginal Ranolazine Fails to Improve Glycaemia in Obese Liver-Specific Pyruvate Dehydrogenase Deficient Male Mice

Christina T. Saed[1,2,3], Seyed Amirhossein Tabatabaei Dakhili[1,2,3], Amanda A. Greenwell[1,2,3], Jordan S.F. Chan[1,2,3], Kunyan Yang[1,2,3], Keshav Gopal[1,2,3], Farah Eaton[1,2,3], Rami Al Batran[4], and John R. Ussher[1,2,3]

[1]Faculty of Pharmacy and Pharmaceutical Sciences, University of Alberta, Edmonton, AB, Canada

[2]Alberta Diabetes Institute, University of Alberta, Edmonton, AB Canada

[3]Cardiovascular Research Institute, University of Alberta, Edmonton, AB Canada

[4]Faculty of Pharmacy, Université de Montréal, Montreal, Quebec, Canada

PUBLISHED: Christina T. Saed, Seyed Amirhossein Tabatabaei Dakhili, Amanda A. Greenwell, Jordan S.F. Chan, Kunyan Yang, Keshav Gopal, Farah Eaton, Rami Al Batran, and John R. Ussher. The antianginal ranolazine fails to improve glycaemia in obese liver-specific pyruvate dehydrogenase deficient male mice. *Basic Clin Pharmacol Toxicol*. 2023 Aug;133(2):194-201.

3.1 Abstract

Recent studies have demonstrated that stimulating pyruvate dehydrogenase (PDH, gene *Pdha1*), the rate-limiting enzyme of glucose oxidation, can reverse obesity-induced non-alcoholic fatty liver disease (NAFLD), which can be achieved via treatment with the antianginal ranolazine. Accordingly, our aim was to determine whether ranolazine's ability to mitigate obesity-induced NAFLD and hyperglycaemia requires increases in hepatic PDH activity. We generated liver-specific PDH-deficient ($Pdha1^{Liver-/-}$) mice, which were provided a high-fat diet for 12 weeks to induce obesity. $Pdha1^{Liver-/-}$ mice and their albumin-Cre (Alb^{Cre}) littermates were randomized to treatment with either vehicle control or ranolazine (50 mg/kg) once daily via oral gavage during the final 5 weeks, following which we assessed glucose and pyruvate tolerance. $Pdha1^{Liver-/-}$ mice exhibited no overt phenotypic differences (e.g. adiposity, glucose tolerance) when compared to their Alb^{Cre} littermates. Of interest, ranolazine treatment improved glucose tolerance and mildly reduced hepatic triacylglycerol content in obese Alb^{Cre} mice but not in obese $Pdha1^{Liver-/-}$ mice. The latter was independent of changes in hepatic mRNA expression of genes involved in regulating lipogenesis. Liver-specific PDH deficiency is insufficient to promote an NAFLD phenotype. Nonetheless, hepatic PDH activity partially contributes to how the antianginal ranolazine improves glucose tolerance and alleviates hepatic steatosis in obesity.

3.2 Introduction

Non-alcoholic fatty liver disease (NAFLD) is a condition in which excess fat/lipid (>5% of liver weight) accumulates in the liver of individuals who are not heavy consumers of alcohol. Although

NAFLD is a reversible condition, if left untreated, it may lead to a more irreversible severe condition referred to as non-alcoholic steatohepatitis (NASH), which is characterised by liver fibrosis and inflammation. Furthermore, NASH can progress to cirrhosis and/or hepatocellular carcinoma (202). NAFLD is also strongly associated with obesity, such that people with both conditions have an increased risk of developing type 2 diabetes (T2D) (203). Unfortunately, there are no therapies approved for the specific treatment of NAFLD/NASH, and it is imperative that we develop new therapies to treat this condition(s) and their associated complications.

Recent studies have demonstrated that genetic deletion of pyruvate dehydrogenase kinase (PDHK), which inhibits pyruvate dehydrogenase (PDH, gene name *Pdha1*), the rate-limiting enzyme of glucose oxidation, can reduce hepatic steatosis and alleviate NAFLD pathology (134). Interestingly, we have demonstrated that ranolazine, a second-line antianginal therapy, alleviated liver steatosis and the associated glucose intolerance in mice with obesity, which was accompanied by an increase in hepatic PDH activity (138). These observations are consistent with previous studies demonstrating that ranolazine stimulates glucose oxidation rates (136, 137). Accordingly, our aim herein was to confirm whether increases in hepatic PDH activity are indeed necessary for the above mentioned salutary actions attributed to ranolazine. In order to address this, we generated liver-specific *Pdha1*-deficient (*Pdha1*$^{\text{Liver}-/-}$) mice using Cre-lox technology and characterised their metabolic phenotype. We next examined whether ranolazine treatment would retain the ability to alleviate hepatic steatosis and glucose intolerance in obese *Pdha1*$^{\text{Liver}-/-}$ mice. We hypothesized that such an outcome would not be observed, reinforcing the importance of PDH activity and glucose oxidation towards the pathology of NAFLD and ranolazine's mechanism of action.

3.3 Methods

3.3.1 Animal Care and Experimentation

All animal procedures were approved by the University of Alberta Health Sciences Animal Welfare Committee and performed according to the regulations and guidelines of the Canadian Council on Animal Care. Animals were housed in a temperature-controlled unit under a12-h light/dark cycle with free access to drinking water and food. To generate *Pdha1*$^{\text{Liver}-/-}$ mice, male albumin-Cre (Alb$^{\text{Cre}}$) (The Jackson Laboratory; Stock no. 003574) were crossed with floxed PDH (gene name *Pdha1*; The Jackson Laboratory; Stock no. 017443). At 6–8 weeks of age, male Alb$^{\text{Cre}}$ and *Pdha1*$^{\text{Liver-/-}}$ mice were placed on either a 10% fat diet (10% LFD; Research Diets D12450J—lean mice), a 45% fat diet (45% HFD; Research Diets D12451), or a 60% fat diet (60% HFD; Research Diets D12492) for 12 weeks to induce experimental obesity and NAFLD. At 7 weeks into the dietary protocol, all obese mice were randomised to receive once-daily treatment with either vehicle control (VC) (sterile water) or ranolazine (S1425, Selleck Chemicals) (50 mg/kg) via oral gavage for 5 weeks. This dose of ranolazine was selected based on our previous studies demonstrating stimulation of hepatic PDH activity (138). At the end of the treatment period, all mice were euthanized via intraperitoneal (IP) injection of sodium pentobarbital (12 mg) (00141704, Bimeda-MTC Animal Health Inc.) following a 16-h fast and 4-h refeed. All mice subsequently had their livers extracted, washed with 1x phosphate buffered saline (PBS) and separated into four lobes that were immediately snap frozen in liquid N_2 using Wollenberger tongs and stored at −80°C. This study was conducted in accordance with the Basic & Clinical Pharmacology & Toxicology policy for experimental and clinical studies, (204) and the operator was blinded from the treatment randomisation of mice for all in vivo physiological assessments.

3.3.2 Nucleic Acid Extraction and PCR Genotyping

DNA was isolated from mouse tail biopsies using a mixture of phenol/chloroform. Briefly, 300 µL of DNA digestion buffer (proteinase K and digestion buffer) was added to each sample in 1.5 ml Eppendorf tubes and incubated overnight at 55°C on a shaker. An equal volume of the phenol/chloroform mixture was added the following day to every tube and centrifuged for 6 min at 11000 rpm. The upper phase was transferred into new 1.5 ml-Eppendorf tubes, and 1 ml of 100% ethanol was added; the tubes were centrifuged at 13000 rpm for 8 min. The supernatants were discarded, and the pellets were washed with 500 µL of 70% ethanol at 13000 rpm for 6 min. The supernatants were discarded, and the tubes were dried for at least 20 min before resuspending each pellet in 10 mM Tris. Then a conventional PCR was performed using the following primers for *IL2*-F: 5′-CTA GGC CAC AGT ATT GAA AGA TCT-3′ and *IL2*-R: 5′-GTA GGT GGA AAT TCT AGC ATC ATC C-3′; Cre-F: 5′-GCG CTC TGG CAG TAA AAA CTA TC-3′ and Cre-R: 5′-GTG AAA CAG CAT TGC TGT CAC TT-3′; *Pdha1*-F: 5′-CGT CTG TTG AGA GAG CAG CA-3′ and *Pdha1*-R: 5′-CGC ACA AGA TAT CCA TTC CA-3′. PCR conditions were as follows: step 1, denaturation (94°C for 3 min); step 2, 35 amplification cycles (55°C for 1 min and 72°C for 30 s); and step 3, extension (72°C for 2 min and 15°C for 10 min).

3.3.3 Body Composition

Conscious lean and obese mice were placed in an EchoMRI-4 in1/700 body composition analyser to assess lean mass and fat mass as described in **Chapter 2.3.2**.

3.3.4 Assessment of Glucose Homeostasis

Mice were transferred to clean cages with all cage enrichments prior to fasting for either 16 h or 24 h with free access to drinking water before undergoing an IP glucose (Millipore Sigma) (2 g/kg)

tolerance test or an IP pyruvate (Millipore Sigma) (2 g/kg) tolerance test, respectively. Blood was collected over the course of 120 min via tail bleed at 0, 15, 30, 60, 90 and 120 min post-glucose, or pyruvate administration, using the Contour Next blood glucose monitoring system (Bayer, NJ, USA).

3.3.5 Western Blotting

Protein was isolated from powdered, frozen mouse liver samples (~20 mg) using a homogenisation buffer containing 50 mM Tris HCl (pH 8 at 4°C), 1 mM ethylenediaminetetraacetic acid (EDTA), 10% glycerol (w/v), 0.02% Brij-35 (w/v), 1 mM dithiothreitol and protease and phosphatase inhibitors (Millipore Sigma). The protein samples were then quantified using a Bradford protein assay kit (Bio-Rad Laboratories) (128). and (15 µg) were then denatured and subjected to western blotting, separated at 100 V for 1 h in 10% sodium dodecyl sulphate-polyacrylamide gel electrophoresis gels and transferred to nitrocellulose membranes (1620115; Bio-Rad Laboratories) for 2 h at 100 V. Following transfer, all membranes were blocked with 5% fat-free milk in Tris-buffered saline tween-20 (P7949; Millipore Sigma) (TBS-T) for 40 min. The membranes were further incubated overnight with primary antibodies at 4°C for the following: long-chain acyl-CoA dehydrogenase (LCAD; ab129711, Abcam), β-hydroxyacyl CoA dehydrogenase (βHAD; ab37673, Abcam), protein kinase B (Akt; 9272S, Cell Signaling), phospho-Akt (P-Akt; 4060S, Cell Signaling), pyruvate dehydrogenase (PDH; 3205S, Cell Signaling), HRP-conjugated mouse monoclonal β-actin (A3854, Millipore Sigma) and heat shock protein-90 (Hsp90; 610418, BD Biosciences). All primary antibodies were prepared in a 1/1000 dilution in 3% bovine serum albumin (BSA) except LCAD and βHAD (1:2000). The following day, all membranes were washed three times for 10 min with TBS-T. Immunodetection was performed using a secondary antibody (1:2000) in 5% fat-free milk in TBS-T and incubated for 90 min with shaking at room

temperature. Protein bands were visualised using enhanced chemiluminescence (PI34580; Thermo Fisher Scientific). Following visualisation of the protein bands, nitrocellulose membranes were incubated in stripping buffer (21059; Thermo Fisher Scientific) for 10 min at room temperature, rinsed once in distilled water and then washed three times for 5 min with TBS-T. The membranes were subsequently blocked with 5% fat-free milk in TBS-T for 40 min and then probed with a new primary antibody (from those listed above), with all steps to the visualisation of protein bands repeated. All chemiluminescent blots were imaged with the ImageQuant™ LAS 4000 mini biomolecular imager, and the intensity of immunoblot signals was quantified using Image Studio Lite Version 5.2 software.

3.3.6 Real-Time PCR Analysis

Total RNA was isolated from powdered liver samples (~15–20 mg) using TRIzol (15596018; Thermo Fisher Scientific). Briefly, RNA was quantified by measuring absorbance at 260 nm using a NanoDrop™ 2000 spectrophotometer (Thermo Fisher Scientific). First-strand cDNA synthesis was prepared using the high-capacity cDNA reverse transcriptase kit (Thermo Fisher Scientific), followed by real-time PCR, which was carried out with a CFX Connect Real-Time PCR machine (Bio-Rad Laboratories) using SYBR Green (KK4601; Kapa Biosystems). Cyclophilin A (Ppia) was used as an internal housekeeping gene to quantify the relative mRNA transcript levels of various genes (**Table 3.1**) using the $2^{-\Delta\Delta Ct}$ method as described in **Chapter 2.3.6**.

3.3.7 Determination of Triacylglycerol (TAG) Content

TAGs were extracted from the powdered frozen livers (~20 mg) using a 2:1 chloroform:methanol solution. This was followed by adding 0.2 volumes of methanol to each sample, which was kept on ice for 10 min prior to centrifugation at 3500 xg for 10 min. The supernatants were transferred

to new tubes, and 0.2 volumes of 0.04% (w/v) CaCl2 were added, followed by centrifugation at 2400 xg for 20 min. The supernatant was discarded, and the remaining TAG extract was washed twice with 150 µL of pure solvent upper phase. Finally, 50 µL of methanol was added to produce a singular phase. The samples were subsequently dried under N2 gas at 60°C, and the remaining TAG-containing pellets were dissolved in 50 µL of 3:2 tert-butyl alcohol X-100 methyl alcohol (1:1) and stored overnight at 4°C. The following day, all samples were quantified for TAG content using a commercially available enzymatic colorimetric assay kit (Wako Pure Chemical Industries) Following the manufacturer's instructions, the same kit was also used to measure the amounts of circulating TAG in mouse plasma samples (4 µL) (205).

3.3.8 Statistical Analysis

The results are presented as means ± standard deviation (SD). The significance of differences was assessed using either a two-tailed, unpaired Student's t-test or a two-way analysis of variance (ANOVA) followed by a Bonferroni post-hoc analysis. Differences were considered significant when $P < 0.05$. All data analysis was performed using GraphPad Prism 9.0 software.

Table 3.1 *Primer Sequences*.

Gene	Forward Primer	Reverse Primer
Ppia	GCTGGACCAAACACAAACG	ATGCCTTCTTTCACCTTCCC
Acaca	TAATGGGCTTCTGTGACTC	CTCAATATCGCCATCAGTCTTG
Chrebp	GAGTGCTTGAGCCTGGCTTACA	GCTCTCCAGATGGCGTTGTTCA
Srebf1	GGAGCCATGGATTGCACATT	GGCCCGGGAAGTCACTGT
Fasn	GGTTACACTGTGCTAGGTGTTG	TCCAGGCGCATGAGGCTCAGC
Pparg	TATGGAGTGACATAGAGTGTGCT	CCACTTCAATCCACCCAGAAAG
Scd1	GCTGGAGTACGTCTGGAGGAA	TCCCGAAGAGGCAGGTGTAG
Ppara	GCAGTGCCCTGAACATCGA	CGCCGAAAGAAGCCCTTAC
Acta2	CCCAGACATCAGGGAGTAATGG	TCTATCGGAACTTCAGCGTCA
Col1a1	TGCTAACGTGGTTCGTGACCG	ACATCTTGAGGTCGCGGCATGT
Col1a2	TTGCTGAGGGCAACAGCAGGTT	AATGTCAAGGAACGGCAGGCGA
Timp	GAGACCACCTTATACCAGCGTT	TACGCCAGGGAACCAAGAAG
Ccn2	TGACCCCTGCGACCCACA	TACACCGACCCACCGAAGCAG

3.4 Results

3.4.1 Generation of *Pdha1*$^{Liver-/-}$ Mice and Characterisation of Their Metabolic Phenotype

In order to generate *Pdha1*$^{Liver-/-}$ mice, we crossed Alb^{Cre} mice with floxed *Pdha1* mice (loxP site flanking exon 8 of *Pdha1* (**Figure 3.1, A and B**). We verified liver-specific PDH deletion via western blotting, where PDH protein was undetectable in livers from *Pdha1*$^{Liver-/-}$ mice but still present in other peripheral tissues, including the soleus, kidney and heart, versus being detected in all these tissues from their Alb^{Cre} littermates **(Figure 3.1, C–F)**.

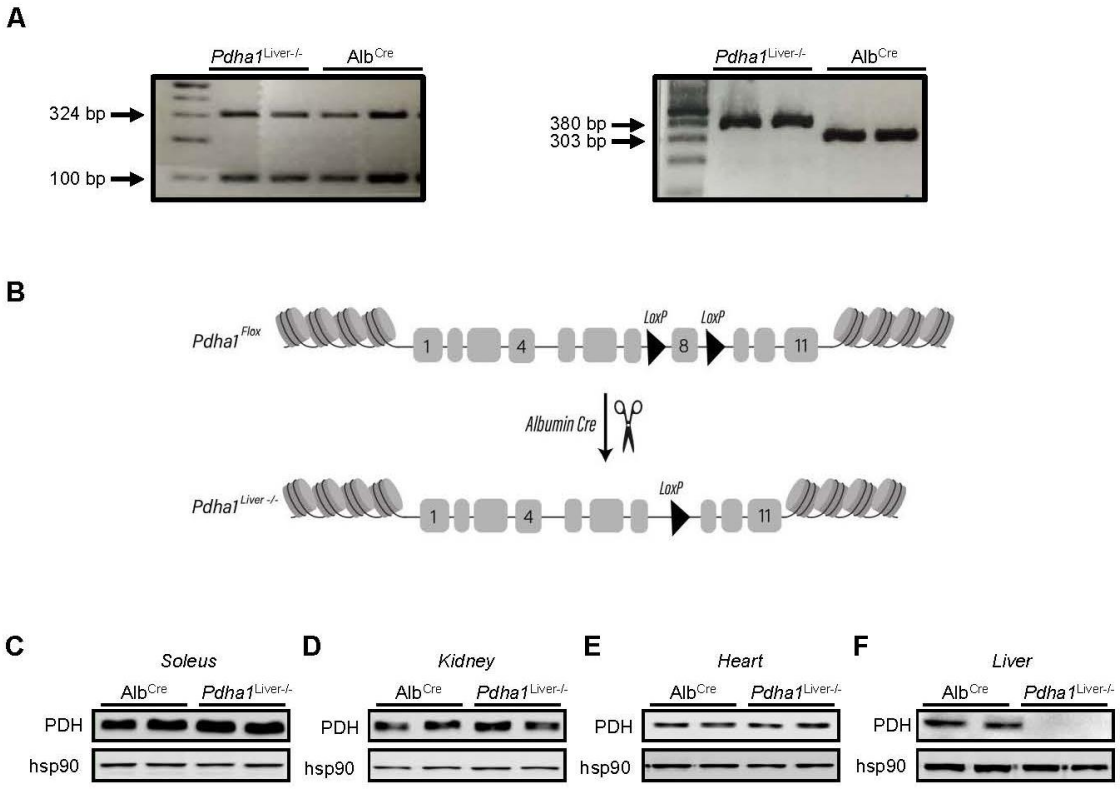
A
Pdha1Liver-/-
AlbCre
324 bp
100 bp
Pdha1Liver-/-
AlbCre
380 bp
303 bp
B
Pdha1Flox
LoxP
LoxP
1
4
8
11
Albumin Cre
Pdha1Liver -/-
LoxP
1
4
11
C
Soleus
AlbCre
Pdha1Liver-/-
PDH
hsp90
D
Kidney
AlbCre
Pdha1Liver-/-
PDH
hsp90
E
Heart
AlbCre
Pdha1Liver-/-
PDH
hsp90
F
Liver
AlbCre
Pdha1Liver-/-
PDH
hsp90

Figure 3.1 *Generation of Liver-Specific Pdha1 Deficient Mice (Pdha1$^{Liver-/-}$) Mice.* **(A)** PCR genotyping of mouse offspring shows the presence of Cre recombinase as amplification of a 100 base pair fragment and interleukin-2 (positive control) as amplification of a 324 base pair fragment, while the floxed *Pdha1* allele amplifies at a 380 base pair fragment and the wild-type *Pdha1* allele amplifies at a 303 base pair fragment. **(B)** Illustration of the *Pdha1* gene (11 exons) and placement of the loxP sites (denoted by black triangles) that flank exon 8, which is excised by Cre recombinase under control of the albumin promoter **(created with Biorender.com)**. **(C-F)** Western blot analysis of protein expression of PDH in **(C)** soleus, **(D)** kidney, **(E)** heart, and **(F)** liver samples in *Pdha1*$^{Liver-/-}$ mice versus their Alb^{Cre} control littermates.

Regardless of whether male *Pdha1*$^{\text{Liver}-/-}$ mice were fed an LFD or HFD for 12 weeks, they gained body weight at a comparable rate to their Alb$^{\text{Cre}}$ littermates while also displaying a similar body composition pattern **(Table 3.2)**. In addition, ad libitum glucose levels were also comparable between male *Pdha1*$^{\text{Liver}-/-}$ mice and their Alb$^{\text{Cre}}$ littermates regardless of diet **(Table 3.2)**.

Table 3.2 *Body Composition in Alb^{Cre} and Pdha1$^{Liver-/-}$ Mice*.

	Lean Alb$^{\text{Cre}}$ Mice		Lean *Pdha1*$^{\text{Liver-/-}}$ Mice		Obese Alb$^{\text{Cre}}$ Mice		obese *Pdha1*$^{\text{Liver-/-}}$ Mice	
	Baseline	12-weeks	Baseline	12-weeks	Baseline	12-weeks	Baseline	12-weeks
Body weight (g)	22.8 ± 2.3	29.7 ± 2.8*	22.7 ± 2.2	28.6 ± 1.6*	23.2 ± 2.4	34.7 ± 3.9*#	22.8 ± 1.8	35.7 ± 3.5*#
Fat mass (g)	1.4 ± 0.4	4.6 ± 2.2*	1.4 ± 0.5	3.3 ± 1.1*	1.2 ± 0.3	8.0 ± 2.9*#	1.6 ± 0.4	7.6 ± 3.9 *#
Fat mass (%)	6.2 ± 1.2	15.1 ± 5.6*	6.0 ± 1.8	11.7 ± 3.6*	5.2 ± 1.2	22.5 ± 6.4*#	7.0 ± 1.7	22.4 ± 8.5*#
Lean mass (g)	19.7 ± 2.4	23.4 ± 0.4*	19.7 ± 2.1	23.5 ± 1.5*	20.0 ± 2.3	25.0 ± 1.9*	19.1 ± 1.6	26.2 ± 3.5*
Lean mass (%)	86.0 ± 2.5	79.4 ± 4.6*	87.4 ± 2.6	82.1 ± 3.6*	86.1 ± 2.1	72.3 ± 6.3*#	83.8 ± 1.7	73.7 ± 11.1*#
Glucose (mM)	11.6 ± 1.7	9.5 ± 1.3	11.3 ± 1.9	10.4 ± 1.1	10.3 ± 0.8	10.1 ± 1.8	10.7 ± 1.9	10.1 ± 1.4

Body weight, fat mass, lean mass, and ad libitum blood glucose levels were measured at baseline and following 12-weeks of provision with either a low-fat diet (lean) or a high-fat diet (obese) (n= 9-14 mice/group). Values represent means ± SD. Differences were determined using a repeated measures two-way ANOVA followed by a Bonferroni post-hoc analysis. $^{*}P < 0.05$, significantly different from the respective baseline. $^{\#}P < 0.05$, significantly different from lean counterpart.

3.4.2 Male *Pdha1*$^{Liver-/-}$ Mice Do Not Exhibit an Exacerbation of Hyperglycaemia When Subjected to Experimental Obesity

Consistent with no body weight phenotype in male *Pdha1*$^{Liver-/-}$ mice fed an LFD for 12 weeks, they also demonstrated no change in glucose tolerance when compared to their male Alb^{Cre} littermates, though a trend towards a mild worsening of pyruvate tolerance was observed **(Figure 3.2, A and B)**. Furthermore, lean male *Pdha1*$^{Liver-/-}$ mice displayed an increase in their circulating TAG levels versus their male Alb^{Cre} littermates, though no change was observed in hepatic TAG content and liver weight. Molecular profiling of their livers also revealed no differences in mRNA expression of key genes in the regulation of lipogenesis and lipid metabolism **(Figure 3.2, C–F)**.

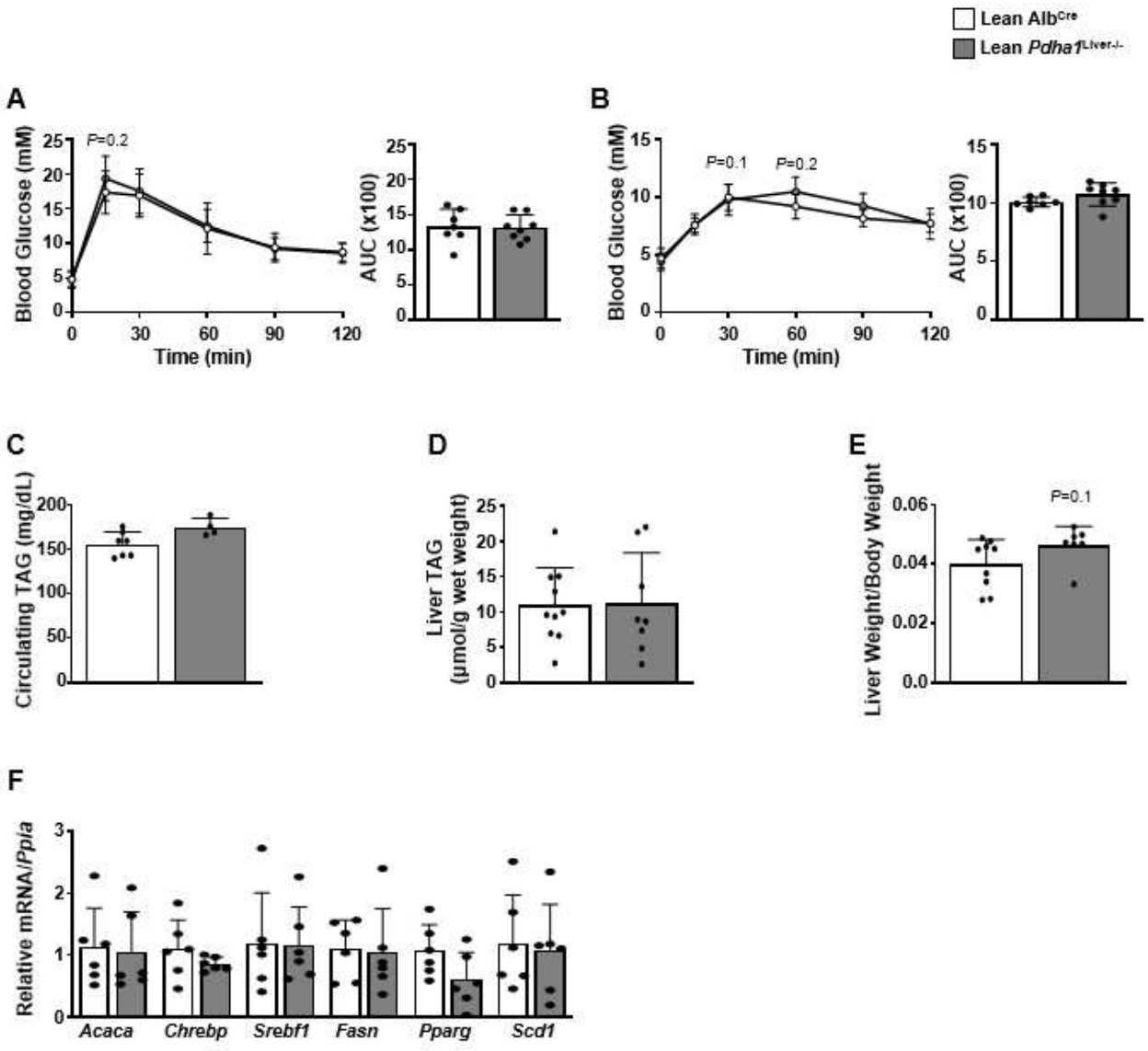
Lean Alb^Cre
Lean Pdha1^Liver-/-
A
Blood Glucose (mM)
P=0.2
Time (min)
AUC (x100)
B
Blood Glucose (mM)
P=0.1
P=0.2
Time (min)
AUC (x100)
C
Circulating TAG (mg/dL)
D
Liver TAG (µmol/g wet weight)
E
Liver Weight/Body Weight
P=0.1
F
Relative mRNA/Ppia
Acaca
Chrebp
Srebf1
Fasn
Pparg
Scd1

Figure 3.2 *Characterizing the Metabolic Phenotype of Pdha1*$^{Liver-/-}$ *Mice Fed a Low-Fat Diet.* **(A)** Glucose tolerance and **(B)** pyruvate tolerance with their respective area under the curves (AUC) in Alb^{Cre} and *Pdha1*$^{Liver-/-}$ mice fed a low-fat diet for 12-weeks (n = 7-8). **(C)** Circulating TAG levels, **(D)** hepatic TAG content, and **(E)** liver weights from Alb^{Cre} and *Pdha1*$^{Liver-/-}$ mice fed a low-fat diet for 12-weeks (n = 4-9). **(F)** mRNA expression of genes involved in regulating lipogenesis (*Acaca*, *Chrebp*, *Srebf1*, *Fasn*, *Pparg*, and *Scd1*) (n = 6) in livers from Alb^{Cre} and *Pdha1*$^{Liver-/-}$ mice fed a low- fat diet for 12-weeks. Values represent means ± SD. Differences were determined using an unpaired 2-tailed Student's t-test or 2-way ANOVA followed by a Bonferroni post-hoc analysis. $^{*}P < 0.05$, significantly different from Alb^{Cre} mice.

Whereas protein expression of fatty acid oxidation markers and Akt phosphorylation remained similar for the most part, other than a decrease in LCAD expression **(Figure 3.3, A-C)**.

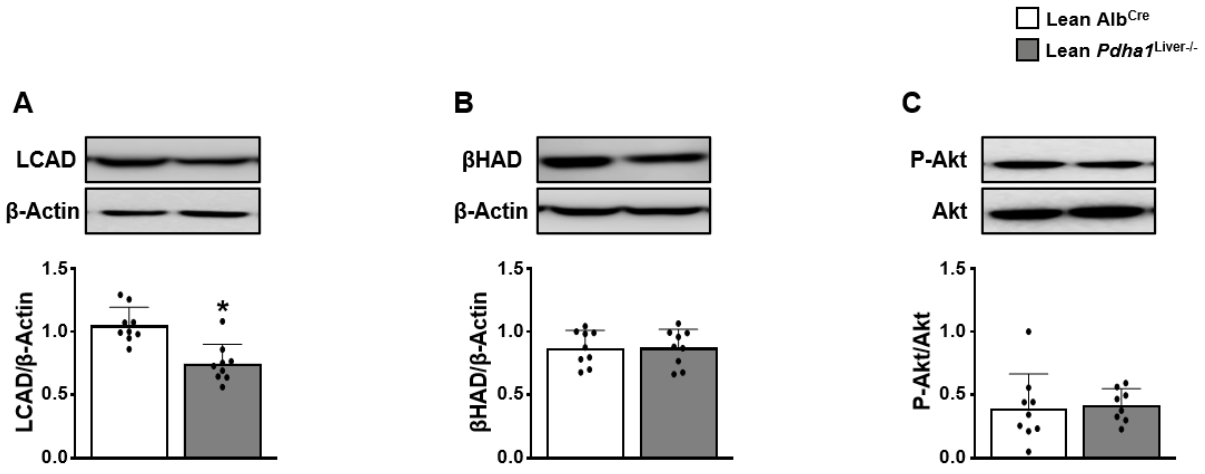

Figure 3.3 *Deletion of Hepatic Pdha1 Had No Effect on Fatty Acids Oxidation in Lean Mice*. Protein expression of key regulators of fatty acid oxidation **(A)** LCAD, **(B)** βHAD, and **(C)** insulin signaling assessed via serine 473 Akt phosphorylation in livers from Alb^{Cre} and $Pdha1^{Liver-/-}$ mice fed a low- fat diet for 12-weeks (n = 8-9). Values represent means ± SD. Differences were determined using an unpaired 2-tailed Student's t-test or 2-way ANOVA followed by a Bonferroni post-hoc analysis. $^{*}P < 0.05$, significantly different from Alb^{Cre} mice.

A similar pattern was observed in male *Pdha1*$^{\text{Liver}-/-}$ mice versus their Alb$^{\text{Cre}}$ littermates fed an HFD for 12 weeks. This included no change in glucose tolerance with a trend towards a mild worsening of pyruvate tolerance **(Figure 3.4, A and B)**, though circulating TAG levels, hepatic TAG content and liver weights were similar **(Figure 3.4, C–E)**. Obese *Pdha1*$^{\text{Liver}-/-}$ mice also displayed no major changes in hepatic mRNA expression of key regulators of lipid metabolism though a reduction in acetyl CoA carboxylase 1 (*Acaca*) mRNA expression (**Figure 3.4F)**.

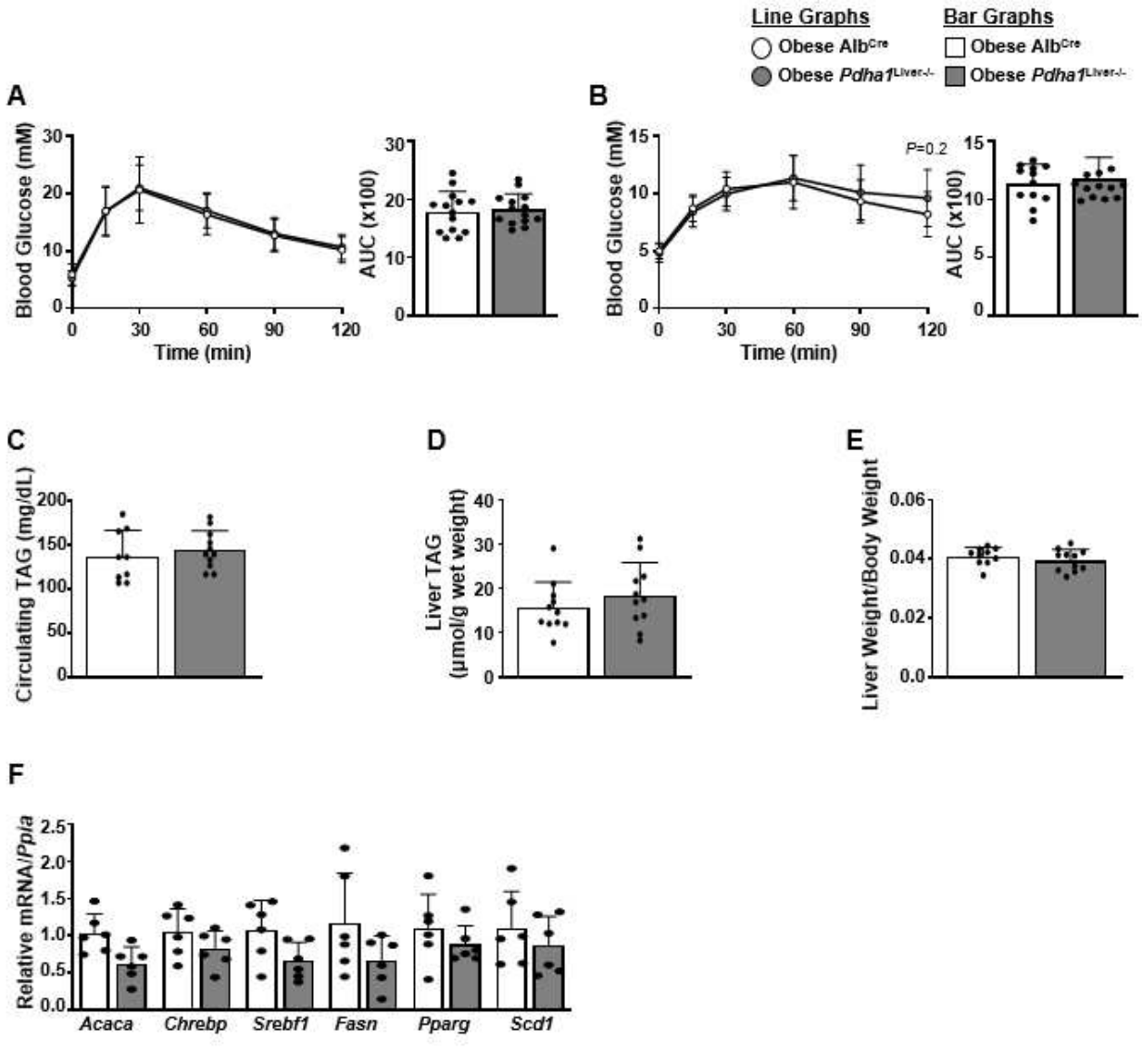
Line Graphs
Obese Alb^Cre
Obese Pdha1^Liver-/-
Bar Graphs
Obese Alb^Cre
Obese Pdha1^Liver-/-
A
Blood Glucose (mM)
Time (min)
AUC (x100)
B
Blood Glucose (mM)
Time (min)
P=0.2
AUC (x100)
C
Circulating TAG (mg/dL)
D
Liver TAG (µmol/g wet weight)
E
Liver Weight/Body Weight
F
Relative mRNA/Ppia
Acaca
Chrebp
Srebf1
Fasn
Pparg
Scd1

Figure 3.4 *Deletion of Hepatic Pdha1 Had No Effect on Glucose Homeostasis in Obese Mice*. **(A)** Glucose tolerance and **(B)** pyruvate tolerance with their respective area under the curves (AUC) in Alb^{Cre} and *Pdha1*$^{Liver-/-}$ mice fed a high-fat diet for 12 weeks (n = 12–14). **(C)** Circulating triacylglycerol (TAG) levels, **(D)** hepatic TAG content and **(E)** liver weights from Alb^{Cre} and *Pdha1*$^{Liver-/-}$ mice fed a high-fat diet for 12 weeks (n = 9–11). **(F)** mRNA expression of genes involved in regulating lipogenesis (*Acaca*, *Chrebp*, *Srebf1*, *Fasn*, *Pparg* and *Scd1*) (n = 6) in livers from Alb^{Cre} and *Pdha1*$^{Liver-/-}$ mice fed a high-fat diet for 12 weeks (n = 8–9). Values represent means ± SD. Differences were determined using an unpaired two-tailed Student's t-test or two-way ANOVA followed by a Bonferroni post-hoc analysis. $^{*}P < 0.05$, significantly different from Alb^{Cre} mice.

Obese *Pdha1*$^{Liver-/-}$ mice displayed a trend towards increased LCAD and βHAD protein expression were observed versus their Alb^{Cre} littermates **(Figure 3.5, A and B)**. In addition, hepatic Akt phosphorylation was similar between obese *Pdha1*$^{Liver-/-}$ mice and their Alb^{Cre} littermates **(Figure 3.5C)**.

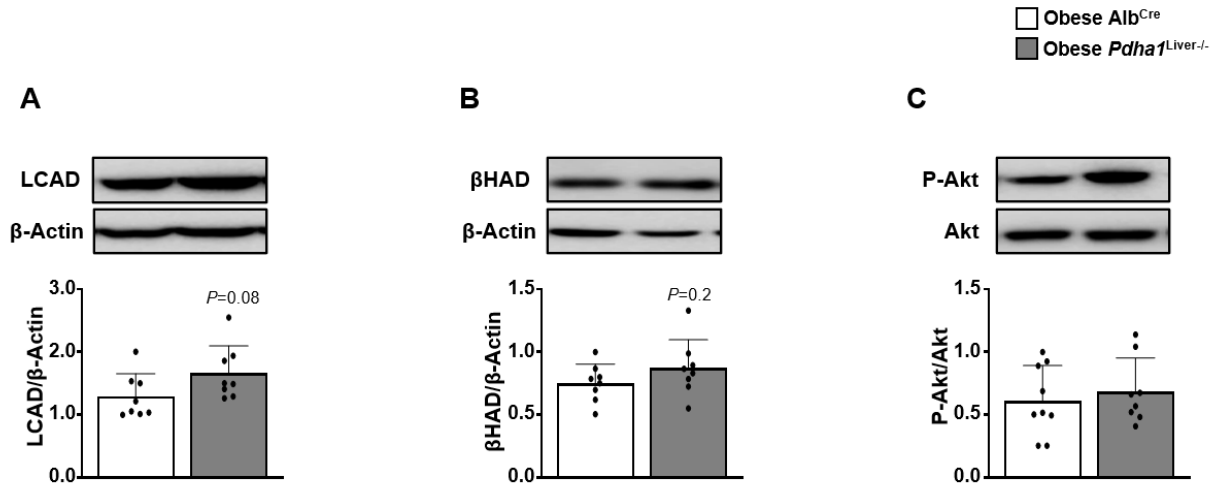

Figure 3.5 *Deletion of Hepatic Pdha1 Had No Effect on Fatty Acids Oxidation in Obese Mice*. protein expression of key regulators of fatty acid oxidation **(A)** LCAD, **(B)** βHAD and **(C)** insulin signaling assessed via serine 473 Akt phosphorylation in livers from Alb^{Cre} and *Pdha1*$^{Liver-/-}$ mice fed a high-fat diet for 12 weeks (n = 8–9). Values represent means ± SD. Differences were determined using an unpaired two-tailed Student's t-test. $^{*}P < 0.05$, significantly different from Alb^{Cre} mice.

3.4.3 Ranolazine Treatment Does Not Mitigate Hepatic Steatosis in Obese Male *Pdha1*$^{\text{Liver}-/-}$ Mice

Our previous studies showed that ranolazine treatment increases hepatic PDH activity and mitigates NAFLD (138). As such, we next subjected male *Pdha1*$^{\text{Liver}-/-}$ mice and their Alb$^{\text{Cre}}$ littermates to our model of experimental obesity (12-week HFD), following which all mice were randomised to treatment with either vehicle control or ranolazine (50 mg/kg once-daily) over the final 5 weeks. Treatment with ranolazine improved glucose tolerance and had no impact on pyruvate tolerance while causing a trend towards mild decreases in circulating TAG levels (16.54% reduction) and hepatic TAG content (16.49% reduction) in obese Alb$^{\text{Cre}}$ mice, actions that were nonexistent in obese *Pdha1*$^{\text{Liver}-/-}$ mice **(Figure 3.6, A–D)**. However, these changes were not associated with a difference in liver weight **(Figure 3.6E)**.

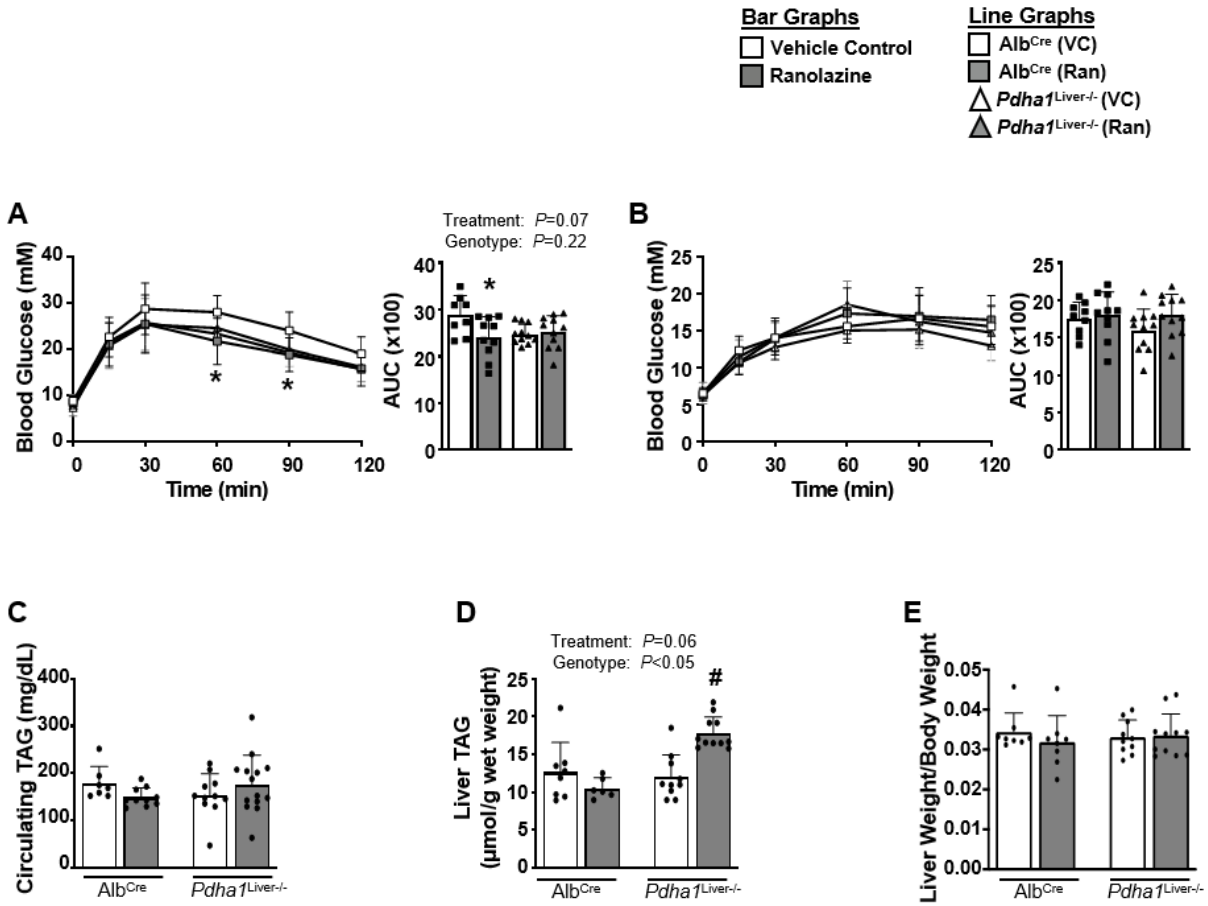
Bar Graphs
Vehicle Control
Ranolazine
Line Graphs
Alb^Cre (VC)
Alb^Cre (Ran)
Pdha1^Liver-/- (VC)
Pdha1^Liver-/- (Ran)
A
Blood Glucose (mM)
Time (min)
Treatment: P=0.07
Genotype: P=0.22
AUC (x100)
B
Blood Glucose (mM)
Time (min)
AUC (x100)
C
Circulating TAG (mg/dL)
Alb^Cre
Pdha1^Liver-/-
D
Treatment: P=0.06
Genotype: P<0.05
Liver TAG (µmol/g wet weight)
Alb^Cre
Pdha1^Liver-/-
E
Liver Weight/Body Weight
Alb^Cre
Pdha1^Liver-/-

Figure 3.6 *Ranolazine Treatment Failed to Mitigate Liver Steatosis in Pdha1*$^{Liver-/-}$ *Mice*. **(A)** Glucose tolerance and **(B)** pyruvate tolerance with their respective area under the curves (AUC) in Alb^{Cre} and *Pdha1*$^{Liver-/-}$ mice treated with either vehicle control (VC) or ranolazine (Ran) (n = 9–11). **(C)** Circulating triacylglycerol (TAG) levels in Alb^{Cre} and *Pdha1*$^{Liver-/-}$ mice treated with either VC or Ran (n = 7–14). **(D)** Hepatic TAG content in Alb^{Cre} and *Pdha1*$^{Liver-/-}$ mice treated with either VC or Ran (n = 6–11). **(E)** Liver weights from Alb^{Cre} and *Pdha1*$^{Liver-/-}$ mice treated with either VC or Ran (n = 6–11). Values represent means ± SD. Differences were determined using an unpaired two-tailed Student's t-test or two-way ANOVA followed by a Bonferroni post-hoc analysis. $^{*}P < 0.05$, significantly different from VC-treated Alb^{Cre} mice. $^{\#}P < 0.05$, significantly different from VC-treated *Pdha1*$^{Liver-/-}$ mice.

Furthermore, the ranolazine-mediated reduction in hepatic steatosis in obese Alb^{Cre} mice was not associated with changes in hepatic mRNA expression of key genes involved in regulating lipogenesis **(Figure 3.7)**. In contrast, ranolazine treatment increased mRNA expression of *Acaca* and fatty acid synthase (*Fasn*) but decreased mRNA expression of peroxisome proliferator activated receptor-α (*Ppara*) in obese *Pdha1*$^{Liver-/-}$ **(Figure 3.7)**.

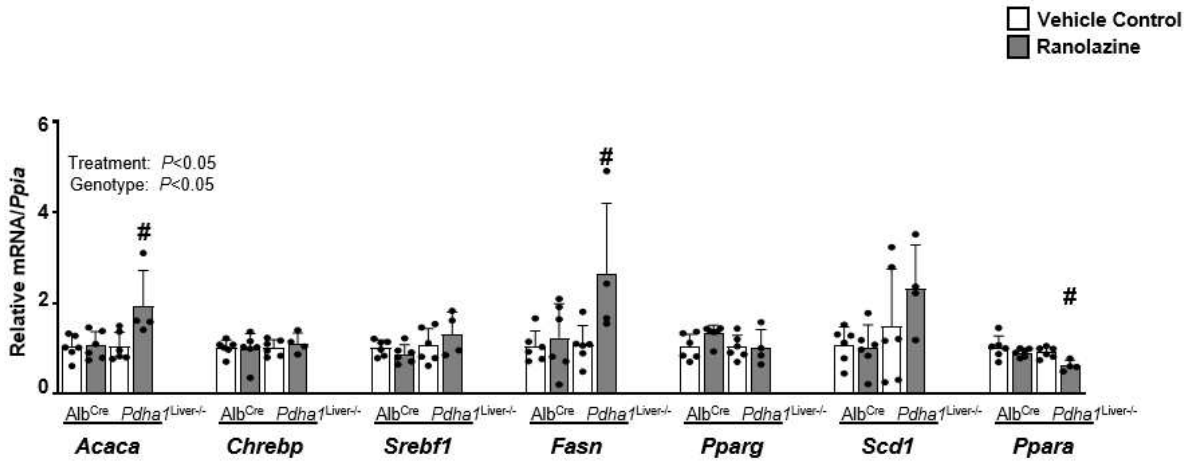

Figure 3.7 *Ranolazine Treatment Failed to Decrease Lipogenesis in Pdha1*$^{Liver-/-}$ *Mice*. mRNA expression of genes involved in regulating lipogenesis and lipid metabolism (*Acaca*, *Chrebp*, *Srebf1*, *Fasn*, *Pparg*, *Scd1* and *Ppara* (n = 4–6) in livers from Alb^{Cre} and *Pdha1*$^{Liver-/-}$ mice treated with either VC or Ran for 5 weeks. Values represent means ± SD. Differences were determined using a two-way ANOVA followed by a Bonferroni post-hoc analysis. $^{*}P < 0.05$, significantly different from VC-treated Alb^{Cre} mice. $^{\#}P < 0.05$, significantly different from VC-treated *Pdha1*$^{Liver-/-}$ mice.

These findings are consistent with ranolazine increasing hepatic TAG content, specifically in obese *Pdha1*$^{\text{Liver}-/-}$ mice **(Figure 3.6D)**. Moreover, hepatic mRNA expression profiles for genes involved in the regulation of fibrosis indicated that these processes were not impacted either by ranolazine treatment or liver-specific *Pdha1* deletion **(Figure 3.8A)**. In agreement with our previous results, ranolazine treatment did not influence protein expression of fatty acid oxidation enzymes or Akt phosphorylation in livers from Alb$^{\text{Cre}}$ and *Pdha1*$^{\text{Liver}-/-}$ mice **(Figure 3.8, B–E)**.

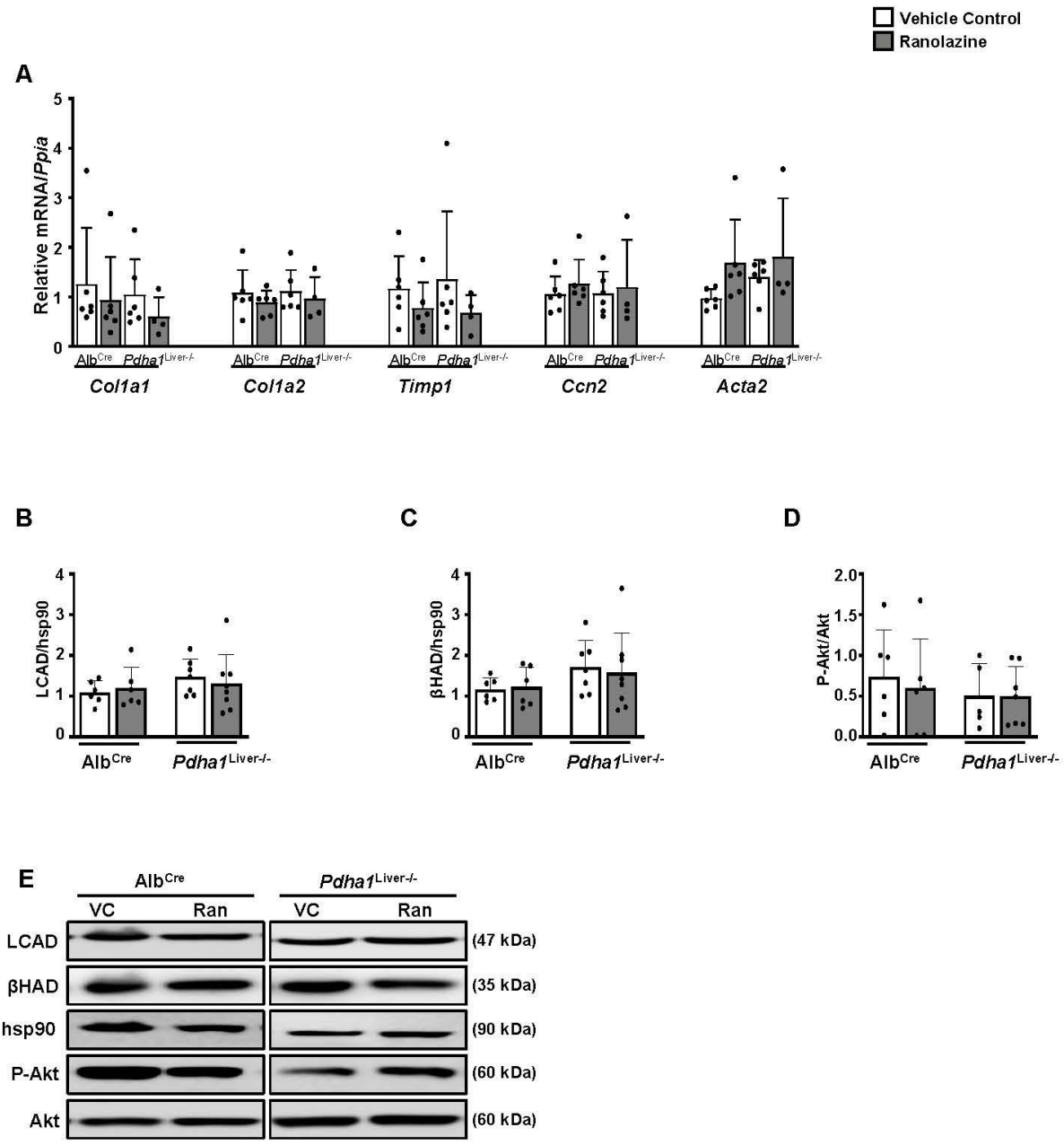
Vehicle Control
Ranolazine
A
Relative mRNA/Ppia
Col1a1
Col1a2
Timp1
Ccn2
Acta2
B
LCAD/hsp90
C
βHAD/hsp90
D
P-Akt/Akt
AlbCre
Pdha1Liver-/-
E
VC
Ran
LCAD
βHAD
hsp90
P-Akt
Akt
(47 kDa)
(35 kDa)
(90 kDa)
(60 kDa)
(60 kDa)

Figure 3.8 *Ranolazine Treatment Failed to Enhance Fatty Acids Oxidation in Pdha1*$^{Liver-/-}$ *Mice*. **(A)** mRNA expression of genes involved in regulating fibrosis (*Col1a1*, *Col1a2*, *Timp1*, *Ccn2* and *Acta2*) (n = 4–6), protein expression of key regulators of fatty acid oxidation **(B)** LCAD, **(C)** βHAD and **(D)** insulin signaling assessed via serine 473 Akt phosphorylation in livers from Alb^{Cre} and *Pdha1*$^{Liver-/-}$ mice treated with either VC or Ran for 5 weeks (n = 5–8). **(E)** Corresponding representative images of western blots for LCAD expression, βHAD expression, and serine 473 Akt phosphorylation. Values represent means ± SD. Differences were determined using a two-way ANOVA followed by a Bonferroni post-hoc analysis. $^{*}P < 0.05$, significantly different from VC-treated Alb^{Cre} mice. $P < 0.05$, significantly different from Ran-treated Alb^{Cre} mice. $^{\#}P < 0.05$, significantly different from VC-treated *Pdha1*$^{Liver-/-}$ mice.

3.5 Discussion

There are two important outcomes reinforced from our study's primary observations. First, reductions in hepatic PDH activity and subsequent glucose oxidation do not directly contribute to the pathology of NAFLD, as hepatic TAG content remained similar in *Pdha1*$^{Liver-/-}$ mice when compared to their Alb^{Cre} littermates, regardless of whether they were fed an LFD or HFD. Second, increases in hepatic PDH activity and glucose oxidation are key mechanisms contributing to the metabolic benefits of the antianginal therapy ranolazine, since ranolazine was unable to improve the pathology of NAFLD and glucose intolerance in obese *Pdha1*$^{Liver-/-}$ mice.

The lack of a major hepatic phenotype in *Pdha1*$^{Liver-/-}$ mice was somewhat surprising, since whole-body genetic deletion of *Pdk2* (encodes for PDHK2) in mice, which results in elevated PDH activity, protected against obesity-induced NAFLD and glucose intolerance (134). Hence, it may be anticipated that *Pdha1*$^{Liver-/-}$ mice, which lack PDH activity specifically in the liver, would exhibit a worsening of NAFLD in response to experimental obesity, and may even demonstrate increases in hepatic steatosis when maintained on standard chow. Conversely, previous studies by Mahmood and colleagues have demonstrated that *Pdha1*$^{Liver-/-}$ mice have reductions in the mRNA expression of genes involved in both lipogenesis and fatty acid oxidation (142). While our results are not compatible with these past findings, Mahmood and colleagues did not observe increases in hepatic TAG content in their colony of *Pdha1*$^{Liver-/-}$ mice, consistent with our own observations, and they did not perform their studies in an obesogenic environment. While a clear explanation for these discrepancies is currently unknown, it may simply indicate that while hepatic PDH activity

is a therapeutic target to decrease hepatic steatosis, changes in PDH activity during obesity are not direct contributors to the pathology of NAFLD per se.

The failure of ranolazine to alleviate hepatic steatosis and improve glucose tolerance in obese *Pdha1*$^{Liver-/-}$ mice is consistent with our hypothesis that increases in hepatic PDH activity and glucose oxidation are key mechanisms required for the salutary metabolic actions of ranolazine in obesity. Such observations support our past findings in animals (138) and are consistent with previous studies in humans, highlighting their potential translational relevance (187, 198). To our surprise, treatment with ranolazine actually increased hepatic TAG content and mRNA expression of key genes involved in regulating lipogenesis in obese *Pdha1*$^{Liver-/-}$ mice. In addition, ranolazine treatment also decreased the mRNA expression of *Ppara* in obese *Pdha1*$^{Liver-/-}$ mice, a key transcription factor regulating fatty acid oxidation. It should be noted, though, that these are only gene expression changes, and it would be important in future studies to assess whether our observations translate into actual changes in metabolic flux through these pathways. While potential increases in lipogenesis and decreases in fatty acid oxidation may explain ranolazine's actions in obese *Pdha1*$^{Liver-/-}$ mice, it is also possible that ranolazine's other actions, including its ability to inhibit the late inward sodium current (135, 185) or to decrease glucagon secretion (206), could be implicated. The latter being consistent with glucagon having been demonstrated to promote hepatic fatty acid oxidation and decrease hepatic steatosis (207). Nonetheless, such actions of ranolazine may be overridden in the context of augmented hepatic PDH activity that would be present in obese Alb^{Cre} mice. There are also a few limitations of our study that need to be considered. As our study was performed entirely in male mice, it is possible that our observations may differ in female mice, especially since female mice are protected against

experimental NAFLD (208). As our assessments of glucose and pyruvate tolerance were performed following an overnight fast, it would also be important for future studies to perform such measurements in response to fasting periods of shorter duration (i.e., 5–6 h) that may be more translationally meaningful (209). Last, we assessed hepatic steatosis in mice in response to feeding, as PDH activity is most relevant in the fed state, where it regulates metabolic flexibility and the transition to using carbohydrates as an oxidative fuel source. However, hepatic TAG content increases during fasting; thus, it would be important to also assess the progression of hepatic steatosis in fasted Alb^{Cre} and $Pdha1^{Liver-/-}$ mice, as well as in response to ranolazine treatment.

Taken together, our results highlight that ranolazine can mitigate obesity-related NAFLD through increases in hepatic PDH activity and glucose oxidation. Such observations are clinically relevant and suggest that ranolazine may be a more preferable antianginal therapy to prescribe to individuals who are also obese. Furthermore, stimulating PDH activity may prove to be a novel strategy for the specific treatment of NAFLD, a condition with no currently approved pharmacotherapies.

Acknowledgements & Grants

This study was supported by an Operating Grant from the Canadian Liver Foundation to JRU and a Project Grant from the Canadian Institutes of Health Research to JRU. CTS was supported by an Alberta Diabetes Institute Graduate Studentship Award and an Antoine Noujaim Graduate Scholarship in Pharmaceutical Sciences. JRU is a Tier 2 Canada Research Chair (Pharmacotherapy of Energy Metabolism in Obesity).

Conflict of interest statement

The authors have no conflicts to declare.

Chapter 4: The Antipsychotic Agent Pimozide Alleviates Steatosis in HepaRG Cells by Activating the IRE1/XBP1 Pathway

Christina T. Saed[1,2,3*], Seyed Amirhossein Tabatabaei Dakhili[1,2,3*], Amanda A. Greenwell[1,2,3], Kunyan Yang[1,2,3], Keshav Gopal[1,2,3], Jordan S.F. Chan[1,2,3], Tanin Shafaati[1,2,3], Indiresh A. Mangra-Bala [1,2,3], Magnus J. Stenlund[1,2,3,] Sally R. Ferrari[1,2,3], Kristil Almahfoud[1,2,3], Farah Eaton[1,2,3], and John R. Ussher[1,2,3]

[1]Faculty of Pharmacy and Pharmaceutical Sciences, University of Alberta, Edmonton, AB Canada

[2]Alberta Diabetes Institute, University of Alberta, Edmonton, AB Canada

[3]Cardiovascular Research Centre, University of Alberta, Edmonton, AB Canada

*Denotes Equal Contribution

UNDER PREPARATION FOR PUBLICATION

4.1 Abstract

Metabolic dysfunction-associated steatotic liver disease (MASLD), which is frequently linked to obesity, is a liver disease that is common worldwide and a major risk factor for type 2 diabetes (T2D). Previous findings from our laboratory have demonstrated that the antipsychotic drug pimozide can inhibit succinyl-CoA:3-ketoacid CoA transferase (SCOT) enzyme within skeletal muscle tissue and improve glycemia in obese mice. In pursuit of additional molecular targets for pimozide related to metabolic disorders, the Similarity Ensemble Approach (SEA) was employed, revealing XBP1 as a potential point of therapeutic engagement. Given the integral involvement of XBP1 within the unfolded protein response (UPR) and its regulatory impact on endoplasmic reticulum (ER) stress, our focus was redirected to inositol-requiring enzyme 1 (IRE1). IRE1 enzyme acts as the proximal sensor of ER stress and is the primary activator of XBP1 through its kinase and endoribonuclease functions. The activation of IRE1 and subsequent splicing of XBP1 mRNA is critical for cellular adaptation to ER stress, influencing the expression of genes integral to protein folding and degradation. These processes are particularly relevant in metabolic conditions such as fatty liver disease, where ER stress is a prominent feature. In vitro analyses utilizing a hepatocyte cell line have revealed that pimozide treatment promotes upregulation of IRE1 and mitigates oleic acid-induced hepatocyte lipid accumulation. Parallel in vivo studies on murine models with induced T2D have documented improved glycemic regulation following pimozide administration, mirroring previous observations yet without substantial changes in levels of hepatic triacylglycerol.

4.2 Introduction

Metabolic dysfunction-associated steatotic liver disease (MASLD) is characterized by the accumulation of lipids within the liver tissue, primarily observed in individuals with minimal alcohol consumption (50). Left untreated, MASLD can progress to metabolic dysfunction-associated steatohepatitis (MASH), a more complex condition marked by liver inflammation and fibrosis, ultimately increasing the risk of cirrhosis and hepatocellular carcinoma (1). MASLD is strongly linked to metabolic syndrome (MetS), with insulin resistance being a crucial contributor in both conditions. Its occurrence increases with obesity, MetS, and type 2 diabetes (T2D), a group of metabolic abnormalities such as abdominal obesity, abnormal levels of lipids in the blood, and inadequate blood glucose control. Using computational modelling, it was discovered that pimozide, which primarily blocks dopamine 2 receptors (D2R), also has an affinity for binding to succinyl-CoA:3-ketoacid CoA transferase (SCOT) (128). SCOT plays a crucial role in the metabolic process of ketone body oxidation, transforming acetoacetate into acetoacetyl-CoA. When pimozide was administered to obese mice, there was a significant elevation in their plasma ketone levels due to reduced SCOT activity in their skeletal muscles and a simultaneous decrease in blood glucose levels. These findings highlight the potential for repositioning pimozide as a novel therapeutic option for T2D.

This finding has sparked increased interest in exploring other potential targets with which pimozide may interact. Initially, through the Similarity Ensemble Approach (SEA) approach, XBP1 (X-box binding protein 1) was recognized as a target in our research (210). SEA is a chemoinformatics tool that predicts potential drug-target interactions by analysing similarities in chemical structure. It operates on the principle of molecular mimicry, suggesting that molecules with similar features are more likely to bind to similar targets. SEA does not rely on the detailed

structural information of the target protein; instead, it utilizes large libraries of compounds with known biological activities, breaking down each molecule into its constituent features like shape, electrostatic charges, and functional groups. These molecular signatures are then used to create a similarity score that quantifies the likeness between different compounds.

XBP1 is a critical part of the endoplasmic reticulum (ER), and its unfolded protein response (UPR), mainly governed by the IRE1 (a key enzyme in UPR), plays a crucial role in maintaining cellular homeostasis by orchestrating adaptive signaling pathways in response to ER stress. Activation of IRE1 induces non-canonical splicing of XBP1 mRNA, generating the stress-responsive transcription factor XBP1s while also stimulating regulated IRE1-dependent decay (RIDD), collectively contributing to the resolution of ER stress and cellular adaptation (211). IRE1 and XBP1 contribute to modulating binding immunoglobulin protein (BiP) expression. This process is essential for the UPR, maintaining proper protein folding and cellular balance. Within obesity and diabetes, these mechanisms are particularly critical. Elevated levels of XBP1 improve glucose tolerance and insulin signaling while concurrently inhibiting lipid synthesis, thus vital in managing these conditions (212). Conversely, disruptions in XBP1 expression are associated with impaired glucose homeostasis (165). Recent studies further highlight the critical role of XBP1, revealing that its genetic deletion exacerbates MASLD progression to MASH and contributes to liver injury (213). Moreover, the deficiency of IRE1α in the liver leads to a moderate increase in liver lipid content, exacerbating liver steatosis (154). Recognizing these interconnected findings, the necessity for a pharmacological approach becomes apparent, precisely one that selectively enhances the protective IRE1/XBP1 signalling pathway to mitigate MASLD. Therefore, our objective in this study is to delve deeper into this molecular interaction. Our study involves using

an in vitro HepaRG model. This human hepatoma cell line closely resembles primary hepatocytes to study the possible role of XBP1 and how pimozide affects it or its related pathway in hepatocytes. We also plan to use in vivo methods to confirm our discoveries in animal models, enabling us to thoroughly evaluate the therapeutic possibilities of repurposing pimozide for treating MASLD.

4.3 Methods

4.3.1 Animal Care and Experimentation

All animal procedures were approved by the University of Alberta Health Sciences Animal Welfare Committee and performed according to the regulations and guidelines of the Canadian Council on Animal Care. The animals were provided unrestricted access to food and water and housed in a temperature-controlled unit with a 12-hour light/dark cycle. Male C57BL/6J mice, aged 8 weeks, obtained from The Jackson Laboratory, were given a week to adapt to our animal facility. After this, they were given either a chow or high-fat diet (HFD) consisting of 60% of calories from lard (Research Diets D12492) for 10 weeks. In order to induce experimental T2D, all HFD-fed animals received a single intraperitoneal (IP) injection of streptozotocin (S0130-1G, Sigma-Aldrich) (STZ; 75 mg/kg) diluted in 0.1 M sodium citrate (pH 5.0), while all lean mice received a single administration of vehicle control at 4-weeks into the dietary protocol. After receiving STZ for four weeks, mice were randomized to receive treatment with pimozide (2062784. Sigma-Aldrich), lurasidone (HY-B0032, MedChemExpress), or vehicle control (corn oil) (10 mg/kg once every 48 h) via oral gavage for 2 weeks. After a 4-hour fast, mice were administered 200 μL of Ensure Original (containing 9 grams of protein) via oral gavage, following a subsequent 1-hour interval

before euthanasia, achieved through an intraperitoneal injection of sodium pentobarbital (12 mg, 00141704, Bimeda-MTC). All mice subsequently had their livers extracted and washed with 1x phosphate-buffered saline (PBS). The livers were then divided into four lobes, which were promptly frozen in liquid nitrogen using Wollenberger tongs and stored at a temperature of -80°C.

4.3.2 Body Composition

Conscious lean and obese mice were subjected to analysis of their body composition, lean mass, and fat mass using the EchoMRI™in1/700) as described in **Chapter 4.3.3**.

4.3.3 Assessment of Glucose Homeostasis

Before conducting an IP glucose (Millipore Sigma (1 g/kg) tolerance test, mice were moved to clean cages with all cage enrichments. They had fasted for 16 h with unrestricted access to drinking water. Blood samples were obtained by performing tail bleeds at specific time intervals (0, 15, 30, 60, 90, and 120-min) after administering glucose using the Contour Next blood glucose monitoring system (Bayer, NJ, USA).

4.3.4 Assessment of Circulating Insulin Levels

Mouse tail blood samples (~5 µL) were taken before and 15-min after glucose injection during the glucose tolerance test. A commercial enzyme-linked immunosorbent assay (ELISA) kit (ALPCO Diagnostics) was used to assess plasma insulin. Samples were placed in a 96-well microplate with 75 µL of working strength conjugation buffer. After incubating the plate in an orbital microplate shaker for 2 h at room temperature, it was washed 6x with a working strength wash buffer. Start the reaction by adding 100 µL tetramethylbenzidine (TMB) to each well for 30-min. The reaction

was stopped by adding 100 µL of stop solution. Plasma insulin levels were calculated after measuring each sample's optical density at 450 nm (Synergy H1 Hybrid Reader; BioTek) (128).

4.3.5 Western Blotting

HepaRG and liver tissues were lysed with RIPA buffer (R0278, Millipore Sigma) supplemented with protease and phosphatase inhibitors (Millipore Sigma). A Bradford protein assay kit (Bio-Rad Laboratories) was then used to quantify the protein samples. The protein samples were then processed and subjected to Western blotting techniques as previously outlined. Inositol-requiring transmembrane kinase endoribonuclease-1α (IRE1α; 3294S, Cell Signaling), binding immunoglobulin protein (BiP; 3177S, Cell Signaling), X-box binding protein 1 (XBP1s; ab220783, Abcam), and heat shock protein-90 (hsp90; 610418, BD Biosciences). All membranes were washed 3x 10-min the following day with tris-buffered saline Tween-20 (TBS-T). Immunodetection was performed using a secondary antibody (1:2000) in 5% fat-free milk in TBS-T and incubated for 90-min with shaking at room temperature. Protein bands were visualized using enhanced chemiluminescence (PI34580; Thermo Fisher Scientific). All antibodies were prepared in a 1/1000 dilution in 5% bovine serum albumin (BSA).

4.3.6 Plasma and Liver Triacylglycerol (TAG)

TAGs were extracted from the powdered frozen livers (~20 mg) using a 2:1 chloroform: methanol solution. This was followed by adding 0.2 volumes of methanol to each sample, which was kept on ice for 10-min before centrifugation at 3,500 x*g*. The supernatants were transferred to new tubes, and 0.2 volumes of 0.04% (w/v) $CaCl_2$ were added, followed by centrifugation at 2,400 x*g* for 20-min. The supernatant was discarded, and the remaining TAG extract was washed twice with 150 µL of pure solvent upper phase. Finally, 50 µL methanol was added to produce a singular

phase. The samples were subsequently dried under N_2 gas at 60°C, and the remaining TAG-containing pellets were dissolved in 50 µL of 3:2 tert-butyl alcohol X-100 methyl alcohol (1:1) and stored overnight at 4°C. All samples were quantified for TAG content the following day using a commercially available enzymatic colourimetric assay kit (Wako Pure Chemical Industries). Following the manufacturer's instructions, the same kit was also used to measure the amounts of circulating TAG in mouse plasma samples (4 µL) (205).

4.3.7 Cell Culture

HepaRG cells were cultured in William's E Medium (12551032, Thermo Fisher Scientific) containing 10% FBS and 1% penicillin/streptomycin (P/S). Cells were incubated in a water-jacketed CO_2 incubator at 37°C with 5% CO_2. Once cells reached 80–90% confluency, they were seeded at 6 well-plates at a cell density of 0.5 x 10^6 cells/well and exposed to 2 mM oleic acid–bovine serum albumin (O3008, Sigma-Aldrich) for 24 h. Within this period, the cells were treated with various compounds, including dimethyl sulfoxide (DMSO), denoted in this paper as a vehicle, pimozide, lurasidone, paliperidone, clozapine (12.5 nm) for 16 h.

4.3.8 Semi-Quantitative PCR (semi-qPCR) and Quantitative Real-time RT-PCR (qPCR)

The cells were cultured, treated according to the instructions, and subsequently harvested. Total RNA was extracted with a TRIzol (15596018; Thermo Fisher Scientific) procedure as specified by the manufacturer and quantified by NanoDrop™ 2000 spectrophotometer. First-strand cDNA was performed using 2000 ng of total RNA with the high-capacity cDNA reverse transcriptase kit (Thermo Fisher Scientific). *XBP1* transcripts (spliced and unspliced) were amplified by RT-PCR using PCR master mix (Thermo Fisher Scientific) and the following primers: human *XBP1* forward (5′-AAACAGAGTAGCAGCTCAGACTGC-3′) and human *XBP1* reverse (5′-

TCCTTCTGGGTAGACCTCTGGGAG-3′). *GAPDH* forward (5′-ACCACAGTCCATGCCATCAC-3′), and *GAPDH* reverse (5′-TCCACCACCCTGTTGCTGTA-3′). The PCR conditions were as follows: step 1, denaturation (95°C for 2-min); step 2, 35 cycles of amplification, with each cycle consisting of heating to 95°C for 30 s, cooling to 60°C for 30 s, and then heating to 72°C for 30-sec, and step 3 involved a final extension at 72°C for 10-min. The PCR product was subjected to digestion with the PstI enzyme to differentiate between unspliced fragments (290 bp and 183 bp) and spliced fragments (473 bp). DNA fragments containing spliced and unspliced human *XBP1* were separated by electrophoresis on a 2.5% agarose gel.

Real-time PCR was carried out with a CFX Connect Real-Time PCR machine (Bio-Rad Laboratories) using SYBR Green (KK4601; Kapa Biosystems). Cyclophilin A (Ppia) was used as an internal housekeeping gene to quantify various genes' relative mRNA transcript levels (**Table 4.1**) using the 2-ΔΔCt method described in **Chapter 2.3.6**.

4.3.9 Oil Red O Staining

For the preparation of frozen sections, mouse liver tissues underwent sequential incubation with 5%, 10%, and 30% sucrose solutions (1–2 mL each) for 12–16 hours at 4°C. Subsequent to this, the tissues were embedded in an OCT compound and preserved at −80°C until analysis. Cryostat sectioning was performed, yielding sections of 8-10 μm thickness. The Oil Red O stock solution (00625-256, Sigma-Aldrich) was prepared by dissolving 0.5 g of Oil Red O powder in 50 mL of isopropanol. For application, 10 mL of the stock stain was combined with 16 mL of glycerol. The sections were air-dried for 30-min, subjected to a 5-min rinse with 60% isopropanol, and stained with a working solution for 1 h. In the case of HepaRG cells, a gentle wash with PBS preceded fixation with 10% formalin for 10-min, post-fixation, the cells were subjected to staining with the

working solution (10 mL of the stock stain mixed with 16 mL of 60% isopropanol) for 1 h. Imaging was done with a Zeiss LSM 710 confocal microscope, and subsequent analysis was performed using FIJI software.

4.3.10 siRNA Transfection

Following the manufacturer's protocol, HepaRG cells were performed using a JetPRIME® siRNA transfection reagent kit (PolyPlus-transfection®). A transfection master mix was prepared by combining 306 ng of SMART Pool ON-TARGET Plus human siRNA (L-004951-02-0005, Dharmacon) with 200 µL of JetPRIME® buffer and 4 µL of JetPRIME® reagent. HepaRG cells were seeded at 0.5 x 10^6 cells/well in 6-well plates and grown for ~ 24 h to attain a confluence of 80% before transfection. The transfection mix was added to the cells and incubated at 37 °C for 48 h. 24-hour post-transfection, 2 mM oleic acid was added for 24 h. Within this period, the cells were treated with vehicle or pimozide (12.5 nm) for 16 h. HepaRG cells were collected and subjected to western blot and semi-quantitative RT-PCR.

4.3.11 Statistical Analysis

The results are presented as means ± standard error of the mean (SEM). The significance of differences was assessed using either a 2-tailed, unpaired Student’s t-test, one-way analysis of variance (ANOVA) or a 2-way ANOVA followed by a Bonferroni post-hoc analysis. Differences were considered significant when $P < 0.05$. All data analysis was performed using GraphPad Prism 9.0 software.

Table 4.1 *Primer Sequences*.

Gene	Forward Primer	Reverse Primer
PPIA	CCCACCGTGTTCTTCGACATT	GGACCCGTATGCTTTAGGATGA
XBP1	CTGCCAGAGATCGAAAGAAGGC	CTCCTGGTTCTCAACTACAAGGC
ACC1	ATGTCTGGCTTGCACCTAGTA	CCCCAAAGCGAGTAACAAATTCT
ACC2	CAAGCCGATCACCAAGAGTAAA	CCCTGAGTTATCAGAGGCTGG
SREBF1	ACAGTGACTTCCCTGGCCTAT	GCATGGACGGGTACATCTTCAA
FAS	AAGGACCTGTCTAGGTTTGATGC	TGGCTTCATAGGTGACTTCCA
PPP1R15A	TCCGACTGCAAAGGCGGCTCA	CAGCCAGGAAATGGACAGTGAC
DDIT3	ACCAAGGGAGAACCAGGAAACG	TCACCATTCGGTCAATCAGAGC
DNAJB9	TCTTAGGTGTGCCAAAATCGG	TGTCAGGGTGGTACTTCATGG
TNF-α	CTCTTCTGCCTGCTGCACTTTG	ATGGGCTACAGGCTTGTCACTC
IL6	AGACAGCCACTCACCTCTTCAG	TTCTGCCAGTGCCTCTTTGCTG
IL1B	CCACAGACCTTCCAGGAGAATG	GTGCAGTTCAGTGATCGTACAGG

4.4 Results

4.4.1 Pimozide Stimulates IRE1/XBP1s Signaling in HepaRG Cells

SEA-mediated discovery of XBP1 as a possible therapeutic target led us to investigate the durability of this protein **(Figure 4.1 and Appendix Table 4.1)**. Subsequent computational modelling and surface analysis indicated that XBP1 is "undruggable," meaning its surface properties and configuration do not easily allow for the binding of small-molecule drugs (**Figure 4.2A**). This revelation necessitated a change in our research trajectory, given the role of XBP1 in MASLD, which led us to investigate the upstream regulator of XBP1, IRE1 (**Figure 4.2B**). To determine if antipsychotic medicines had consistent effects on IRE1, we conducted a comprehensive investigation that included a range of (Pimozide, Paliperidone, Clozapine, and Lurasidone); among all these drugs, only pimozide demonstrated a notable capability to increase IRE1 expression **(Figure 4.2C)**. These findings are consistent with our SEA findings, showing that none of the examined drugs possess XBP1 as a possible target **(Appendix Tables 4.2-4.4)**. This discovery necessitates additional exploration into the distinct molecular paths by which pimozide influences ER stress responses. IRE1 serves as a detector of unfolded proteins in the ER stress response, and it acts as an endoribonuclease, which triggers the splicing of XBP1 mRNA. We looked further into XBP1 expression to validate the distinct regulatory actions of pimozide on the endoplasmic reticulum stress response. Pimozide treatment substantially increased the transcription of XBP1 mRNA and the splicing into its active form, XBP1s (**Figure 4.2, D and E**).

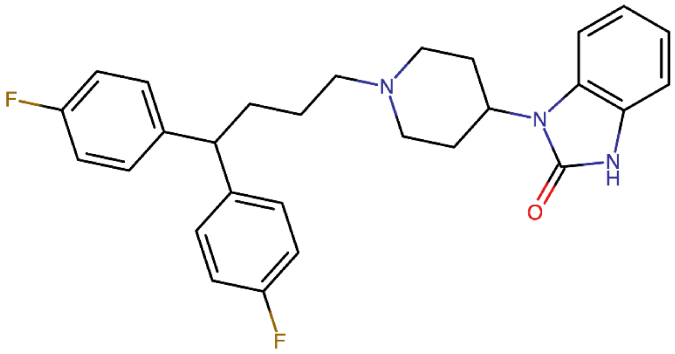

Pimozide

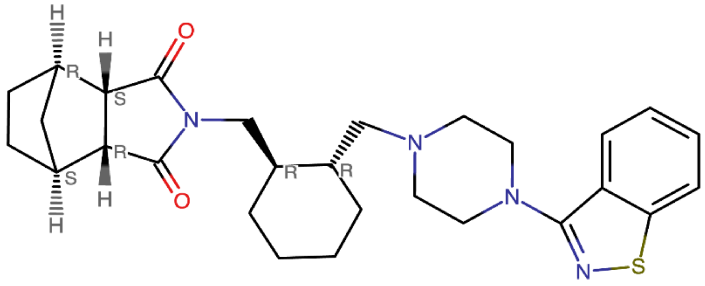

Lurasidone

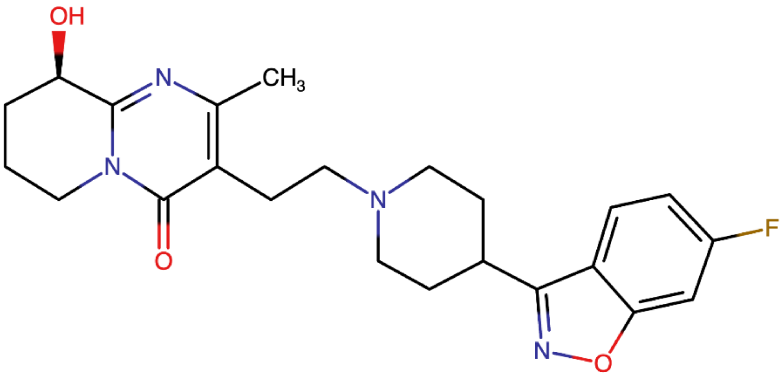

Paliperidone

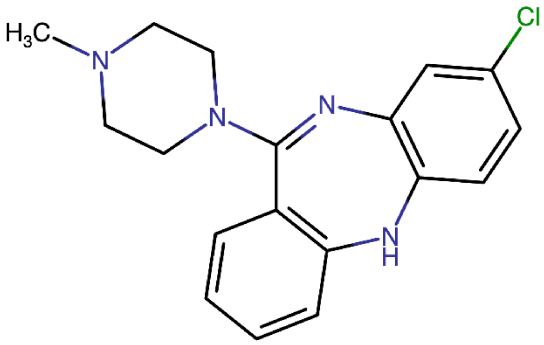

Clozapine

Figure 4.1 *Chemical Structure of Drugs Tested.*

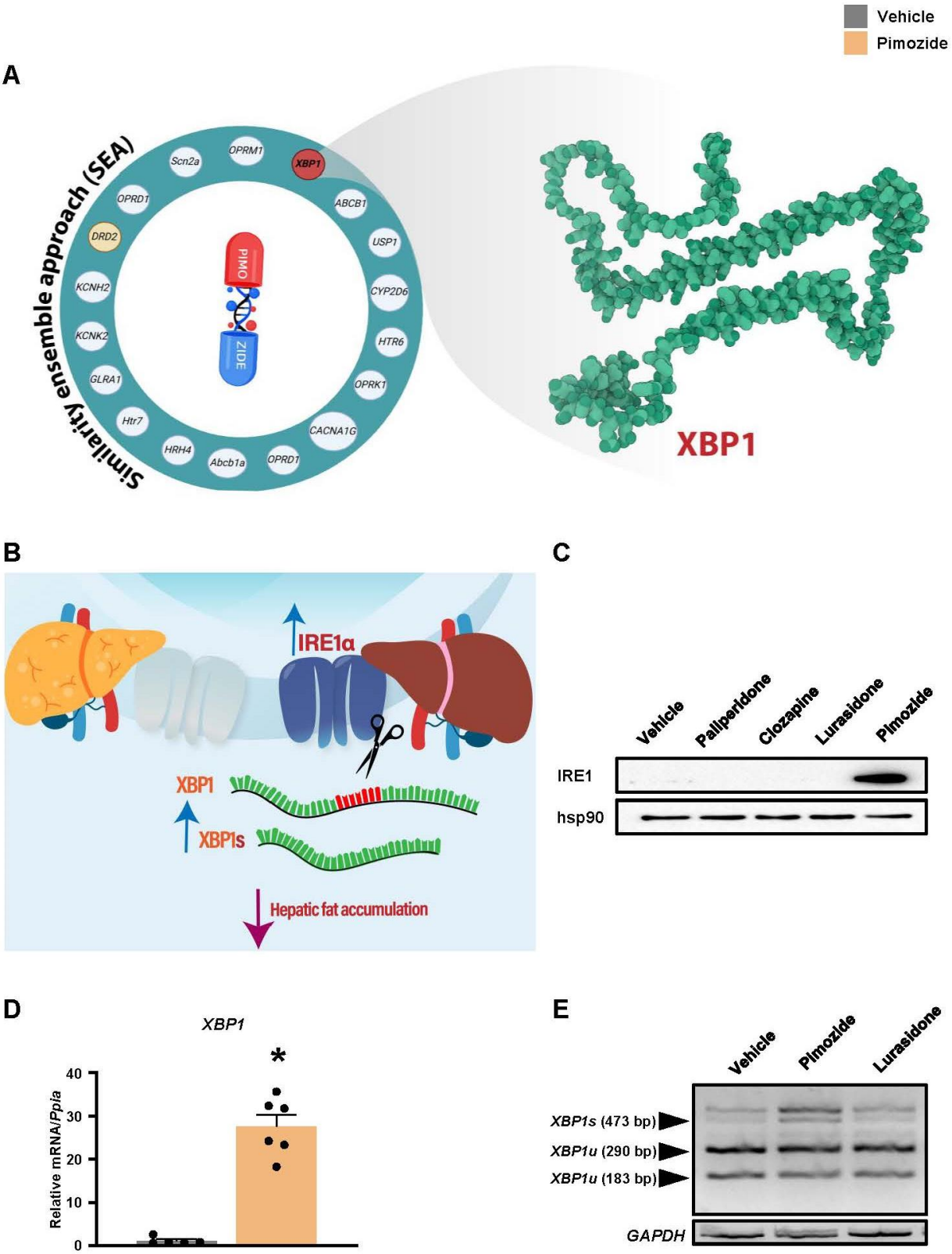
Vehicle
Pimozide
A
Similarity ensemble approach (SEA)
Scn2a
OPRM1
XBP1
ABCB1
USP1
CYP2D6
HTR6
OPRK1
CACNA1G
OPRD1
Abcb1a
HRH4
Htr7
GLRA1
KCNK2
KCNH2
DRD2
OPRD1
PIMO
ZIDE
XBP1
B
IRE1α
XBP1
XBP1s
Hepatic fat accumulation
C
Vehicle
Paliperidone
Clozapine
Lurasidone
Pimozide
IRE1
hsp90
D
XBP1
*
Relative mRNA/Ppia
40
30
20
10
0
E
Vehicle
Pimozide
Lurasidone
XBP1s (473 bp)
XBP1u (290 bp)
XBP1u (183 bp)
GAPDH

Figure 4.2 *Pimozide Enhances the Expression of IRE1/XBP1 Signaling Pathway*. **(A)** Predicted protein structure for XBP1 (AlphaFold), **(B)** Schematic represents the proposed mechanism by which pimozide (PMZ) influences hepatic lipid metabolism. The illustration hypothesizes that PMZ acts on the inositol-requiring enzyme 1 alpha (IRE1α) to modulate its activity. Subsequent activation of IRE1α leads to increased X-box binding protein 1 (XBP1) mRNA splicing, producing its active form, XBP1s. This activation cascade is suggested to result in the attenuation of hepatic fat accumulation. **(C)** Protein expression of IRE1 in HepaRG cells treated with either vehicle, paliperidone, clozapine, lurasidone, or pimozide (12.5 nM). **(D)** *XBP1* mRNA expression level in HepaRG cells treated with either vehicle or pimozide (12.5 nM) (n = 6). **(E)** HepaRG cells treated with either vehicle, pimozide, or lurasidone (12.5 nM), Post-treatment, spliced and unspliced *XBP1* mRNA were assessed using semi-quantitative RT-PCR, followed by PstI restriction enzyme digestion. *GAPDH* was used as a loading control. Values represent means ± standard error of the mean. Differences were determined using an unpaired 2-tailed Student's t-test. $*P < 0.05$, significantly different from vehicle-treated cells.

In our study, lurasidone was used as an atypical (second-generation) antipsychotic that can also antagonize D2R, hence counteracting pimozide's canonical actions on D2R. As anticipated, pimozide treatment also increased protein expressions of IRE1-XBP1s and resulted in an upregulation of the major ER chaperone, binding immunoglobulin protein (BiP) (**Figure 4.3, A-D**).

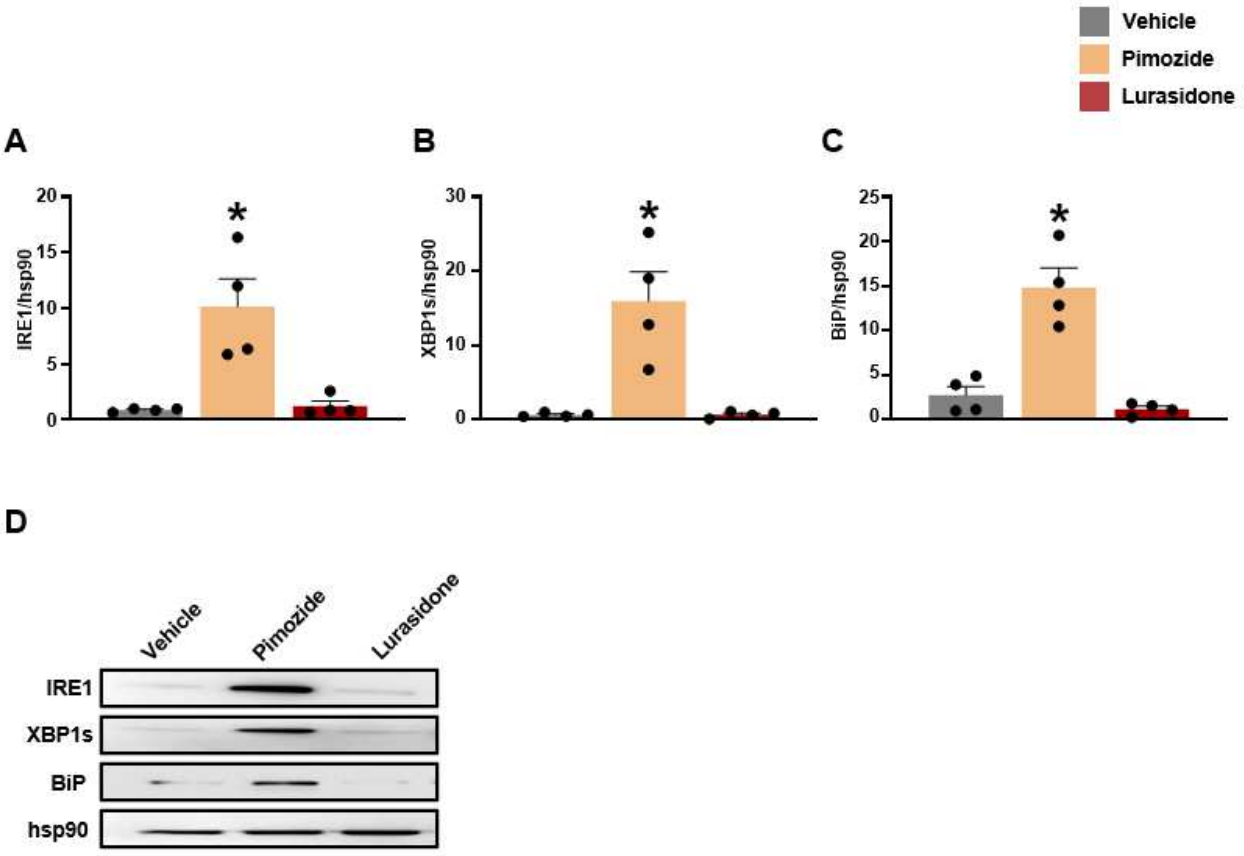

Figure 4.3 *Pimozide Stimulates IRE1/XBP1s Signaling in HepaRG Cells***.** Protein expression of **(A)** IRE1, **(B)** XBP1s, **(C)** BiP in HepaRG cells treated with either vehicle, pimozide, or Lurasidone (12.5 nM). **(E)** Corresponding representative images of western blots for the IRE1, XBP1s, and BiP (n = 4). Values represent means ± standard error of the mean. Differences were determined using a one-way ANOVA followed by a Bonferroni post-hoc analysis. *$P < 0.05$, significantly different from both vehicle and lurasidone-treated cells.

4.4.2 Pimozide Treatment Selectively Induces IRE1/XBP1s Signaling in HepaRG Cells

Next, we checked the protein kinase RNA-like ER kinase (PERK) activated during the UPR. Following 16 h of pimozide treatment, the mRNA expression genes regulated by the PERK UPR signaling pathway protein phosphatase 1 regulatory subunit 15A (*PPP1R15A*), DNA damage-inducible transcript 3 (*DDIT3*), DNAJ homolog subfamily B member 9 (*DNAJB9*) were upregulated (**Figure 4.4, A-C**). We then wanted to confirm whether the pimozide-induced IRE1 activation related to the observed upregulation of XBP1 expression, as shown in (**Figure 4.2D**). Upon knocking down IRE1, we observed that pimozide failed to increase XBP1 expression (**Figure 4.4D and E**).

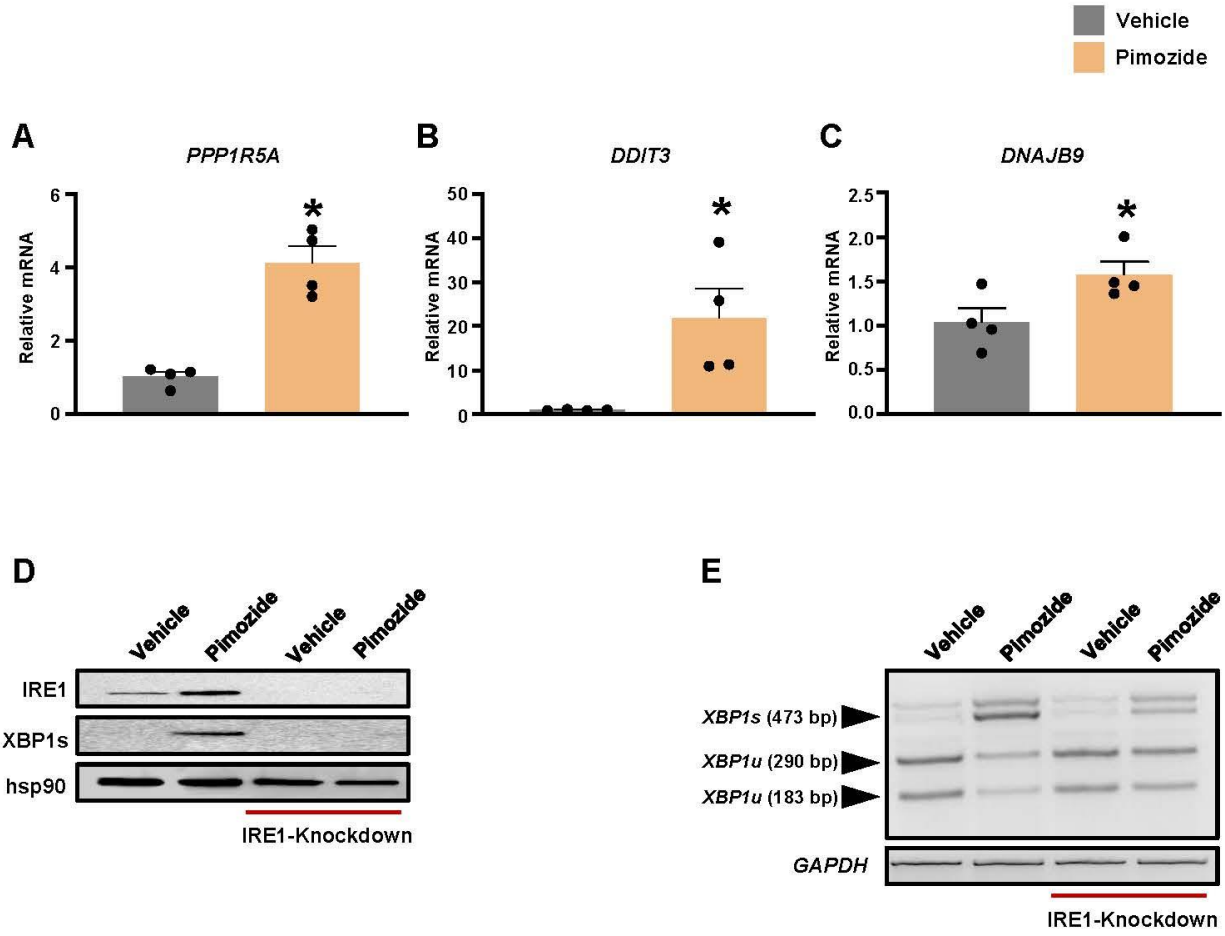
Vehicle
Pimozide
A
PPP1R5A
Relative mRNA
6
4
2
0
*
B
DDIT3
Relative mRNA
50
40
30
20
10
0
*
C
DNAJB9
Relative mRNA
2.5
2.0
1.5
1.0
0.5
0.0
*
D
Vehicle
Pimozide
Vehicle
Pimozide
IRE1
XBP1s
hsp90
IRE1-Knockdown
E
Vehicle
Pimozide
Vehicle
Pimozide
XBP1s (473 bp)
XBP1u (290 bp)
XBP1u (183 bp)
GAPDH
IRE1-Knockdown

Figure 4.4 *Selectively Induces IRE1/XBP1s Signaling in HepaRG Cells*. mRNA expression of genes involved in IRE1-regulated genes **(A)** *PPP1R5A*, **(B)** *DDIT3*, and **(C)** *DNAJB9* in HepaRG cells treated with either vehicle or pimozide (12.5 nM) (n = 4). **(D)** HepaRG cells were transfected with scrambled control siRNA or *IRE1* siRNA and treated with either vehicle control or pimozide (12.5 nM). After 48 h, the cells were harvested for immunoblotting. **(E)** HepaRG cells transfected with IRE1 siRNA and treated with either vehicle or pimozide (12.5 nM), post-treatment, spliced and unspliced *XBP1* mRNA were assessed using semi-quantitative RT-PCR, followed by PstI restriction enzyme digestion. *GAPDH* was used as a loading control. Values represent means ± standard error of the mean. Differences were determined using an unpaired 2-tailed Student's t-test. **P* < 0.05, significantly different from vehicle-treated cells.

4.4.3 Pimozide Treatment Suppresses Lipid Accumulation in HepaRG Cells Without Affecting De Novo Lipogenesis

Previous studies have highlighted the crucial role of upregulating IRE1 and XBP1 in alleviating fatty liver conditions. We next assessed the therapeutic potential associated with increased IRE1/XBP1s activity in this context. We next evaluated the therapeutic potential associated with increased IRE1/XBP1s activity in this context. Treatment with pimozide resulted in a significant decrease in lipid accumulation in HepaRG cells subjected to 2 mM oleic acid, as shown by Oil Red O staining (**Figure 4.5A**). The observed impact was attributed to the interaction of pimozide with its unique target, XBP1-IRE, instead of its canonical action method through dopamine receptors. The deduction is supported by the lack of detectable dopamine receptors in the hepatic tissue of the mice (**Figure 4.5B**). Next, compared to the control group, we evaluated gene expression of crucial de novo lipogenesis transcription factors and inflammation markers in cells treated with pimozide. Surprisingly, there was no change in the expression of key lipogenic genes, including acetyl CoA carboxylase 1 and 2 (*ACC1* and *ACC2*), sterol regulatory element binding protein 1c (*SREBP1*), fatty acid synthase (*FAS*), Interleukin-6 (*IL6*), Interleukin-1 beta (IL-1β), while there was a trend towards reducing tumour necrosis factor-alpha (*TNF-α*), a key regulator of the immune cells (**Figure 4.5C**).

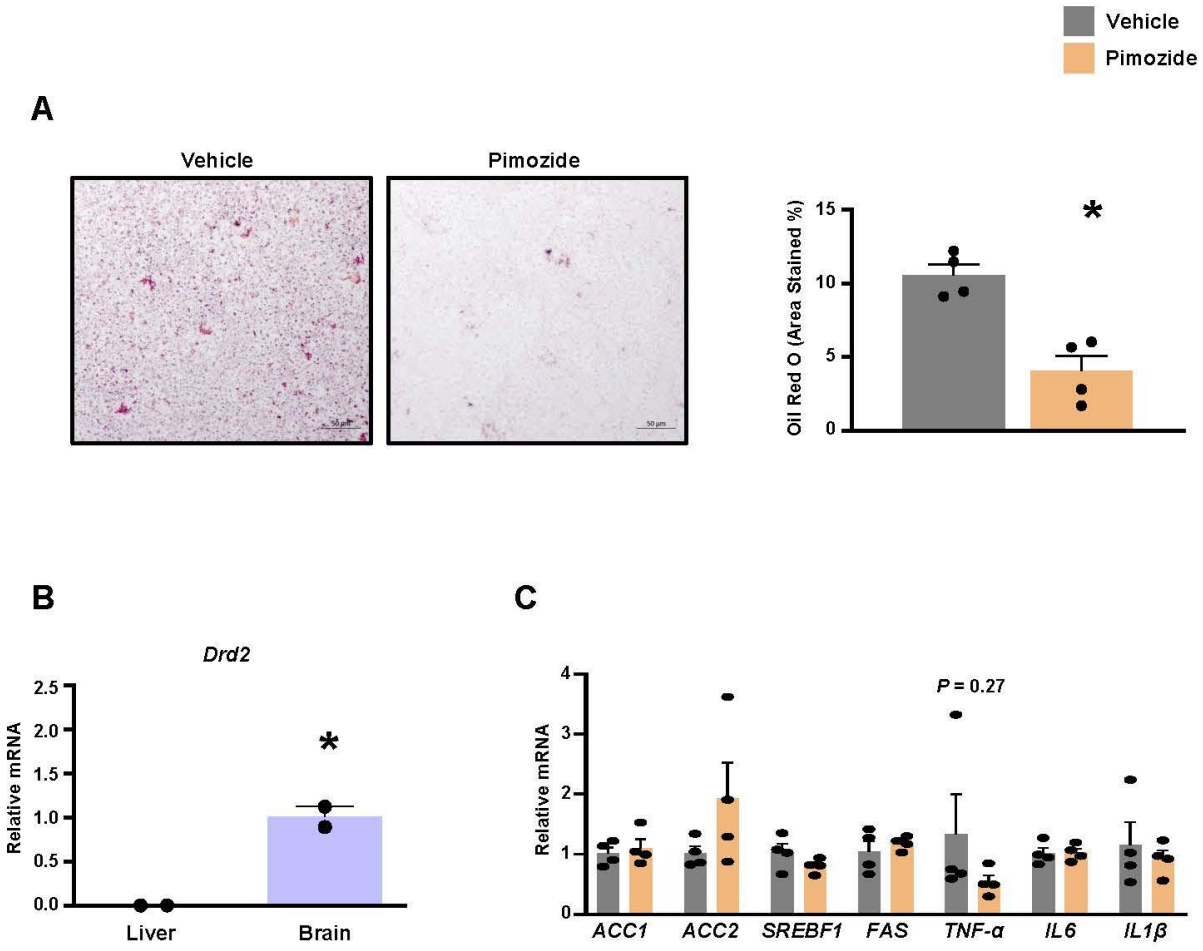
Vehicle
Pimozide
A
Vehicle
Pimozide
Oil Red O (Area Stained %)
15
10
5
0
*
B
Drd2
Relative mRNA
2.5
2.0
1.5
1.0
0.5
0.0
*
Liver
Brain
C
Relative mRNA
4
3
2
1
0
P = 0.27
ACC1
ACC2
SREBF1
FAS
TNF-α
IL6
IL1β

Figure 4.5 *Pimozide Treatment Suppresses Lipid Accumulation in HepaRG Cells Without Affecting De Novo Lipogenesis*. **(A)** Representative images of Oil Red O staining of HepaRG cells treated with either vehicle or pimozide (12.5 nM) (n = 4). **(B)** mRNA expression of gene dopamine 2 receptor (*D2rd*) in livers and brains from mice (n=2). **(C)** mRNA expression of genes involved in regulating lipogenesis and inflammation (*ACC1*, *ACC2*, *SREBF1*, *FAS*, *TNF-α*, *IL6*, *IL1β*) in HepaRG cells treated with either vehicle or pimozide (12.5 nM) (n = 4). Values represent means ± standard error of the mean. Differences were determined using an unpaired 2-tailed Student's t-test. *$P < 0.05$, significantly different from vehicle-treated cells.

4.4.4 Pimozide Treatment Does Not Mitigate Hepatic Steatosis in Male Mice Subjected to Experimental T2D.

To further elucidate whether our in vitro observation can be translated to an in vivo model. We used the experimental T2D model, which encompasses HFD supplementation for 10 weeks with a single injection of streptozotocin (STZ, 75 mg/kg) provided at the 4-week time. Pimozide treatment did not impact body weight or fat mass (**Figure 4.6, A-C**). Consistent with our previous studies, pimozide treatment markedly improved glucose tolerance test without affecting insulin sensitivity in male mice subjected to T2D, while lurasidone treatment had no effect (**Figure 4.6, D-F**).

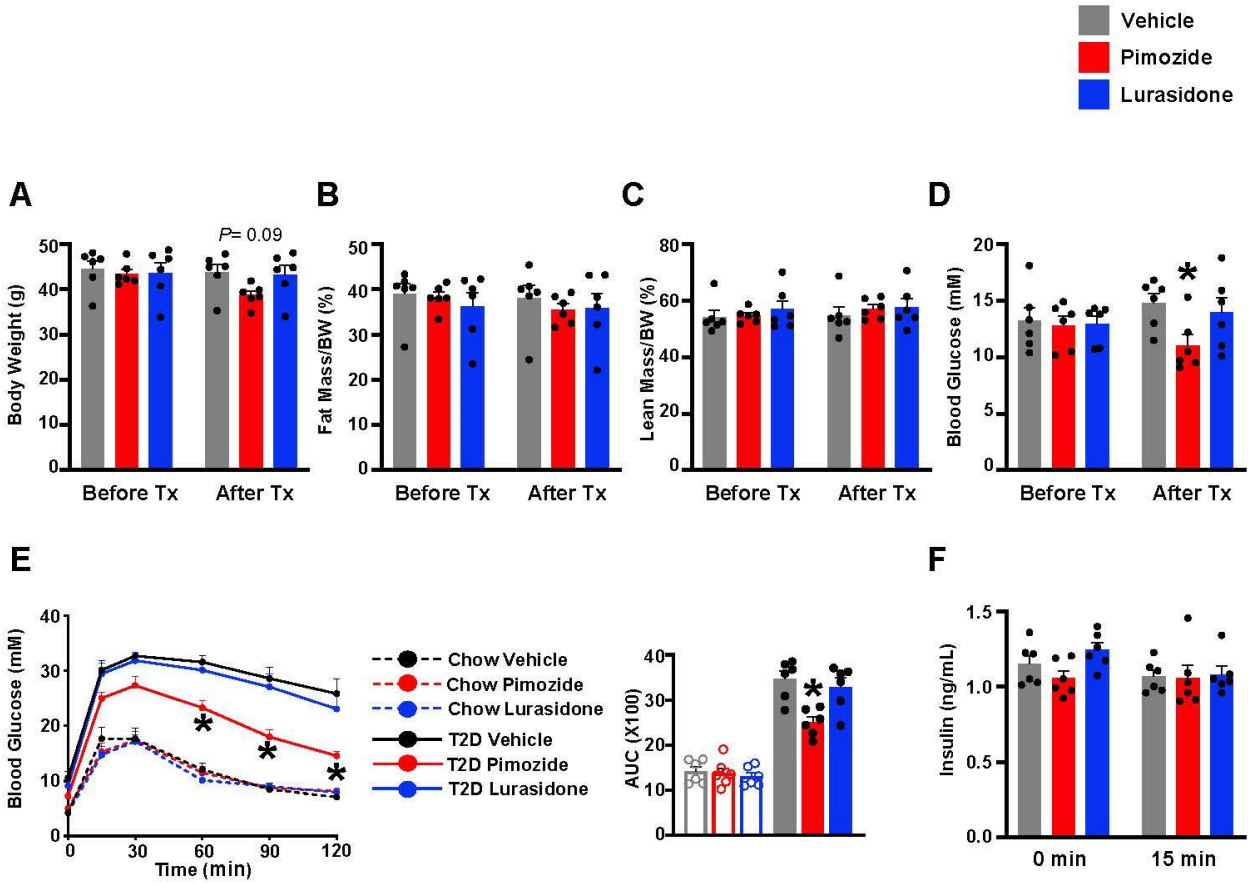
Vehicle
Pimozide
Lurasidone
A
B
C
D
P= 0.09
Body Weight (g)
Fat Mass/BW (%)
Lean Mass/BW (%)
Blood Glucose (mM)
Before Tx
After Tx
E
F
Blood Glucose (mM)
Time (min)
Chow Vehicle
Chow Pimozide
Chow Lurasidone
T2D Vehicle
T2D Pimozide
T2D Lurasidone
AUC (X100)
Insulin (ng/mL)
0 min
15 min

Figure 4.6 *Pimozide Treatment Improved Glucose Homeostasis in Male Mice Subjected to Experimental T2D*. **(A)** Body weight, **(B)** % fat mass, **(C)** % lean mass, and **(D)** ad libitum blood glucose levels of male mice subjected to experimental T2D before and after 2 weeks of treatment with either vehicle, pimozide, or lurasidone (10 mg/kg every 48 h) for 2 weeks (n = 6). **(E)** Glucose tolerance and its associated area under the curve (AUC) of lean mice fed a chow diet and experimental T2D mice (n = 6) 2 weeks post-treatment. **(F)** Plasma insulin levels before (0 min) and (15 min) after IP glucose injection. Values represent means ± standard error of the mean. Differences were determined using one-way ANOVA or 2-way ANOVA followed by a Bonferroni post-hoc analysis. *$P < 0.05$, significantly different from vehicle-treated mice.

Next, we assessed hepatic steatosis in experimental T2D treated with pimozide. However, no changes were observed in liver weights, hepatic TAG content, and circulating TAG following pimozide treatment, as shown in Oil Red O staining (**Figure 4.7, A-D**). Expanding on our earlier observation of pimozide-mediated improvement in hepatic steatosis through upregulating the IRE1-XBP1 pathway in HepaRG cells, we measured the hepatic protein expressions of IRE1, XBP1, and BiP in experimental T2D male mice. However, in line with the absence of improvement in hepatic steatosis, pimozide-treated mice with experimental T2D did not exhibit an upregulation in these protein levels (**Figure 4.7, E-H**).

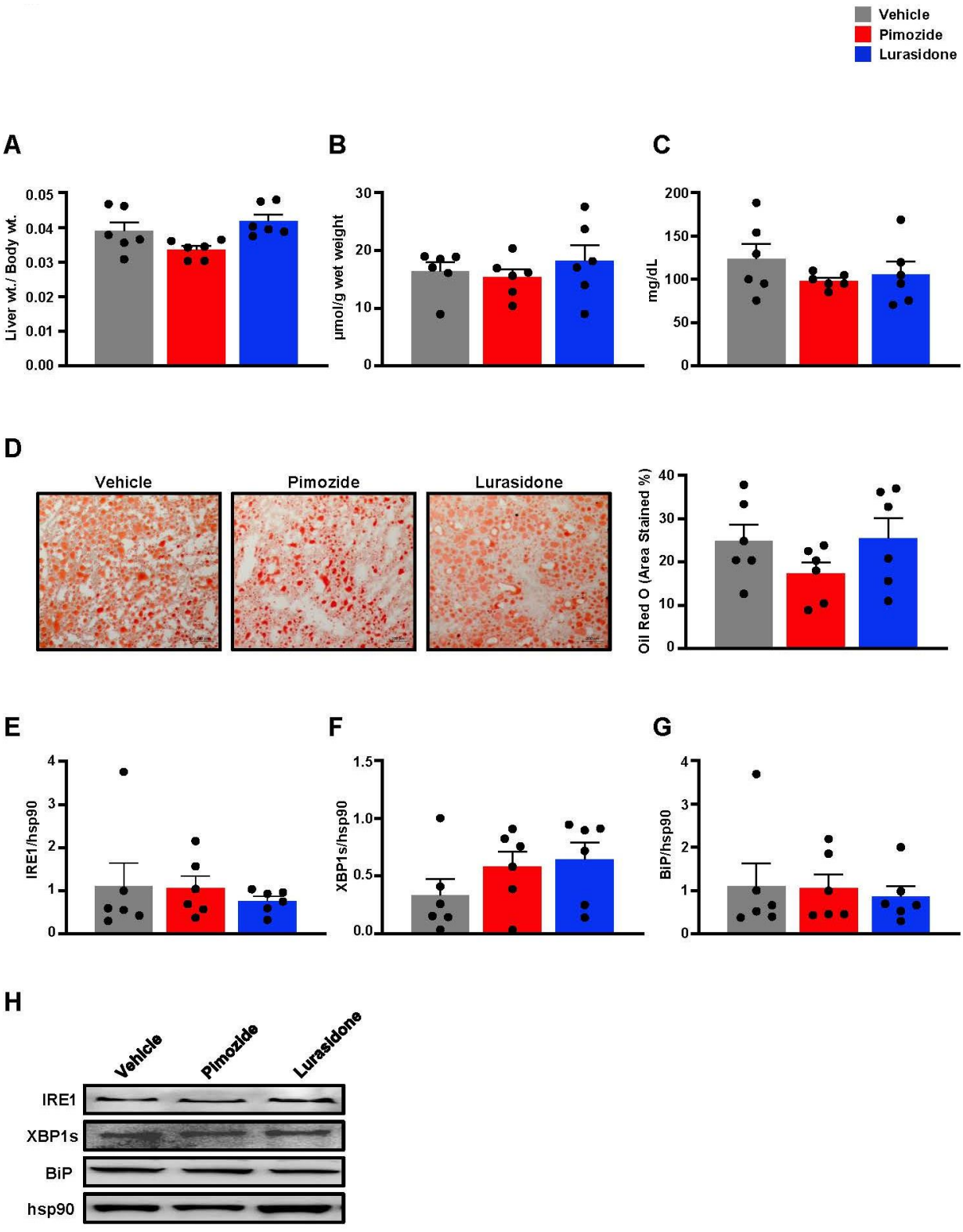
Vehicle
Pimozide
Lurasidone
A
Liver wt./ Body wt.
0.05
0.04
0.03
0.02
0.01
0.00
B
µmol/g wet weight
30
20
10
0
C
mg/dL
200
150
100
50
0
D
Vehicle
Pimozide
Lurasidone
Oil Red O (Area Stained %)
40
30
20
10
0
E
IRE1/hsp90
4
3
2
1
0
F
XBP1s/hsp90
1.5
1.0
0.5
0.0
G
BiP/hsp90
4
3
2
1
0
H
Vehicle
Pimozide
Lurasidone
IRE1
XBP1s
BiP
hsp90

Figure 4.7 *Pimozide Treatment Does Not Mitigate Hepatic Steatosis in Male Mice Subjected to Experimental T2D*. **(A)** Liver weights, **(B)** hepatic TAG content, **(C)** circulating TAG levels, **(D)** representative images of Oil Red O staining of mice livers in male mice subjected to T2D treated with either vehicle, pimozide, or lurasidone (10 mg/kg every 48 h) for 2 weeks (n = 6). **(E)** IRE1, **(F)** XBP1s, **(G)** BiP in livers from male mice subjected to T2D treated with either vehicle, pimozide, or lurasidone (10 mg/kg every 48 h) for 2 weeks (n = 6). **(H)** Corresponding representative images of western blots for the IRE1, XBP1s, and BiP (n = 6). Values represent means ± standard error of the mean. Differences were determined using a one-way ANOVA followed by a Bonferroni post-hoc analysis.

4.5 Discussion

Pimozide, an older-generation antipsychotic agent typically employed for managing tics in individuals with Tourette syndrome, acts primarily by inhibiting D2R (214). Our previous research demonstrated its binding affinity to SCOT, enhancing glucose tolerance in obese mice (128). Since the SCOT enzyme (114, 215) nor D2R expression is detected in the liver (www.proteinatlas.org; Date Accessed: March 16, 2024), the observed effect of pimozide in our current investigation is attributed to its modulation of a novel target as pimozide's action on hepatocytes is unlikely to be mediated through its canonical D2R. Moreover, our investigation reveals that pimozide, compared to other antipsychotic D2R antagonists, has a distinct ability to increase IRE1 levels, indicating possible therapeutic benefits. This finding highlights the significance of investigating different targets for repurposing pimozide in liver-related illnesses providing novel perspectives on its mechanism of action beyond its conventional application in neuropsychiatric disorders.

While pimozide treatment effectively ameliorated steatosis, our investigation indicated no discernible impact on lipogenesis markers. This observation may be due to hepatocyte heterogeneity, where cells exhibit varying abilities to retain lipids and distinct metabolic profiles (216). Furthermore, the deletion of IRE1, specifically in hepatocytes, did not affect the process of lipogenesis; however, it specifically hindered the assembly and release of VLDL, resulting in hepatic steatosis and hypolipidemia (160). Thus, the exact mechanism by which ER stress influences lipid accumulation and/or release via the IRE1α/XBP1 pathway is a topic of debate. Interestingly, cells treated with pimozide showed a downward trend in the levels of *TNF-α*, a crucial cytokine that promotes inflammation. Studies have shown that the activation of XBP1 can

reduce the inflammatory reactions caused by TNF-α in cultured human umbilical vein endothelial cells. Increased expression of spliced XBP1 has been associated with decreased upregulation of inflammatory biomarkers, such as Intercellular Adhesion Molecule 1 and Monocyte Chemoattractant Protein-1, produced by TNF-α (217). This suggests that spliced XBP1 has a suppressive effect on TNF-α-driven inflammatory pathways.

Eukaryotic initiation factor 2 alpha (eIF2α) also plays a vital role in the cellular response to ER stress. The cell activates the UPR to restore homeostasis. Phosphorylation of eIF2α is a key aspect of this response, possibly evolving as a transient signal in stressed cells. However, sustained eIF2α phosphorylation can be detrimental and lead to cell death (218). Our data showed that treatment with pimozide activates *PP1R15A*, *DDIT3*, and *DNAJB9*, collectively known as growth arrest and DNA damage-inducible protein 34. Previous studies revealed that the activation of DNA damage-inducible protein 34, coupled with the ensuing delayed dephosphorylation of eIF2α, serves as a regulatory mechanism facilitating the translation of specific mRNAs (154); notably, this includes transcripts such as BiP. Our findings contribute to a nuanced understanding of the molecular pathways through which pimozide modulates cellular responses to ER stress.

Unfortunately, given that pimozide therapy could not lower the hepatic TAG content in mice with experimental T2D, those findings do not seem to apply to MASLD linked to T2D. Although HepaRG cells were used as the in vitro model in our investigation, providing a helpful platform for the initial phases of drug development, it is crucial to acknowledge the inherent constraints of laboratory-based assays. The intricacies of biological processes within living creatures necessitate the cautious extrapolation of these in vitro discoveries to in vivo scenarios. The transition from

laboratory research conducted outside of a living organism to real-life situations within living organisms can pose difficulties and variations because of the intricate nature of biological systems. In vitro, investigations are limited in accurately replicating the interactions between a pharmaceutical chemical and the various substances and cell types found in a living organism. This constraint can affect the transfer of results from controlled laboratory experiments to practical, real-world applications. Biomedical researchers employ many techniques, such as animal models, tissue cultures, and computational simulations, to investigate human diseases and disorders. Although in vitro experiments have the benefit of repeatability, they may not accurately reflect in vivo responses due to variations in biokinetics factors and the atypical behaviour of malignant cell lines usually employed in vitro (219). Although in vitro research is both cost-effective and ethically preferable, it lacks the intricate nature of organ systems seen in living animals. This constraint impedes the ability to translate in vitro discoveries to human reactions, particularly in relation to biochemical processes such as metabolization.

Pimozide is frequently used orally as an antipsychotic medicine in therapeutic settings. It is approved for treating disorders such as Tourette syndrome, schizophrenia, and psychosis. Significant hepatic metabolism occurs with pimozide, and no human cases of hepatotoxicity or acute liver injury have been documented. Recent research has shown that pimozide may effectively reduce the viability of HCC by potentially decreasing the expression of epithelial cell adhesion molecules. It is imperative to emphasize that this impact has solely been investigated using in vitro models, as shown by experiments done using Hep3B, HepG2, and Sk-Hep-1 (220). Currently, there is a lack of clinical trials investigating the efficacy of pimozide in the treatment of hepatocellular carcinoma in human patients.

Pimozide's favourable impact on glycemic control seems primarily observed in individuals with obesity and/or T2D, as current preclinical evidence indicates (128, 221). However, this beneficial effect does not appear to extend to individuals with T2D who also have MASLD. One drawback of our work is that we only assessed hepatic steatosis by quantifying tissue TAG content using the Bligh and Dyer method (199), which involves extracting chloroform:methanol. In future studies, it will be crucial to validate our findings by employing pulse-chase analysis to examine the kinetics of apolipoprotein B (apoB), very-low-density lipoprotein triglyceride (VLDL-TAG) secretion, and fatty acid oxidation. This approach will offer valuable insights into the fundamental cellular mechanisms associated with lipid metabolism.

In summary, although the encouraging results indicate that the antipsychotic treatment pimozide exhibits novel effects in mitigating steatosis in HepaRG cells, this potential does not seem to extend to MASLD associated with T2D.

Acknowledgement

CTS was supported by an Alberta Diabetes Institute Graduate Studentship Award, an Antoine Noujaim Graduate Scholarship in Pharmaceutical Sciences, Alberta Graduate Excellence Scholarship, and Graduate Student Engagement Scholarship. JRU is a Tier 2 Canada Research Chair (Pharmacotherapy of Energy Metabolism in Obesity).

Conflict of Interest

The authors have no conflicts to declare.

Chapter 5: Discussion

5.1 Metabolic Dysfunction-Associated Steatohepatitis Liver Disease and Liver Glucose Metabolism

5.1.1 Overview

MASLD is now the predominant chronic liver disease globally due to its intricate etiology and diagnostic challenges. Glucose overconsumed in the diet is processed through glycolysis in the liver. This process ultimately results in the transformation of glucose into fatty acids, which are subsequently converted into TAG and secreted as VLDL. Insulin regulates hepatic glucose production by managing the breakdown of fats in adipose tissues, which decreases the amount of fatty acids entering the liver. This leads to lower levels of hepatic acetyl-CoA and reduced PDC activity, resulting in a decrease in the conversion of pyruvate to glucose in the liver. In individuals with MASLD and insulin resistance, the rapid breakdown of fat in adipose tissue results in higher glucose production in the liver, increasing the process of DNL creation in the liver (222). In addition, PDH activity is inhibited in malnutrition and diabetes by phosphorylating the PDHα subunit, a primary cause of glucose intolerance (223-225). Interestingly, due to poor insulin control of hepatic glucose uptake and synthesis, hepatic glucose production in obesity and insulin resistance remains normal or higher despite hyperinsulinemia (226). Significantly, MASLD is characterized by impaired PDH activity, which exacerbates the metabolic dysregulation of the disease.

The impairment of PDH activity in metabolic syndrome has also been extensively investigated in numerous studies (227-229). The current research has demonstrated that ranolazine, a second-line antianginal drug, improves heart function via activating PDH (182, 230-232). Our latest study found that it may be beneficial in treating MASLD associated with obesity (138). Subsequently, we aimed to determine whether ranolazine provides similar benefits in MASLD associated with T2D **(Chapter 2)** and whether its effects on hepatic PDH are direct, as examined in our later study **(Chapter 3)**. The results in **Chapter 2** found no notable alterations in body weight, fat mass, or glycemia in lean or T2D mice after receiving ranolazine treatment. Furthermore, ranolazine did not influence insulin sensitivity, hepatic glucose production, or hepatic steatosis in mice with T2D. No significant changes were observed in the expression of key lipogenesis or fatty acid oxidation regulators. While prior research revealed that ranolazine could increase hepatic PDH activity in obese mice, this effect was not observed in T2D mice, showing any change in hepatic PDH status following ranolazine treatment in this setting.

As discussed in **Chapter 2**, the lack of effectiveness of ranolazine treatment in improving MASLD in experimental T2D mice may be due to its inability to increase hepatic PDH activity and glucose utilization in these mice. In the comparison between obesity and T2D, there is a significant difference in hepatic PDH activity. Research has revealed specific patterns showing that increased hepatic PDH activity in obese mice is associated with protective effects against obesity-associated MetS, such as MASLD, by enhancing glucose oxidation rates (117). Obese mice with increased hepatic PDH activity typically show enhancements in glucose metabolism and general metabolic health, which may help reduce the development or advancement of MASLD. Targeting hepatic PDKs is a promising technique to restore metabolic balance in obesity and diabetes by controlling

PDH activity (133). The regulatory mechanisms governing PDH activity (e.g insulin resistance, elevated fatty acids, and inflammatory pathway) may differ in T2D mice, suggesting a potential divergence in the modulation of PDH function in the context of diabetes (233). Studies emphasize the crucial function of PDKs in regulating the activity of the PDC and glucose metabolism in different tissues, such as the liver and muscle, suggesting that targeting PDK could be a novel approach in T2D (234-236). The complex relationship between PDK expression, PDC activity, and metabolic diseases highlights the numerous mechanisms that control glucose use and energy metabolism in various physiological situations.

In **Chapter 3**, we investigated the metabolic characteristics of *Pdha1*$^{\text{Liver}-/-}$ mice and their response to induced obesity and ranolazine therapy. *Pdha1*$^{\text{Liver}-/-}$ mice did not exhibit significant alterations in body weight, body composition, or glucose levels compared to control mice, irrespective of the diet. Furthermore, they did not show worsened high blood glucose levels when exposed to experimental obesity. Lean *Pdha1*$^{\text{Liver}-/-}$ mice had higher amounts of circulating TAG, but their hepatic TAG content did not change. Molecular profiling identified no substantial changes in gene expression associated with lipogenesis or lipid metabolism. Ranolazine therapy did not improve hepatic steatosis, glucose tolerance, or pyruvate tolerance in obese *Pdha1*$^{\text{Liver}-/-}$ mice. Ranolazine decreased TAG levels in the blood and liver of obese control mice but not in *Pdha1*$^{\text{Liver}-/-}$ animals. Ranolazine changed mRNA expression associated with lipogenesis in *Pdha1*$^{\text{Liver}-/-}$ mice but did not affect fibrosis-related gene expression. The results indicate that deleting hepatic PDH affects the responsiveness to ranolazine treatment in obese mice, showing a complicated relationship between PDH activity and ranolazine's effectiveness in reducing hepatic steatosis.

The human PDHα component is encoded by two genes: *PDHA1* on chromosome X, expressed in somatic cells, and *PDHA2* on chromosome 4, expressed exclusively in the testes (237-240). Deleting *Pdha1* leads to systemic PDC insufficiency, a metabolic disease that causes substantial damage to the central nervous system (241). *PDHA1* deficiency is linked to multiple neurodegenerative disorders such as Alzheimer's disease, epilepsy, and Leigh's syndrome (242-244), with symptoms ranging from severe lactic acidosis leading to death to long-term dementia. Previous research showed that PDH heart knockout mice displayed diastolic dysfunction, as evidenced by a decreased mitral E/A ratio. This indicates that limiting glucose oxidation in the hearts of *Pdha1* cardiac knockout mice is enough to cause a cardiomyopathy-like condition (245). Similarly, in the heart and muscle knockout mouse model, male mice died within 7 days after weaning when fed a rodent chow diet but survived with a high-fat diet. These mice displayed left ventricular hypertrophy and diminished left ventricular systolic function compared to wild-type male mice (246). These findings underscore the importance of PDH in maintaining cardiac function and overall metabolic homeostasis. Consequently, we posited that *Pdha1* liver knockout mice would manifest severe liver damage and glucose intolerance. Surprisingly, male *Pdha1*$^{\text{Liver}-/-}$ mice did not change body weight or glucose tolerance compared to their male Alb$^{\text{Cre}}$ littermates after being fed a low-fat diet for 12 weeks, although worsening pyruvate tolerance was seen. Our results align with the research conducted by Choi *et al*., who examined mice lacking the liver's PDH enzyme. Similarly, we did not detect any alterations in body composition or blood glucose levels, as liver glucose consumption is just one of the factors influencing total glucose metabolism (247). Nevertheless, we characterized different mouse models fed with an HFD. Elevated PDH levels may signify variations in tissue function and energy utilization during the progression of obesity (248). Given the pivotal roles of the liver and adipose tissue in fatty acid synthesis (249),

a limitation of our study was that the primary focus was on the alterations in hepatic mRNA and protein expression of key regulators of lipid metabolism without exploring other relevant variables or organs such as adipose tissue. Potential compensatory mechanisms in the adipose tissue of *Pdha1*$^{\text{Liver}-/-}$ mice were not considered.

A limitation of our study is that we did not do a pharmacokinetic assessment after administering ranolazine through oral gavage, nor did we quantify the levels of the drug in the bloodstream. This hinders our capacity to fully comprehend the systemic exposure and pharmacological impacts of ranolazine within the framework of our animal model. Incorporating these data in future research is essential for a comprehensive assessment of the drug's pharmacokinetic profile and its relationship with therapeutic results. The dose of ranolazine selected for this study was determined based on our prior research, which involved administering 50 mg once daily and observing positive effects on fatty liver and glucose intolerance. However, it is crucial to take into account the pharmacokinetics of ranolazine, particularly its brief half-life of approximately 2 to 6 hours. Considering the fast clearance, future investigations should examine the possible advantages of delivering ranolazine twice daily to provide more stable plasma levels and potentially improve its therapeutic effectiveness. Another limitation of our work is that the levels of alanine aminotransferase (ALT) and aspartate aminotransferase (AST) in our diabetic mouse model were much higher than the standard ranges observed in healthy mice. Typically, ALT levels in mice in good health range from 17 to 77 U/L, whereas the levels of AST range from 54 to 298 U/L (250). The increased levels of ALT and AST in our model indicate possible hepatic stress or damage that exceeds the usual expectations in normal type 2 diabetes models. This disparity could impact the understanding of metabolic and hepatic results and should be taken into account when

extrapolating our findings to other investigations. Subsequent research should clarify the reasons behind these increased enzyme levels and evaluate their influence on the development and effectiveness of disease pathogenesis and treatment.

Future research could investigate adipose tissue changes to understand the metabolic adjustments that have been reported further. Studying the rates of acetate oxidation in adipose tissue could provide valuable insights into metabolic modifications related to PDH deficiency.

5.1.2 Future Directions

Studies have shown that PDKs, specifically PDK2 and PDK4, have a role in altering metabolic processes, causing insulin resistance, and regulating glucose metabolism. Targeting PDKs could provide a new and innovative approach to controlling metabolic diseases such as MASLD and T2D (251). PDK inhibitors, such as dichloroacetate (DCA) and AZD7545, have been studied for their possible therapeutic effects on metabolic diseases by altering PDK activity (252). Studies have examined DCA's metabolic impact in individuals with diabetes, revealing encouraging results. DCA has decreased plasma glucose and lipids in individuals with diabetes (253). Dichloroacetate exhibited an antidiabetic effect by diminishing gluconeogenesis. A solitary administration of DCA in normal rats resulted in a reduction of plasma pyruvate levels and fasting plasma glucose levels, while treatment with DCA in diabetic ob/ob mice resulted in decreased gluconeogenesis and levels of glucose, suggesting the beneficial use of DCA in T2D related metabolic diseases (254). DCA broadly targets PDKs in peripheral tissues, whereas AZD7545, a novel inhibitor specifically targeting PDK2, demonstrates a higher level of specificity. This

selectivity leads to a more noticeable increase in the activity of the PDC in the liver compared to skeletal muscle and heart tissues (249, 255). AZD7545 has demonstrated the ability to activate PDH in vivo and improve blood glucose control by targeting specific domains of PDKs, such as the lipoamide-binding domain (213, 214). Preclinical studies have further supported AZD7545's efficacy in activating PDH in vivo and improving blood glucose control in obese rats (215). This targeted approach highlights its therapeutic potential in enhancing glucose metabolism and addressing metabolic disorders. A previous study found that the expression of PDK4 was higher in the muscle of insulin-resistant mice compared to their liver. As a result, the liver's pyruvate dehydrogenase complex (PDC) has lower activity than the muscle of PDK4 knockout mice fed an HFD (256). This indicates that PDK4 plays a more critical role in the muscle than in the liver. In contrast, PDK2 exhibits more significant levels of expression in the liver than PDK4. Therefore, the increased expression of PDK2 in the liver could serve as a more suitable model for investigating MASLD.

5.2 Metabolic Dysfunction-Associated Steatohepatitis Liver Disease and Endoplasmic Reticulum Stress

5.2.1 Overview

The study in **Chapter 4** investigates the therapeutic efficacy of pimozide in treating MASLD and T2D. The findings demonstrate that pimozide interacts with SCOT in skeletal muscle, affecting glucose metabolism. Additionally, pimozide binds exclusively to IRE1, a crucial regulator of ER. The administration of pimozide in HepaRG cells leads to a notable increase in the expression of IRE1 and XBP1s mRNA and protein levels. This indicates the activation of the UPR, which

subsequently results in a reduction in lipid accumulation. Curiously, the cause of this effect is ascribed to the drug's interaction with the IRE1-XBP1 pathway instead of its recognized impact on dopamine receptors, which were not found in liver tissues. The effectiveness of pimozide in laboratory conditions differs from its effectiveness in living organisms. While it improved steatosis in HepaRG, it does not impact hepatic steatosis in mice, suggesting a complicated relationship between pimozide's effects on cells and the body's overall metabolism. The research emphasizes the need for more studies to clarify the complete spectrum of effects of pimozide and its potential usefulness in treating metabolic diseases.

The observed disparity between the results obtained from our in vitro experiments and those done on in vivo mice can be ascribed to using HepaRG, a human hepatic cell line, for our initial in vitro investigations. Although mice and humans share genetic and physiological similarities, evolutionary divergence can result in different reactions to experimental interventions. The translatability of study findings may be impacted by changes in genetic networks that link genes to diseases between mice and humans, which can result in mice not always precisely reflecting human responses (257). The intricate nature of human diseases may not be adequately represented by mouse models, resulting in variations in how therapies or disease processes are observed in people compared to mice. The limitations of mouse models in accurately depicting the complex nature of human diseases can impede the translation of findings from human cell studies to rodent models (258). Although mice have proven to help study human biology and disease, they may not always accurately mimic the course of human diseases. The effectiveness of treatments in healing diseases in mice may not be replicated in humans, underscoring the difficulties in converting discoveries from animal models to practical applications (257). The response of mice to

experimental interventions frequently differs from that of humans, highlighting the importance of caution when extending findings from human cell line investigations to mouse models. Understanding the evolved distinctions and resemblances between mice and humans is essential for appropriately interpreting research findings.

The disparity in drug response between in vitro systems, such as HepaRG cells, and in vivo environments is a widely acknowledged constraint in pharmacokinetic and drug metabolism research. Although HepaRG cells exhibit advanced functional features, such as the presence of phase I and II enzymes and transporters, they do not fully duplicate the dynamic drug handling and flow in a real organism. Within a living organism, medications undergo intricate absorption, distribution, metabolism, and excretion processes. These processes are affected by blood flow throughout the body, interactions with different types of cells, and ongoing mechanisms of transformation and elimination. Nevertheless, in vitro systems such as HepaRG cells usually entail stagnant settings where the medication is supplied to the culture medium and digested by the cells, but without the ongoing removal and input of fresh drugs as would happen in the circulation. This can result in the medication and its metabolites building up in the culture media, which can saturate metabolic pathways and cause non-physiological interactions. Additionally, the drug transport mechanisms in HepaRG cells may not accurately replicate those found in human liver tissue due to variations in the expression levels of transport proteins and the lack of natural organ structure and intercellular connections. Consequently, the drug's concentration within cells and the surrounding environment may not correctly represent its concentration within the tissues of a living organism. Therefore, although HepaRG cells offer essential insights into liver metabolism and toxicity in controlled settings, it is crucial to be cautious when applying these findings to anticipate

how drugs will behave in the body and how they will affect patients. In order to improve the accuracy and applicability of drug metabolism and pharmacokinetic studies utilizing HepaRG cells, it is essential to conduct bridging studies that involve more sophisticated in vitro models or include in vivo data. Pimozide undergoes metabolism via both CYP3A4 and CYP2D6 enzymes. The presence of genetic variations in CYP2D6 can affect the pharmacokinetics of pimozide. While HepaRG cells exhibit CYP2D6 expression, this enzyme's levels and functional activity in HepaRG cells are often lower than primary human hepatocytes (259). The decrease in activity can affect the precision of forecasts for CYP2D6-mediated drug metabolism and interactions when employing HepaRG cells. Therefore, although HepaRG cells are a valuable model for studying metabolism in a laboratory setting, validating the findings related to CYP2D6 metabolism with additional data obtained from in vitro or in vivo experiments is necessary. It is important to comprehend how drugs behave in clinical situations fully, especially those extensively metabolized by CYP2D6. A limitation of our study is that we did not directly measure the levels of pimozide in the liver in our in vivo model. Not incorporating this information limits our comprehension of the hepatic storage and local breakdown of pimozide, hindering our ability to evaluate its pharmacodynamics and potential hepatotoxic consequences. Measuring the amount of pimozide in the liver would give us important information about how it is spread throughout the liver, how quickly it is broken down, and how it interacts with enzymes in the liver. This would help us better understand how effectively pimozide reduces fatty liver. Incorporating these data in future research would provide a more thorough assessment of pimozide's in vivo pharmacokinetic and pharmacodynamic properties.

A limitation of our study is that we did not thoroughly investigate the range of targets affected by pimozide. The drug's well-established dopaminergic action is widely acknowledged. However,

there is a growing understanding that pimozide can prevent the phosphorylation of a critical tyrosine residue, which is necessary to activate the signal transducer and activator of transcription 5 (STAT5) (260, 261). The inhibitory impact of pimozide on STAT5 phosphorylation suggests its participation in a broader range of metabolic pathways. The involvement of STAT5 in hepatic steatosis is intricate and exhibits some conflicting aspects. Deficiency in STAT5, specifically in the context of growth hormone (GH)-dependent signalling, has been associated with hepatic lipids accumulation and changes in the activity of genes responsible for fatty acid metabolism. On the other hand, when STAT5 is activated, it seems to have a beneficial effect in avoiding fat accumulation in the liver, indicating an essential role in preserving liver health and metabolic equilibrium. Furthermore, studies conducted on male mice lacking hepatic STAT5a/b have shown that the absence of GH-dependent STAT5 signalling is associated with increased activity of STAT1 and STAT3, which contributes to liver diseases (262). In addition, suppressing STAT5 activity using dominant-negative STAT5 resulted in an elevated lipid uptake in a mouse hepatoma cell line (263). Suppressing STAT5 has also been linked to potential consequences in ER stress; studies indicate that the inhibition of STAT5 may trigger the activation of ER stress pathways (264). Additional research is necessary to determine if its impact on ER stress directly causes the observed effects of pimozide or if they result from the suppression of STAT5 signaling.

5.2.2 Future Directions

Subsequent investigations to validate the interaction between pimozide and IRE1, methods such as co-immunoprecipitation and bimolecular fluorescence complementation assays could be employed to elucidate the molecular specificity and functional consequences of this drug-target

engagement. These robust analytical approaches may provide a comprehensive understanding of the binding affinity and the subsequent biological effects induced by pimozide on the IRE1 protein complex within cellular systems. Pimozide treatment reduced steatosis in HepaRG cells, which coincided with the increase in the expression of IRE1. In order to ascertain whether IRE1 facilitates pimozide's effect on steatosis attenuation, we would want to knockdown IRE1 and examine the possibility of steatosis after IRE1 depletion provides clarity on the reliance of pimozide's therapeutic actions on the IRE1 signalling pathway.

The aim is to determine whether pimozide affects the PERK/eIF2α/ATF4 pathway of the UPR, which regulates lipid homeostasis in MASLD (265-267); PERK activates the phosphorylation of eukaryotic initiation factor 2 alpha (eIF2α), which in turn promotes the selective translation of activating transcription factor 4 (ATF4). This signalling cascade regulates hepatic lipid metabolism and forms steatosis in MASLD. Additionally, the ATF6 branch of the UPR also has a role in causing ER stress and MASLD (268). When there is stress in the ER, ATF6 moves to the Golgi apparatus, which is broken down by proteolytic cleavage, releasing its active form, ATF6f. ATF6f subsequently moves into the nucleus to activate genes linked with endo ER protein folding, lipid metabolism, and ER-associated degradation. ATF6 activation contributes to the adaptive response to ER stress in MASLD by affecting the production of lipid droplets and lipid metabolism.

In our in vivo animal models, pimozide treatment did not enhance the IRE1-XBP1 pathway, leading to no amelioration of hepatic steatosis. The results of this study do not render IRE1 an ineffective target for the treatment of MASLD. However, additional research is required to ascertain the applicability of our findings across various liver cell lines, hence offering further

elucidation on the fundamental mechanisms and prospective therapeutic targets associated with liver-related illnesses. We previously used HepaRG cells, which exhibit gene expression, biotransformation activities, and responses to inducers of cytochrome P450 enzymes that closely resemble those of human hepatocytes, present a more dependable and physiologically significant in vitro model as compared to experiments conducted on mice. We will use various human liver cell lines, including HepG2, Huh7, Hep3B, and SK-Hep-1. We also plan to use a mouse liver cell line, Hepa1c1c7.

Our SEA data results indicate that pimozide interacts with calcium voltage-gated channel subunit alpha1 G (CACNA1G). In addition, MASLD and HCC tissue samples show overexpression of CACNA1G and other calcium signalling genes (269). This indicates that the disruption of calcium signalling pathways involving CACNA1G may have a role in the development and advancement of MASLD. In addition, a model of MASLD using human pluripotent stem cells showed that the development of a MASLD-like condition was linked to an increase in the expression of CACNA1G , along with other genes (270). This supports the notion that CACNA1G may have a function in the development of MASLD (269, 271-273). Hence, we plan to conduct a more in-depth investigation.

Ketogenesis is a process that exclusively occurs in hepatocytes. This is due to the abundant expression of mitochondrial HMGCS2 in hepatocytes, which is needed for ketogenesis. Additionally, hepatocytes lack SCOT, which is responsible for breaking down ketone bodies (114). As a result, hepatocytes do not use the ketone bodies they produce. In a recent study, macrophage-specific SCOT knockout mice fed with 60% HFD for 8 weeks. While the SCOT-Macrophage-KO

animals showed comparable levels of total ketone bodies in their blood plasma compared to their littermate controls, disruptions in glycosaminoglycan metabolism were found in both cultured macrophages without SCOT and in the liver tissue of mice with SCOT deficiency in macrophages (274). The occurrence of these metabolic disturbances was found to be associated with the development of hepatic fibrogenesis. Transcriptional changes associated with fibrogenesis were observed in the livers of SCOT-Macrophage-KO mice. These changes included increased expression of mRNAs for the angiogenic factor (vascular endothelial growth factor C), the mitogen (platelet-derived growth factor A), and the pro-fibrotic cytokine Il13 (274).

In a previous study, we established that pimozide can inhibit SCOT in the muscles (128); however, its effects on macrophages remain unknown. Nevertheless, there is a potential for the in vivo impact of pimozide to vary due to communication between macrophages and hepatocytes. Therefore, we aim to examine the interaction between HepaRG cells and macrophages treated with pimozide to gain a deeper understanding of the underlying mechanism and assess potential therapeutic benefits.

5.3 Concluding Remarks

MASLD and T2D are characterized by a disturbance in converting energy, indicating various possible targets for treatment to reverse the disease's pathology and prevent it from advancing to more severe stages (117, 275). The illness is commonly linked to systemic metabolic dysfunctions, such as hyperglycemia, insulin resistance, and obesity, highlighting its significant impact on energy metabolism that extends beyond liver-related disorders. Thus, enhancing PDH could be a

potential therapeutic target for treating hepatic steatosis (276, 277). Unfortunately, ranolazine treatment did not mitigate MASLD associated with T2D. Therefore, targeting PDK may have therapeutic potential in rectifying aberrant metabolic pathways implicated in fatty liver disease.

Persistent ER stress can lead to the loss of physiological function, cell death in liver cells, and more severe consequences, including liver damage and disease progression (278). Chronic ER stress is associated with the progression of MASLD to more severe stages like MASH and fibrosis, highlighting its detrimental impact on liver health (279). However, acute ER stress can be beneficial by activating adaptive responses that aim to restore cellular homeostasis and promote cell survival under stress conditions. IRE1 is a crucial component of ER stress responses, and targeting this pathway can have therapeutic implications for liver diseases like MASLD (280). Although pimozide treatment failed to alleviate hepatic steatosis in a murine model, the drug could upregulate IRE1 expression and reduce steatosis in hepatocyte-like cells, such as HepaRG.

Ultimately, while ranolazine was effective in boosting PDH activity in MASLD related to obesity, it may not have the same outcome in MASLD associated with T2D. Additional investigation into the pathways via which pimozide decreases steatosis in HepaRG cells will aid in determining if pimozide might be repurposed for treating MASLD related to MetS.

Bibliography

1. Haas JT, Francque S, Staels B. Pathophysiology and Mechanisms of Nonalcoholic Fatty Liver Disease. Annual Review of Physiology2016. p. 181-205.

2. Perry RJ, Samuel VT, Petersen KF, Shulman GI. The role of hepatic lipids in hepatic insulin resistance and type 2 diabetes. Nature. 2014;510(7503):84-91.

3. Sun DQ, Targher G, Byrne CD, Wheeler DC, Wong VW, Fan JG, et al. An international Delphi consensus statement on metabolic dysfunction-associated fatty liver disease and risk of chronic kidney disease. Hepatobiliary Surg Nutr. 2023;12(3):386-403.

4. Chan WK, Chuah KH, Rajaram RB, Lim LL, Ratnasingam J, Vethakkan SR. Metabolic Dysfunction-Associated Steatotic Liver Disease (MASLD): A State-of-the-Art Review. J Obes Metab Syndr. 2023;32(3):197-213.

5. Han SK, Baik SK, Kim MY. Non-alcoholic fatty liver disease: Definition and subtypes. Clin Mol Hepatol. 2023;29(suppl):S5-S16.

6. Ayonrinde OT. Historical narrative from fatty liver in the nineteenth century to contemporary NAFLD - Reconciling the present with the past. JHEP Rep. 2021;3(3):100261.

7. Liu Y, Zhong GC, Tan HY, Hao FB, Hu JJ. Nonalcoholic fatty liver disease and mortality from all causes, cardiovascular disease, and cancer: a meta-analysis. Scientific reports. 2019;9(1):11124.

8. Paik JM, Golabi P, Younossi Y, Mishra A, Younossi ZM. Changes in the Global Burden of Chronic Liver Diseases From 2012 to 2017: The Growing Impact of NAFLD. Hepatology. 2020;72(5):1605-16.

9. Younossi Z, Anstee QM, Marietti M, Hardy T, Henry L, Eslam M, et al. Global burden of NAFLD and NASH: Trends, predictions, risk factors and prevention. Nature Reviews Gastroenterology and Hepatology. 2018;15(1):11-20.

10. Devarbhavi H, Asrani SK, Arab JP, Nartey YA, Pose E, Kamath PS. Global burden of liver disease: 2023 update. J Hepatol. 2023;79(2):516-37.

11. Younossi ZM, Golabi P, Paik JM, Henry A, Van Dongen C, Henry L. The global epidemiology of nonalcoholic fatty liver disease (NAFLD) and nonalcoholic steatohepatitis (NASH): a systematic review. Hepatology. 2023;77(4):1335-47.

12. Mantovani A, Byrne CD, Bonora E, Targher G. Nonalcoholic fatty liver disease and risk of incident type 2 diabetes: A meta-analysis. Diabetes Care. 2018;41(2):372-82.

13. Monetti M, Levin MC, Watt MJ, Sajan MP, Marmor S, Hubbard BK, et al. Dissociation of Hepatic Steatosis and Insulin Resistance in Mice Overexpressing DGAT in the Liver. Cell Metabolism. 2007;6(1):69-78.

14. Fan R, Wang J, Du J. Association between body mass index and fatty liver risk: A dose-response analysis. Sci Rep. 2018;8(1):15273.

15. Huang JF, Tsai PC, Yeh ML, Huang CF, Huang CI, Hsieh MH, et al. Risk stratification of non-alcoholic fatty liver disease across body mass index in a community basis. J Formos Med Assoc. 2020;119(1 Pt 1):89-96.

16. Fabbrini E, Sullivan S, Klein S. Obesity and nonalcoholic fatty liver disease: biochemical, metabolic, and clinical implications. Hepatology. 2010;51(2):679-89.

17. Godoy-Matos AF, Silva Junior WS, Valerio CM. NAFLD as a continuum: from obesity to metabolic syndrome and diabetes. Diabetol Metab Syndr. 2020;12:60.

18. Loomba R, Friedman SL, Shulman GI. Mechanisms and disease consequences of nonalcoholic fatty liver disease. Cell. 2021;184(10):2537-64.

19. Friedman SL, Neuschwander-Tetri BA, Rinella M, Sanyal AJ. Mechanisms of NAFLD development and therapeutic strategies. Nat Med. 2018;24(7):908-22.

20. Engin AB. What Is Lipotoxicity? Adv Exp Med Biol. 2017;960:197-220.

21. Boren J, Watts GF, Adiels M, Soderlund S, Chan DC, Hakkarainen A, et al. Kinetic and Related Determinants of Plasma Triglyceride Concentration in Abdominal Obesity: Multicenter Tracer Kinetic Study. Arterioscler Thromb Vasc Biol. 2015;35(10):2218-24.

22. Chen Z, Tian R, She Z, Cai J, Li H. Role of oxidative stress in the pathogenesis of nonalcoholic fatty liver disease. Free Radic Biol Med. 2020;152:116-41.

23. Hardy T, Oakley F, Anstee QM, Day CP. Nonalcoholic Fatty Liver Disease: Pathogenesis and Disease Spectrum. Annu Rev Pathol. 2016;11:451-96.

24. Borrelli A, Bonelli P, Tuccillo FM, Goldfine ID, Evans JL, Buonaguro FM, et al. Role of gut microbiota and oxidative stress in the progression of non-alcoholic fatty liver disease to hepatocarcinoma: Current and innovative therapeutic approaches. Redox Biol. 2018;15:467-79.

25. Ma Q. Role of nrf2 in oxidative stress and toxicity. Annu Rev Pharmacol Toxicol. 2013;53:401-26.

26. Li L, Fu J, Liu D, Sun J, Hou Y, Chen C, et al. Hepatocyte-specific Nrf2 deficiency mitigates high-fat diet-induced hepatic steatosis: Involvement of reduced PPARgamma expression. Redox Biol. 2020;30:101412.

27. Li J, Wang T, Liu P, Yang F, Wang X, Zheng W, et al. Hesperetin ameliorates hepatic oxidative stress and inflammation via the PI3K/AKT-Nrf2-ARE pathway in oleic acid-induced HepG2 cells and a rat model of high-fat diet-induced NAFLD. Food Funct. 2021;12(9):3898-918.

28. Qu LL, Yu B, Li Z, Jiang WX, Jiang JD, Kong WJ. Gastrodin Ameliorates Oxidative Stress and Proinflammatory Response in Nonalcoholic Fatty Liver Disease through the AMPK/Nrf2 Pathway. Phytother Res. 2016;30(3):402-11.

29. Arroyave-Ospina JC, Wu Z, Geng Y, Moshage H. Role of Oxidative Stress in the Pathogenesis of Non-Alcoholic Fatty Liver Disease: Implications for Prevention and Therapy. Antioxidants (Basel). 2021;10(2).

30. Ramanathan R, Ali AH, Ibdah JA. Mitochondrial Dysfunction Plays Central Role in Nonalcoholic Fatty Liver Disease. Int J Mol Sci. 2022;23(13).

31. Zheng Y, Wang S, Wu J, Wang Y. Mitochondrial metabolic dysfunction and non-alcoholic fatty liver disease: new insights from pathogenic mechanisms to clinically targeted therapy. J Transl Med. 2023;21(1):510.

32. Shin S, Kim J, Lee JY, Kim J, Oh CM. Mitochondrial Quality Control: Its Role in Metabolic Dysfunction-Associated Steatotic Liver Disease (MASLD). J Obes Metab Syndr. 2023;32(4):289-302.

33. Sokolowska E, Blachnio-Zabielska A. The Role of Ceramides in Insulin Resistance. Front Endocrinol (Lausanne). 2019;10:577.

34. Pagadala M, Kasumov T, McCullough AJ, Zein NN, Kirwan JP. Role of ceramides in nonalcoholic fatty liver disease. Trends Endocrinol Metab. 2012;23(8):365-71.

35. Postic C, Girard J. Contribution of de novo fatty acid synthesis to hepatic steatosis and insulin resistance: lessons from genetically engineered mice. J Clin Invest. 2008;118(3):829-38.

36. Poss AM, Summers SA. Too Much of a Good Thing? An Evolutionary Theory to Explain the Role of Ceramides in NAFLD. Front Endocrinol (Lausanne). 2020;11:505.

37. Hajduch E, Lachkar F, Ferre P, Foufelle F. Roles of Ceramides in Non-Alcoholic Fatty Liver Disease. J Clin Med. 2021;10(4).

38. Han HS, Kang G, Kim JS, Choi BH, Koo SH. Regulation of glucose metabolism from a liver-centric perspective. Exp Mol Med. 2016;48(3):e218.

39. Ramatchandirin B, Pearah A, He L. Regulation of Liver Glucose and Lipid Metabolism by Transcriptional Factors and Coactivators. Life (Basel). 2023;13(2).

40. Schneeweiss B, Graninger W, Ferenci P, Eichinger S, Grimm G, Schneider B, et al. Energy metabolism in patients with acute and chronic liver disease. Hepatology. 1990;11(3):387-93.

41. Dewidar B, Mastrototaro L, Englisch C, Ress C, Granata C, Rohbeck E, et al. Alterations of hepatic energy metabolism in murine models of obesity, diabetes and fatty liver diseases. EBioMedicine. 2023;94:104714.

42. Ren M, Li J, Xue R, Wang Z, Coll SL, Meng Q. Liver function and energy metabolism in hepatocellular carcinoma developed in patients with hepatitis B-related cirrhosis. Medicine (Baltimore). 2019;98(19):e15528.

43. Rui L. Energy metabolism in the liver. Compr Physiol. 2014;4(1):177-97.

44. Shao M, Ye Z, Qin Y, Wu T. Abnormal metabolic processes involved in the pathogenesis of non-alcoholic fatty liver disease (Review). Exp Ther Med. 2020;20(5):26.

45. McGlinchey AJ, Govaere O, Geng D, Ratziu V, Allison M, Bousier J, et al. Metabolic signatures across the full spectrum of non-alcoholic fatty liver disease. JHEP Rep. 2022;4(5):100477.

46. Deprince A, Haas JT, Staels B. Dysregulated lipid metabolism links NAFLD to cardiovascular disease. Mol Metab. 2020;42:101092.

47. Ismaiel A, Dumitrascu DL. Cardiovascular Risk in Fatty Liver Disease: The Liver-Heart Axis-Literature Review. Front Med (Lausanne). 2019;6:202.

48. Chao HW, Chao SW, Lin H, Ku HC, Cheng CF. Homeostasis of Glucose and Lipid in Non-Alcoholic Fatty Liver Disease. Int J Mol Sci. 2019;20(2).

49. Sanyal AJ, Brunt EM, Kleiner DE, Kowdley KV, Chalasani N, Lavine JE, et al. Endpoints and clinical trial design for nonalcoholic steatohepatitis. Hepatology. 2011;54(1):344-53.

50. Takahashi Y, Fukusato T. Histopathology of nonalcoholic fatty liver disease/nonalcoholic steatohepatitis. World J Gastroenterol. 2014;20(42):15539-48.

51. Browning JD, Szczepaniak LS, Dobbins R, Nuremberg P, Horton JD, Cohen JC, et al. Prevalence of hepatic steatosis in an urban population in the United States: impact of ethnicity. Hepatology. 2004;40(6):1387-95.

52. Dyson JK, Anstee QM, McPherson S. Non-alcoholic fatty liver disease: a practical approach to diagnosis and staging. Frontline Gastroenterol. 2014;5(3):211-8.

53. Williams CD, Stengel J, Asike MI, Torres DM, Shaw J, Contreras M, et al. Prevalence of nonalcoholic fatty liver disease and nonalcoholic steatohepatitis among a largely middle-aged population utilizing ultrasound and liver biopsy: a prospective study. Gastroenterology. 2011;140(1):124-31.

54. Burt AD, Lackner C, Tiniakos DG. Diagnosis and Assessment of NAFLD: Definitions and Histopathological Classification. Semin Liver Dis. 2015;35(3):207-20.

55. Karlas T, Petroff D, Garnov N, Bohm S, Tenckhoff H, Wittekind C, et al. Non-invasive assessment of hepatic steatosis in patients with NAFLD using controlled attenuation parameter and 1H-MR spectroscopy. PLoS One. 2014;9(3):e91987.

56. Schwimmer JB, Middleton MS, Behling C, Newton KP, Awai HI, Paiz MN, et al. Magnetic resonance imaging and liver histology as biomarkers of hepatic steatosis in children with nonalcoholic fatty liver disease. Hepatology. 2015;61(6):1887-95.

57. Ferrannini E, Bjorkman O, Reichard GA, Jr., Pilo A, Olsson M, Wahren J, et al. The disposal of an oral glucose load in healthy subjects. A quantitative study. Diabetes. 1985;34(6):580-8.

58. Chen LQ, Cheung LS, Feng L, Tanner W, Frommer WB. Transport of sugars. Annu Rev Biochem. 2015;84:865-94.

59. de Souza Cordeiro LM, Bainbridge L, Devisetty N, McDougal DH, Peters DJM, Chhabra KH. Loss of function of renal Glut2 reverses hyperglycaemia and normalises body weight in mouse models of diabetes and obesity. Diabetologia. 2022;65(6):1032-47.

60. Burcelin R, del Carmen Munoz M, Guillam MT, Thorens B. Liver hyperplasia and paradoxical regulation of glycogen metabolism and glucose-sensitive gene expression in GLUT2-null hepatocytes. Further evidence for the existence of a membrane-based glucose release pathway. J Biol Chem. 2000;275(15):10930-6.

61. Guillam MT, Burcelin R, Thorens B. Normal hepatic glucose production in the absence of GLUT2 reveals an alternative pathway for glucose release from hepatocytes. Proc Natl Acad Sci U S A. 1998;95(21):12317-21.

62. Rajas F, Gautier-Stein A, Mithieux G. Glucose-6 Phosphate, A Central Hub for Liver Carbohydrate Metabolism. Metabolites. 2019;9(12).

63. Murray B, Rosenbloom C. Fundamentals of glycogen metabolism for coaches and athletes. Nutr Rev. 2018;76(4):243-59.

64. Adeva-Andany MM, Gonzalez-Lucan M, Donapetry-Garcia C, Fernandez-Fernandez C, Ameneiros-Rodriguez E. Glycogen metabolism in humans. BBA Clin. 2016;5:85-100.

65. Adeva-Andany MM, Perez-Felpete N, Fernandez-Fernandez C, Donapetry-Garcia C, Pazos-Garcia C. Liver glucose metabolism in humans. Biosci Rep. 2016;36(6).

66. Ge T, Yang J, Zhou S, Wang Y, Li Y, Tong X. The Role of the Pentose Phosphate Pathway in Diabetes and Cancer. Front Endocrinol (Lausanne). 2020;11:365.

67. Jin ES, Lee MH, Murphy RE, Malloy CR. Pentose phosphate pathway activity parallels lipogenesis but not antioxidant processes in rat liver. Am J Physiol Endocrinol Metab. 2018;314(6):E543-E51.

68. Ham M, Choe SS, Shin KC, Choi G, Kim JW, Noh JR, et al. Glucose-6-Phosphate Dehydrogenase Deficiency Improves Insulin Resistance With Reduced Adipose Tissue Inflammation in Obesity. Diabetes. 2016;65(9):2624-38.

69. Chandramouli V, Ekberg K, Schumann WC, Kalhan SC, Wahren J, Landau BR. Quantifying gluconeogenesis during fasting. Am J Physiol. 1997;273(6):E1209-15.

70. Jensen J, Rustad PI, Kolnes AJ, Lai YC. The role of skeletal muscle glycogen breakdown for regulation of insulin sensitivity by exercise. Front Physiol. 2011;2:112.

71. Hers HG, Hue L. Gluconeogenesis and related aspects of glycolysis. Annu Rev Biochem. 1983;52:617-53.

72. Owen OE, Kalhan SC, Hanson RW. The key role of anaplerosis and cataplerosis for citric acid cycle function. J Biol Chem. 2002;277(34):30409-12.

73. Petersen MC, Vatner DF, Shulman GI. Regulation of hepatic glucose metabolism in health and disease. Nat Rev Endocrinol. 2017;13(10):572-87.

74. Chourpiliadis C, Mohiuddin SS. Biochemistry, Gluconeogenesis. StatPearls. Treasure Island (FL) with ineligible companies. Disclosure: Shamim Mohiuddin declares no relevant financial relationships with ineligible companies.2024.

75. Onyango AN. Excessive gluconeogenesis causes the hepatic insulin resistance paradox and its sequelae. Heliyon. 2022;8(12):e12294.

76. Xiang J, Chen C, Liu R, Gou D, Chang L, Deng H, et al. Gluconeogenic enzyme PCK1 deficiency promotes CHK2 O-GlcNAcylation and hepatocellular carcinoma growth upon glucose deprivation. J Clin Invest. 2021;131(8).

77. Xu D, Wang Z, Xia Y, Shao F, Xia W, Wei Y, et al. The gluconeogenic enzyme PCK1 phosphorylates INSIG1/2 for lipogenesis. Nature. 2020;580(7804):530-5.

78. Millward CA, Desantis D, Hsieh CW, Heaney JD, Pisano S, Olswang Y, et al. Phosphoenolpyruvate carboxykinase (Pck1) helps regulate the triglyceride/fatty acid cycle and development of insulin resistance in mice. J Lipid Res. 2010;51(6):1452-63.

79. Ye Q, Liu Y, Zhang G, Deng H, Wang X, Tuo L, et al. Deficiency of gluconeogenic enzyme PCK1 promotes metabolic-associated fatty liver disease through PI3K/AKT/PDGF axis activation in male mice. Nat Commun. 2023;14(1):1402.

80. Hliwa A, Ramos-Molina B, Laski D, Mika A, Sledzinski T. The Role of Fatty Acids in Non-Alcoholic Fatty Liver Disease Progression: An Update. Int J Mol Sci. 2021;22(13).

81. Iqbal J, Hussain MM. Intestinal lipid absorption. Am J Physiol Endocrinol Metab. 2009;296(6):E1183-94.

82. Zilversmit DB. Formation and transport of chylomicrons. Fed Proc. 1967;26(6):1599-605.

83. Hudgins LC, Hellerstein M, Seidman C, Neese R, Diakun J, Hirsch J. Human fatty acid synthesis is stimulated by a eucaloric low fat, high carbohydrate diet. J Clin Invest. 1996;97(9):2081-91.

84. Ferre P, Foufelle F. SREBP-1c transcription factor and lipid homeostasis: clinical perspective. Horm Res. 2007;68(2):72-82.

85. Schlein C, Fischer AW, Sass F, Worthmann A, Todter K, Jaeckstein MY, et al. Endogenous Fatty Acid Synthesis Drives Brown Adipose Tissue Involution. Cell Rep. 2021;34(2):108624.

86. Pepino MY, Kuda O, Samovski D, Abumrad NA. Structure-function of CD36 and importance of fatty acid signal transduction in fat metabolism. Annu Rev Nutr. 2014;34:281-303.

87. Glatz JFC, Luiken J. Dynamic role of the transmembrane glycoprotein CD36 (SR-B2) in cellular fatty acid uptake and utilization. J Lipid Res. 2018;59(7):1084-93.

88. Zeng H, Qin H, Liao M, Zheng E, Luo X, Xiao A, et al. CD36 promotes de novo lipogenesis in hepatocytes through INSIG2-dependent SREBP1 processing. Mol Metab. 2022;57:101428.

89. Shao W, Yu Z, Chiang Y, Yang Y, Chai T, Foltz W, et al. Curcumin prevents high fat diet induced insulin resistance and obesity via attenuating lipogenesis in liver and inflammatory pathway in adipocytes. PLoS One. 2012;7(1):e28784.

90. Prasad S, Gupta SC, Tyagi AK, Aggarwal BB. Curcumin, a component of golden spice: from bedside to bench and back. Biotechnol Adv. 2014;32(6):1053-64.

91. Liu Y, Cheng F, Luo Y, Zhan Z, Hu P, Ren H, et al. PEGylated Curcumin Derivative Attenuates Hepatic Steatosis via CREB/PPAR-gamma/CD36 Pathway. Biomed Res Int. 2017;2017:8234507.

92. Vacca M, Allison M, Griffin JL, Vidal-Puig A. Fatty Acid and Glucose Sensors in Hepatic Lipid Metabolism: Implications in NAFLD. Semin Liver Dis. 2015;35(3):250-61.

93. Trefts E, Gannon M, Wasserman DH. The liver. Curr Biol. 2017;27(21):R1147-R51.

94. Gaggini M, Carli F, Rosso C, Buzzigoli E, Marietti M, Della Latta V, et al. Altered amino acid concentrations in NAFLD: Impact of obesity and insulin resistance. Hepatology. 2018;67(1):145-58.

95. Lake AD, Novak P, Shipkova P, Aranibar N, Robertson DG, Reily MD, et al. Branched chain amino acid metabolism profiles in progressive human nonalcoholic fatty liver disease. Amino Acids. 2015;47(3):603-15.

96. Wewer Albrechtsen NJ, Junker AE, Christensen M, Haedersdal S, Wibrand F, Lund AM, et al. Hyperglucagonemia correlates with plasma levels of non-branched-chain amino acids in patients with liver disease independent of type 2 diabetes. Am J Physiol Gastrointest Liver Physiol. 2018;314(1):G91-G6.

97. Wiklund P, Zhang X, Pekkala S, Autio R, Kong L, Yang Y, et al. Insulin resistance is associated with altered amino acid metabolism and adipose tissue dysfunction in normoglycemic women. Sci Rep. 2016;6:24540.

98. Yoon MS. The Emerging Role of Branched-Chain Amino Acids in Insulin Resistance and Metabolism. Nutrients. 2016;8(7).

99. Amanatidou AI, Mikropoulou EV, Amerikanou C, Milanovic M, Stojanoski S, Bjelan M, et al. Plasma Amino Acids in NAFLD Patients with Obesity Are Associated with Steatosis and Fibrosis: Results from the MAST4HEALTH Study. Metabolites. 2023;13(8).

100. Acevedo A, Jones AE, Danna BT, Turner R, Montales KP, Beninca C, et al. The BCKDK inhibitor BT2 is a chemical uncoupler that lowers mitochondrial ROS production and de novo lipogenesis. bioRxiv. 2023.

101. Wang W, Zhang F, Xia Y, Zhao S, Yan W, Wang H, et al. Defective branched chain amino acid catabolism contributes to cardiac dysfunction and remodeling following myocardial infarction. Am J Physiol Heart Circ Physiol. 2016;311(5):H1160-H9.

102. White PJ, McGarrah RW, Grimsrud PA, Tso SC, Yang WH, Haldeman JM, et al. The BCKDH Kinase and Phosphatase Integrate BCAA and Lipid Metabolism via Regulation of ATP-Citrate Lyase. Cell Metab. 2018;27(6):1281-93 e7.

103. Zhou M, Shao J, Wu CY, Shu L, Dong W, Liu Y, et al. Targeting BCAA Catabolism to Treat Obesity-Associated Insulin Resistance. Diabetes. 2019;68(9):1730-46.

104. Bollinger E, Peloquin M, Libera J, Albuquerque B, Pashos E, Shipstone A, et al. BDK inhibition acts as a catabolic switch to mimic fasting and improve metabolism in mice. Mol Metab. 2022;66:101611.

105. Lian K, Guo X, Wang Q, Liu Y, Wang RT, Gao C, et al. PP2Cm overexpression alleviates MI/R injury mediated by a BCAA catabolism defect and oxidative stress in diabetic mice. Eur J Pharmacol. 2020;866:172796.

106. Lo EKK, Felicianna, Xu JH, Zhan Q, Zeng Z, El-Nezami H. The Emerging Role of Branched-Chain Amino Acids in Liver Diseases. Biomedicines. 2022;10(6).

107. Ghimire P, Dhamoon AS. Ketoacidosis. StatPearls. Treasure Island (FL) ineligible companies. Disclosure: Amit Dhamoon declares no relevant financial relationships with ineligible companies.2023.

108. Westman EC, Tondt J, Maguire E, Yancy WS, Jr. Implementing a low-carbohydrate, ketogenic diet to manage type 2 diabetes mellitus. Expert Rev Endocrinol Metab. 2018;13(5):263-72.

109. Alves-Bezerra M, Cohen DE. Triglyceride Metabolism in the Liver. Compr Physiol. 2017;8(1):1-8.

110. Newman JC, Verdin E. beta-Hydroxybutyrate: A Signaling Metabolite. Annu Rev Nutr. 2017;37:51-76.

111. Green A, Bishop RE. Ketoacidosis - Where Do the Protons Come From? Trends Biochem Sci. 2019;44(6):484-9.

112. d'Avignon DA, Puchalska P, Ercal B, Chang Y, Martin SE, Graham MJ, et al. Hepatic ketogenic insufficiency reprograms hepatic glycogen metabolism and the lipidome. JCI Insight. 2018;3(12).

113. Adeva-Andany MM, Funcasta-Calderon R, Fernandez-Fernandez C, Castro-Quintela E, Carneiro-Freire N. Metabolic effects of glucagon in humans. J Clin Transl Endocrinol. 2019;15:45-53.

114. Orii KE, Fukao T, Song XQ, Mitchell GA, Kondo N. Liver-specific silencing of the human gene encoding succinyl-CoA: 3-ketoacid CoA transferase. Tohoku J Exp Med. 2008;215(3):227-36.

115. Cheng CW, Biton M, Haber AL, Gunduz N, Eng G, Gaynor LT, et al. Ketone Body Signaling Mediates Intestinal Stem Cell Homeostasis and Adaptation to Diet. Cell. 2019;178(5):1115-31 e15.

116. Thorens B, Mueckler M. Glucose transporters in the 21st Century. American Journal of Physiology - Endocrinology and Metabolism. 2010;298(2):E141-E5.

117. Saed CT, Tabatabaei Dakhili SA, Ussher JR. Pyruvate Dehydrogenase as a Therapeutic Target for Nonalcoholic Fatty Liver Disease. ACS Pharmacology and Translational Science. 2021;4(2):582-8.

118. Merritt ME, Harrison C, Sherry AD, Malloy CR, Burgess SC. Flux through hepatic pyruvate carboxylase and phosphoenolpyruvate carboxykinase detected by hyperpolarized 13C magnetic resonance. Proceedings of the National Academy of Sciences of the United States of America. 2011;108(47):19084-9.

119. Patel MS, Korotchkina LG. Regulation of the pyruvate dehydrogenase complex. Biochemical Society Transactions. 2006;34(2):217-22.

120. Patel MS, Nemeria NS, Furey W, Jordan F. The pyruvate dehydrogenase complexes: Structure-based function and regulation. Journal of Biological Chemistry. 2014;289(24):16615-23.

121. Jing E, O'Neill BT, Rardin MJ, Kleinridders A, Ilkeyeva OR, Ussar S, et al. Sirt3 regulates metabolic flexibility of skeletal muscle through reversible enzymatic deacetylation. Diabetes. 2013;62(10):3404-17.

122. Zhang X, Ji R, Liao X, Castillero E, Kennel PJ, Brunjes DL, et al. MicroRNA-195 regulates metabolism in failing myocardium via alterations in sirtuin 3 expression and mitochondrial protein acetylation. Circulation. 2018;137(19):2052-67.

123. Almutairi M, Gopal K, Greenwell AA, Young A, Gill R, Aburasayn H, et al. The GLP-1 Receptor Agonist Liraglutide Increases Myocardial Glucose Oxidation Rates via Indirect Mechanisms and Mitigates Experimental Diabetic Cardiomyopathy. Canadian Journal of Cardiology. 2021;37(1):140-50.

124. O'Brien M, Chalker J, Slade L, Gardiner D, Mailloux RJ. Protein S-glutathionylation alters superoxide/hydrogen peroxide emission from pyruvate dehydrogenase complex. Free Radical Biology and Medicine. 2017;106:302-14.

125. Choi CS, Ghoshal P, Srinivasan M, Kim S, Cline G, Patel MS. Liver-specific pyruvate dehydrogenase complex deficiency upregulates lipogenesis in adipose tissue and improves peripheral insulin sensitivity. Lipids. 2010;45(11):987-95.

126. Jeoung NH, Harris RA. Pyruvate dehydrogenase kinase-4 deficiency lowers blood glucose and improves glucose tolerance in diet-induced obese mice. American Journal of Physiology - Endocrinology and Metabolism. 2008;295(1):E46-E54.

127. Apontes P, Liu Z, Su K, Benard O, Youn DY, Li X, et al. Mangiferin stimulates carbohydrate oxidation and protects against metabolic disorders induced by high-fat diets. Diabetes. 2014;63(11):3626-36.

128. Al Batran R, Gopal K, Capozzi ME, Chahade JJ, Saleme B, Tabatabaei-Dakhili SA, et al. Pimozide Alleviates Hyperglycemia in Diet-Induced Obesity by Inhibiting Skeletal Muscle Ketone Oxidation. Cell Metabolism. 2020;31(5):909-19.e8.

129. Muoio DM, Noland RC, Kovalik JP, Seiler SE, Davies MN, Debalsi KL, et al. Muscle-specific deletion of carnitine acetyltransferase compromises glucose tolerance and metabolic flexibility. Cell Metabolism. 2012;15(5):764-77.

130. Broderick TL, Quinney HA, Lopaschuk GD. Carnitine stimulation of glucose oxidation in the fatty acid perfused isolated working rat heart. Journal of Biological Chemistry. 1992;267(6):3758-63.

131. Stacpoole PW, Henderson GN, Yan Z, James MO. Clinical pharmacology and toxicology of dichloroacetate. Environmental Health Perspectives. 1998;106(SUPPL. 4):989-94.

132. Tso SC, Qi X, Gui WJ, Wu CY, Chuang JL, Wernstedt-Asterholm I, et al. Structure-guided development of specific pyruvate dehydrogenase kinase inhibitors targeting the ATP-binding pocket. Journal of Biological Chemistry. 2014;289(7):4432-43.

133. Wu CY, Tso SC, Chuang JL, Gui WJ, Lou M, Sharma G, et al. Targeting hepatic pyruvate dehydrogenase kinases restores insulin signaling and mitigates ChREBP-mediated lipogenesis in diet-induced obese mice. Molecular Metabolism. 2018;12:12-24.

134. Go Y, Jeong JY, Jeoung NH, Jeon JH, Park BY, Kang HJ, et al. Inhibition of pyruvate dehydrogenase kinase 2 protects against hepatic steatosis through modulation of tricarboxylic acid cycle anaplerosis and ketogenesis. Diabetes. 2016;65(10):2876-87.

135. Sossalla S, Maier LS. Role of ranolazine in angina, heart failure, arrhythmias, and diabetes. Pharmacology and Therapeutics. 2012;133(3):311-23.

136. McCormack JG, Baracos VE, Barr R, Lopaschuk GD. Effects of ranolazine on oxidative substrate preference in epitrochlearis muscle. Journal of Applied Physiology. 1996;81(2):905-10.

137. McCormack JG, Barr RL, Wolff AA, Lopaschuk GD. Ranolazine stimulates glucose oxidation in normoxic, ischemic, and reperfused ischemic rat hearts. Circulation. 1996;93(1):135-42.

138. Batran RA, Gopal K, Aburasayn H, Eshreif A, Almutairi M, Greenwell AA, et al. The antianginal ranolazine mitigates obesity-induced nonalcoholic fatty liver disease and increases hepatic pyruvate dehydrogenase activity. JCI Insight. 2019;4(1).

139. Puchalska P, Crawford PA. Multi-dimensional Roles of Ketone Bodies in Fuel Metabolism, Signaling, and Therapeutics. Cell Metabolism. 2017;25(2):262-84.

140. Williamson JR, Scholz R, Browning ET. Control mechanisms of gluconeogenesis and ketogenesis. II. Interactions between fatty acid oxidation and the citric acid cycle in perfused rat liver. Journal of Biological Chemistry. 1969;244(17):4617-27.

141. Cappel DA, Deja S, Duarte JAG, Kucejova B, Iñigo M, Fletcher JA, et al. Pyruvate-Carboxylase-Mediated Anaplerosis Promotes Antioxidant Capacity by Sustaining TCA Cycle and Redox Metabolism in Liver. Cell Metabolism. 2019;29(6):1291-305.e8.

142. Mahmood S, Birkaya B, Rideout TC, Patel MS. Lack of mitochondria-generated acetyl-coa by pyruvate dehydrogenase complex downregulates gene expression in the hepatic de novo lipogenic pathway. American Journal of Physiology - Endocrinology and Metabolism. 2016;311(1):E117-E27.

143. Randle PJ, Garland PB, Hales CN, Newsholme EA. THE GLUCOSE FATTY-ACID CYCLE ITS ROLE IN INSULIN SENSITIVITY AND THE METABOLIC DISTURBANCES OF DIABETES MELLITUS. The Lancet. 1963;281(7285):785-9.

144. Savage DB, Petersen KF, Shulman GI. Disordered lipid metabolism and the pathogenesis of insulin resistance. Physiological Reviews. 2007;87(2):507-20.

145. Timmers S, Nabben M, Bosma M, Van Bree B, Lenaers E, Van Beurden D, et al. Augmenting muscle diacylglycerol and triacylglycerol content by blocking fatty acid oxidation does not impede insulin sensitivity. Proceedings of the National Academy of Sciences of the United States of America. 2012;109(29):11711-6.

146. Steinberg GR, Kemp BE. AMPK in health and disease. Physiological Reviews. 2009;89(3):1025-78.

147. Day EA, Ford RJ, Steinberg GR. AMPK as a Therapeutic Target for Treating Metabolic Diseases. Trends in Endocrinology and Metabolism. 2017;28(8):545-60.

148. Zaki MH, Boyd KL, Vogel P, Kastan MB, Lamkanfi M, Kanneganti TD. The NLRP3 inflammasome protects against loss of epithelial integrity and mortality during experimental colitis. Immunity. 2010;32(3):379-91.

149. Urano F, Wang X, Bertolotti A, Zhang Y, Chung P, Harding HP, et al. Coupling of stress in the ER to activation of JNK protein kinases by transmembrane protein kinase IRE1. Science. 2000;287(5453):664-6.

150. McGuckin MA, Eri RD, Das I, Lourie R, Florin TH. ER stress and the unfolded protein response in intestinal inflammation. Am J Physiol Gastrointest Liver Physiol. 2010;298(6):G820-32.

151. Rawson RB. The SREBP pathway--insights from Insigs and insects. Nat Rev Mol Cell Biol. 2003;4(8):631-40.

152. Ron D, Walter P. Signal integration in the endoplasmic reticulum unfolded protein response. Nat Rev Mol Cell Biol. 2007;8(7):519-29.

153. Wang JM, Qiu Y, Yang Z, Kim H, Qian Q, Sun Q, et al. IRE1alpha prevents hepatic steatosis by processing and promoting the degradation of select microRNAs. Sci Signal. 2018;11(530).

154. Zhang K, Wang S, Malhotra J, Hassler JR, Back SH, Wang G, et al. The unfolded protein response transducer IRE1alpha prevents ER stress-induced hepatic steatosis. EMBO J. 2011;30(7):1357-75.

155. Reimold AM, Iwakoshi NN, Manis J, Vallabhajosyula P, Szomolanyi-Tsuda E, Gravallese EM, et al. Plasma cell differentiation requires the transcription factor XBP-1. Nature. 2001;412(6844):300-7.

156. Kaser A, Lee AH, Franke A, Glickman JN, Zeissig S, Tilg H, et al. XBP1 links ER stress to intestinal inflammation and confers genetic risk for human inflammatory bowel disease. Cell. 2008;134(5):743-56.

157. Ozcan L, Ergin AS, Lu A, Chung J, Sarkar S, Nie D, et al. Endoplasmic reticulum stress plays a central role in development of leptin resistance. Cell Metab. 2009;9(1):35-51.

158. Lee AH, Scapa EF, Cohen DE, Glimcher LH. Regulation of hepatic lipogenesis by the transcription factor XBP1. Science. 2008;320(5882):1492-6.

159. Duwaerts CC, Siao K, Soon RK, Jr., Her C, Iwawaki T, Kohno K, et al. Hepatocyte-specific deletion of XBP1 sensitizes mice to liver injury through hyperactivation of IRE1alpha. Cell Death Differ. 2021;28(5):1455-65.

160. Wang S, Chen Z, Lam V, Han J, Hassler J, Finck BN, et al. IRE1alpha-XBP1s induces PDI expression to increase MTP activity for hepatic VLDL assembly and lipid homeostasis. Cell Metab. 2012;16(4):473-86.

161. Bartoszewska S, Slawski J, Collawn JF, Bartoszewski R. Dual RNase activity of IRE1 as a target for anticancer therapies. J Cell Commun Signal. 2023;17(4):1145-61.

162. Tsuchiya Y, Saito M, Kadokura H, Miyazaki JI, Tashiro F, Imagawa Y, et al. IRE1-XBP1 pathway regulates oxidative proinsulin folding in pancreatic beta cells. J Cell Biol. 2018;217(4):1287-301.

163. Shan B, Wang X, Wu Y, Xu C, Xia Z, Dai J, et al. The metabolic ER stress sensor IRE1alpha suppresses alternative activation of macrophages and impairs energy expenditure in obesity. Nat Immunol. 2017;18(5):519-29.

164. Reimold AM, Etkin A, Clauss I, Perkins A, Friend DS, Zhang J, et al. An essential role in liver development for transcription factor XBP-1. Genes Dev. 2000;14(2):152-7.

165. Ozcan U, Cao Q, Yilmaz E, Lee AH, Iwakoshi NN, Ozdelen E, et al. Endoplasmic reticulum stress links obesity, insulin action, and type 2 diabetes. Science. 2004;306(5695):457-61.

166. Lee K, Chan JY, Liang C, Ip CK, Shi YC, Herzog H, et al. XBP1 maintains beta cell identity, represses beta-to-alpha cell transdifferentiation and protects against diabetic beta cell failure during metabolic stress in mice. Diabetologia. 2022;65(6):984-96.

167. Lee AH, Heidtman K, Hotamisligil GS, Glimcher LH. Dual and opposing roles of the unfolded protein response regulated by IRE1alpha and XBP1 in proinsulin processing and insulin secretion. Proc Natl Acad Sci U S A. 2011;108(21):8885-90.

168. Yamagata K, Furuta H, Oda N, Kaisaki PJ, Menzel S, Cox NJ, et al. Mutations in the hepatocyte nuclear factor-4alpha gene in maturity-onset diabetes of the young (MODY1). Nature. 1996;384(6608):458-60.

169. Moore BD, Jin RU, Lo H, Jung M, Wang H, Battle MA, et al. Transcriptional Regulation of X-Box-binding Protein One (XBP1) by Hepatocyte Nuclear Factor 4alpha (HNF4Alpha) Is Vital to Beta-cell Function. J Biol Chem. 2016;291(12):6146-57.

170. Sun J, Ni Q, Xie J, Xu M, Zhang J, Kuang J, et al. beta-Cell Dedifferentiation in Patients With T2D With Adequate Glucose Control and Nondiabetic Chronic Pancreatitis. J Clin Endocrinol Metab. 2019;104(1):83-94.

171. Lipson KL, Fonseca SG, Ishigaki S, Nguyen LX, Foss E, Bortell R, et al. Regulation of insulin biosynthesis in pancreatic beta cells by an endoplasmic reticulum-resident protein kinase IRE1. Cell Metab. 2006;4(3):245-54.

172. Hassler JR, Scheuner DL, Wang S, Han J, Kodali VK, Li P, et al. The IRE1alpha/XBP1s Pathway Is Essential for the Glucose Response and Protection of beta Cells. PLoS Biol. 2015;13(10):e1002277.

173. Sharma RB, Landa-Galvan HV, Alonso LC. Living Dangerously: Protective and Harmful ER Stress Responses in Pancreatic beta-Cells. Diabetes. 2021;70(11):2431-43.

174. Wang ZV, Hill JA. Protein quality control and metabolism: bidirectional control in the heart. Cell Metab. 2015;21(2):215-26.

175. Steiger D, Yokota T, Li J, Ren S, Minamisawa S, Wang Y. The serine/threonine-protein kinase/endoribonuclease IRE1alpha protects the heart against pressure overload-induced heart failure. J Biol Chem. 2018;293(25):9652-61.

176. Yao S, Miao C, Tian H, Sang H, Yang N, Jiao P, et al. Endoplasmic reticulum stress promotes macrophage-derived foam cell formation by up-regulating cluster of differentiation 36 (CD36) expression. J Biol Chem. 2014;289(7):4032-42.

177. Duan Q, Ni L, Wang P, Chen C, Yang L, Ma B, et al. Deregulation of XBP1 expression contributes to myocardial vascular endothelial growth factor-A expression and angiogenesis during cardiac hypertrophy in vivo. Aging Cell. 2016;15(4):625-33.

178. Jiang S, Yan C, Fang QC, Shao ML, Zhang YL, Liu Y, et al. Fibroblast growth factor 21 is regulated by the IRE1alpha-XBP1 branch of the unfolded protein response and counteracts endoplasmic reticulum stress-induced hepatic steatosis. J Biol Chem. 2014;289(43):29751-65.

179. Herrema H, Zhou Y, Zhang D, Lee J, Salazar Hernandez MA, Shulman GI, et al. XBP1s Is an Anti-lipogenic Protein. J Biol Chem. 2016;291(33):17394-404.

180. So JS, Hur KY, Tarrio M, Ruda V, Frank-Kamenetsky M, Fitzgerald K, et al. Silencing of lipid metabolism genes through IRE1alpha-mediated mRNA decay lowers plasma lipids in mice. Cell Metab. 2012;16(4):487-99.

181. Zhu X, Xiong T, Liu P, Guo X, Xiao L, Zhou F, et al. Quercetin ameliorates HFD-induced NAFLD by promoting hepatic VLDL assembly and lipophagy via the IRE1a/XBP1s pathway. Food Chem Toxicol. 2018;114:52-60.

182. Clarke B, Wyatt KM, McCormack JG. Ranolazine increases active pyruvate dehydrogenase in perfused normoxic rat hearts: evidence for an indirect mechanism. J Mol Cell Cardiol. 1996;28(2):341-50.

183. Marchesini G, Brizi M, Morselli-Labate AM, Bianchi G, Bugianesi E, McCullough AJ, et al. Association of nonalcoholic fatty liver disease with insulin resistance. American Journal of Medicine. 1999;107(5):450-5.

184. Starley BQ, Calcagno CJ, Harrison SA. Nonalcoholic fatty liver disease and hepatocellular carcinoma: A weighty connection. Hepatology. 2010;51(5):1820-32.

185. Undrovinas AI, Belardinelli L, Undrovinas NA, Sabbah HN. Ranolazine improves abnormal repolarization and contraction in left ventricular myocytes of dogs with heart failure by inhibiting late sodium current. Journal of Cardiovascular Electrophysiology. 2006;17(SUPPL. 1):S169-S77.

186. Dhalla AK, Yang M, Ning Y, Kahlig KM, Krause M, Rajamani S, et al. Blockade of na+ channels in pancreatic α-cells has antidiabetic effects. Diabetes. 2014;63(10):3545-56.

187. Eckel RH, Henry RR, Yue P, Dhalla A, Wong P, Jochelson P, et al. Effect of ranolazine monotherapy on glycemic control in subjects with type 2 diabetes. Diabetes Care. 2015;38(7):1189-96.

188. Morrow DA, Scirica BM, Chaitman BR, McGuire DK, Murphy SA, Prokopczuk EK, et al. Evaluation of the Glycometabolic Effects of Ranolazine in Patients With and Without Diabetes Mellitus in the MERLIN-TIMI 36 Randomized Controlled Trial. Circulation. 2009;119(15):2032-9.

189. Gopal K, Al Batran R, Altamimi TR, Greenwell AA, Saed CT, Tabatabaei Dakhili SA, et al. FoxO1 inhibition alleviates type 2 diabetes-related diastolic dysfunction by increasing myocardial pyruvate dehydrogenase activity. Cell Reports. 2021;35(1).

190. Livak KJ, Schmittgen TD. Analysis of relative gene expression data using real-time quantitative PCR and the 2-ΔΔCT method. Methods. 2001;25(4):402-8.

191. Bolzán AD, Bianchi MS. Genotoxicity of Streptozotocin. Mutation Research - Reviews in Mutation Research. 2002;512(2-3):121-34.

192. Johnston APW, Campbell JE, Found JG, Riddell MC, Hawke TJ. Streptozotocin induces G2 arrest in skeletal muscle myoblasts and impairs muscle growth in vivo. American Journal of Physiology - Cell Physiology. 2007;292(3):C1033-C40.

193. Raza H, John A. Streptozotocin-induced cytotoxicity, oxidative stress and mitochondrial dysfunction in human hepatoma HepG2 cells. International Journal of Molecular Sciences. 2012;13(5):5751-67.

194. Mailloux RJ, Gardiner D, O'Brien M. 2-Oxoglutarate dehydrogenase is a more significant source of O2·−/H2O2 than pyruvate dehydrogenase in cardiac and liver tissue. Free Radical Biology and Medicine. 2016;97:501-12.

195. Kleinert M, Clemmensen C, Hofmann SM, Moore MC, Renner S, Woods SC, et al. Animal models of obesity and diabetes mellitus. Nature Reviews Endocrinology. 2018;14(3):140-62.

196. Galgani JE, Fernandez-Verdejo R. Pathophysiological role of metabolic flexibility on metabolic health. Obes Rev. 2021;22(2):e13131.

197. Goodpaster BH, Sparks LM. Metabolic Flexibility in Health and Disease. Cell Metabolism. 2017;25(5):1027-36.

198. Esenboğa K, Kurtul A, Nazman H, Tekin CG, Özyüncü N, Tan TS, et al. Evaluation of the Impact of Ranolazine Treatment on Liver Function Tests in Patients With Coronary Heart Disease and Nonalcoholic Fatty Liver Disease. Angiology. 2022;73(1):73-8.

199. Bligh EG, Dyer WJ. A rapid method of total lipid extraction and purification. Canadian journal of biochemistry and physiology. 1959;37(8):911-7.

200. Jornayvaz FR, Shulman GI. Diacylglycerol activation of protein kinase Cepsilon and hepatic insulin resistance. Cell Metab. 2012;15(5):574-84.

201. Sandhiya S, Dkhar SA, Pillai AA, George M, Jayaraman B, Chandrasekaran A. Comparison of ranolazine and trimetazidine on glycemic status in diabetic patients with coronary artery disease - a randomized controlled trial. J Clin Diagn Res. 2015;9(1):OC01-OC5.

202. Swain MG, Ramji A, Patel K, Sebastiani G, Shaheen AA, Tam E, et al. Burden of nonalcoholic fatty liver disease in Canada, 2019-2030: a modelling study. CMAJ open. 2020;8(2):E429-E36.

203. Targher G, Marchesini G, Byrne CD. Risk of type 2 diabetes in patients with non-alcoholic fatty liver disease: Causal association or epiphenomenon? Diabetes and Metabolism. 2016;42(3):142-56.

204. Tveden-Nyborg P, Bergmann TK, Jessen N, Simonsen U, Lykkesfeldt J. BCPT policy for experimental and clinical studies. Basic and Clinical Pharmacology and Toxicology. 2021;128(1):4-8.

205. Saed CT, Greenwell AA, Tabatabaei Dakhili SA, Gopal K, Eaton F, Ussher JR. The anti-anginal ranolazine does not confer beneficial actions against hepatic steatosis in male mice subjected to high-fat diet and streptozotocin-induced type 2 diabetes. Can J Physiol Pharmacol. 2022;100(5):393-401.

206. Dhalla AK, Yang M, Ning Y, Kahlig KM, Krause M, Rajamani S, et al. Blockade of Na+ channels in pancreatic alpha-cells has antidiabetic effects. Diabetes. 2014;63(10):3545-56.

207. Longuet C, Sinclair EM, Maida A, Baggio LL, Maziarz M, Charron MJ, et al. The Glucagon Receptor Is Required for the Adaptive Metabolic Response to Fasting. Cell Metabolism. 2008;8(5):359-71.

208. Giles DA, Moreno-Fernandez ME, Stankiewicz TE, Graspeuntner S, Cappelletti M, Wu D, et al. Thermoneutral housing exacerbates nonalcoholic fatty liver disease in mice and allows for sex-independent disease modeling. Nature Medicine. 2017;23(7):829-38.

209. Ayala JE, Samuel VT, Morton GJ, Obici S, Croniger CM, Shulman GI, et al. Standard operating procedures for describing and performing metabolic tests of glucose homeostasis in mice. DMM Disease Models and Mechanisms. 2010;3(9-10):525-34.

210. Keiser MJ, Roth BL, Armbruster BN, Ernsberger P, Irwin JJ, Shoichet BK. Relating protein pharmacology by ligand chemistry. Nat Biotechnol. 2007;25(2):197-206.

211. Zhang K, Kaufman RJ. Signaling the unfolded protein response from the endoplasmic reticulum. J Biol Chem. 2004;279(25):25935-8.

212. Kammoun HL, Chabanon H, Hainault I, Luquet S, Magnan C, Koike T, et al. GRP78 expression inhibits insulin and ER stress-induced SREBP-1c activation and reduces hepatic steatosis in mice. J Clin Invest. 2009;119(5):1201-15.

213. Olivares S, Henkel AS. Hepatic Xbp1 Gene Deletion Promotes Endoplasmic Reticulum Stress-induced Liver Injury and Apoptosis. J Biol Chem. 2015;290(50):30142-51.

214. Cavanna AE, Seri S. Tourette's syndrome. BMJ. 2013;347:f4964.

215. Tanaka H, Iguchi N, Miyagawa Y, Koga M, Kohroki J, Nishimune Y. Differential expression of succinyl CoA transferase (SCOT) genes in somatic and germline cells of the mouse testis. Int J Androl. 2003;26(1):52-6.

216. Coassolo L, Liu T, Jung Y, Taylor NP, Zhao M, Charville GW, et al. Mapping transcriptional heterogeneity and metabolic networks in fatty livers at single-cell resolution. iScience. 2023;26(1):105802.

217. Chen L, Xie ZY, Liu L, Zhu L, Wang F, Fan P, et al. Nuclear factor-kappa B-dependent X-box binding protein 1 signalling promotes the proliferation of nucleus pulposus cells under tumour necrosis factor alpha stimulation. Cell Prolif. 2019;52(2):e12542.

218. Srivastava SP, Kumar KU, Kaufman RJ. Phosphorylation of eukaryotic translation initiation factor 2 mediates apoptosis in response to activation of the double-stranded RNA-dependent protein kinase. J Biol Chem. 1998;273(4):2416-23.

219. Saeidnia S, Manayi A, Abdollahi M. From in vitro Experiments to in vivo and Clinical Studies; Pros and Cons. Curr Drug Discov Technol. 2015;12(4):218-24.

220. Fako V, Yu Z, Henrich CJ, Ransom T, Budhu AS, Wang XW. Inhibition of wnt/beta-catenin Signaling in Hepatocellular Carcinoma by an Antipsychotic Drug Pimozide. Int J Biol Sci. 2016;12(7):768-75.

221. Tabatabaei Dakhili SA, Greenwell AA, Yang K, Abou Farraj R, Saed CT, Gopal K, et al. The Antipsychotic Dopamine 2 Receptor Antagonist Diphenylbutylpiperidines Improve Glycemia in Experimental Obesity by Inhibiting Succinyl-CoA:3-Ketoacid CoA Transferase. Diabetes. 2023;72(1):126-34.

222. Leavens KF, Birnbaum MJ. Insulin signaling to hepatic lipid metabolism in health and disease. Crit Rev Biochem Mol Biol. 2011;46(3):200-15.

223. Jeoung NH, Wu P, Joshi MA, Jaskiewicz J, Bock CB, Depaoli-Roach AA, et al. Role of pyruvate dehydrogenase kinase isoenzyme 4 (PDHK4) in glucose homoeostasis during starvation. Biochem J. 2006;397(3):417-25.

224. Wu P, Inskeep K, Bowker-Kinley MM, Popov KM, Harris RA. Mechanism responsible for inactivation of skeletal muscle pyruvate dehydrogenase complex in starvation and diabetes. Diabetes. 1999;48(8):1593-9.

225. Pilegaard H, Birk JB, Sacchetti M, Mourtzakis M, Hardie DG, Stewart G, et al. PDH-E1alpha dephosphorylation and activation in human skeletal muscle during exercise: effect of intralipid infusion. Diabetes. 2006;55(11):3020-7.

226. Cryer PE. Minireview: Glucagon in the pathogenesis of hypoglycemia and hyperglycemia in diabetes. Endocrinology. 2012;153(3):1039-48.

227. Wu P, Sato J, Zhao Y, Jaskiewicz J, Popov KM, Harris RA. Starvation and diabetes increase the amount of pyruvate dehydrogenase kinase isoenzyme 4 in rat heart. Biochem J. 1998;329 (Pt 1)(Pt 1):197-201.

228. Wu P, Blair PV, Sato J, Jaskiewicz J, Popov KM, Harris RA. Starvation increases the amount of pyruvate dehydrogenase kinase in several mammalian tissues. Arch Biochem Biophys. 2000;381(1):1-7.

229. Sugden MC, Holness MJ. Therapeutic potential of the mammalian pyruvate dehydrogenase kinases in the prevention of hyperglycaemia. Curr Drug Targets Immune Endocr Metabol Disord. 2002;2(2):151-65.

230. Fang YH, Piao L, Hong Z, Toth PT, Marsboom G, Bache-Wiig P, et al. Therapeutic inhibition of fatty acid oxidation in right ventricular hypertrophy: exploiting Randle's cycle. J Mol Med (Berl). 2012;90(1):31-43.

231. McCormack JG, Barr RL, Wolff AA, Lopaschuk GD. Ranolazine stimulates glucose oxidation in normoxic, ischemic, and reperfused ischemic rat hearts. Circulation. 1996;93(1):135-42.

232. Clarke B, Spedding M, Patmore L, McCormack JG. Protective effects of ranolazine in guinea-pig hearts during low-flow ischaemia and their association with increases in active pyruvate dehydrogenase. Br J Pharmacol. 1993;109(3):748-50.

233. Lee IK. The role of pyruvate dehydrogenase kinase in diabetes and obesity. Diabetes Metab J. 2014;38(3):181-6.

234. Wang X, Shen X, Yan Y, Li H. Pyruvate dehydrogenase kinases (PDKs): an overview toward clinical applications. Biosci Rep. 2021;41(4).

235. Zhang S, Hulver MW, McMillan RP, Cline MA, Gilbert ER. The pivotal role of pyruvate dehydrogenase kinases in metabolic flexibility. Nutr Metab (Lond). 2014;11(1):10.

236. Jeon JH, Thoudam T, Choi EJ, Kim MJ, Harris RA, Lee IK. Loss of metabolic flexibility as a result of overexpression of pyruvate dehydrogenase kinases in muscle, liver and the immune system: Therapeutic targets in metabolic diseases. J Diabetes Investig. 2021;12(1):21-31.

237. Pinheiro A, Faustino I, Silva MJ, Silva J, Sa R, Sousa M, et al. Human testis-specific PDHA2 gene: methylation status of a CpG island in the open reading frame correlates with transcriptional activity. Mol Genet Metab. 2010;99(4):425-30.

238. Huang YJ, Walker D, Chen W, Klingbeil M, Komuniecki R. Expression of pyruvate dehydrogenase isoforms during the aerobic/anaerobic transition in the development of the parasitic nematode Ascaris suum: altered stoichiometry of phosphorylation/inactivation. Arch Biochem Biophys. 1998;352(2):263-70.

239. Dahl HH, Brown RM, Hutchison WM, Maragos C, Brown GK. A testis-specific form of the human pyruvate dehydrogenase E1 alpha subunit is coded for by an intronless gene on chromosome 4. Genomics. 1990;8(2):225-32.

240. Takakubo F, Dahl HH. The expression pattern of the pyruvate dehydrogenase E1 alpha subunit genes during spermatogenesis in adult mouse. Exp Cell Res. 1992;199(1):39-49.

241. Quintana E, Gort L, Busquets C, Navarro-Sastre A, Lissens W, Moliner S, et al. Mutational study in the PDHA1 gene of 40 patients suspected of pyruvate dehydrogenase complex deficiency. Clin Genet. 2010;77(5):474-82.

242. Turner DA. Contrasting Metabolic Insufficiency in Aging and Dementia. Aging Dis. 2021;12(4):1081-96.

243. Chen W, Sun X, Zhan L, Zhou W, Bi T. Conditional Knockout of Pdha1 in Mouse Hippocampus Impairs Cognitive Function: The Possible Involvement of Lactate. Front Neurosci. 2021;15:767560.

244. Yan S, Xu X, Qi F, Guo X, Luo J, Li Y. Editorial: Application of gene editing in pathology dissection of neurodegenerative diseases. Front Neurosci. 2022;16:1092176.

245. Gopal K, Almutairi M, Al Batran R, Eaton F, Gandhi M, Ussher JR. Cardiac-Specific Deletion of Pyruvate Dehydrogenase Impairs Glucose Oxidation Rates and Induces Diastolic Dysfunction. Front Cardiovasc Med. 2018;5:17.

246. Sidhu S, Gangasani A, Korotchkina LG, Suzuki G, Fallavollita JA, Canty JM, Jr., et al. Tissue-specific pyruvate dehydrogenase complex deficiency causes cardiac hypertrophy and sudden death of weaned male mice. Am J Physiol Heart Circ Physiol. 2008;295(3):H946-H52.

247. Choi CS, Ghoshal P, Srinivasan M, Kim S, Cline G, Patel MS. Liver-specific pyruvate dehydrogenase complex deficiency upregulates lipogenesis in adipose tissue and improves peripheral insulin sensitivity. Lipids. 2010;45(11):987-95.

248. Pendleton AL, Humphreys LR, Davis MA, Camacho LE, Anderson MJ, Limesand SW. Increased pyruvate dehydrogenase activity in skeletal muscle of growth-restricted ovine fetuses. Am J Physiol Regul Integr Comp Physiol. 2019;317(4):R513-R20.

249. Roche TE, Hiromasa Y. Pyruvate dehydrogenase kinase regulatory mechanisms and inhibition in treating diabetes, heart ischemia, and cancer. Cell Mol Life Sci. 2007;64(7-8):830-49.

250. Jha A, Krithika R, Manjeet D, Verma RJ. Protective effect of black tea infusion on aflatoxin-induced hepatotoxicity in mice. J Clin Exp Hepatol. 2013;3(1):29-36.

251. Ferguson D, Finck BN. Emerging therapeutic approaches for the treatment of NAFLD and type 2 diabetes mellitus. Nat Rev Endocrinol. 2021;17(8):484-95.

252. James MO, Jahn SC, Zhong G, Smeltz MG, Hu Z, Stacpoole PW. Therapeutic applications of dichloroacetate and the role of glutathione transferase zeta-1. Pharmacol Ther. 2017;170:166-80.

253. Stacpoole PW, Moore GW, Kornhauser DM. Metabolic effects of dichloroacetate in patients with diabetes mellitus and hyperlipoproteinemia. N Engl J Med. 1978;298(10):526-30.

254. Katayama Y, Kawata Y, Moritoh Y, Watanabe M. Dichloroacetate, a pyruvate dehydrogenase kinase inhibitor, ameliorates type 2 diabetes via reduced gluconeogenesis. Heliyon. 2022;8(2):e08889.

255. Morrell JA, Orme J, Butlin RJ, Roche TE, Mayers RM, Kilgour E. AZD7545 is a selective inhibitor of pyruvate dehydrogenase kinase 2. Biochem Soc Trans. 2003;31(Pt 6):1168-70.

256. Jeoung NH, Harris RA. Pyruvate dehydrogenase kinase-4 deficiency lowers blood glucose and improves glucose tolerance in diet-induced obese mice. Am J Physiol Endocrinol Metab. 2008;295(1):E46-54.

257. Perlman RL. Mouse models of human disease: An evolutionary perspective. Evol Med Public Health. 2016;2016(1):170-6.

258. Souto EP, Dobrolecki LE, Villanueva H, Sikora AG, Lewis MT. In Vivo Modeling of Human Breast Cancer Using Cell Line and Patient-Derived Xenografts. J Mammary Gland Biol Neoplasia. 2022;27(2):211-30.

259. Ashraf MN, Asghar MW, Rong Y, Doschak MR, Kiang TKL. Advanced In Vitro HepaRG Culture Systems for Xenobiotic Metabolism and Toxicity Characterization. Eur J Drug Metab Pharmacokinet. 2019;44(4):437-58.

260. Nelson EA, Walker SR, Xiang M, Weisberg E, Bar-Natan M, Barrett R, et al. The STAT5 Inhibitor Pimozide Displays Efficacy in Models of Acute Myelogenous Leukemia Driven by FLT3 Mutations. Genes Cancer. 2012;3(7-8):503-11.

261. Nelson EA, Walker SR, Weisberg E, Bar-Natan M, Barrett R, Gashin LB, et al. The STAT5 inhibitor pimozide decreases survival of chronic myelogenous leukemia cells resistant to kinase inhibitors. Blood. 2011;117(12):3421-9.

262. Moll HP, Mohrherr J, Blaas L, Musteanu M, Stiedl P, Grabner B, et al. A Mouse Model to Assess STAT3 and STAT5A/B Combined Inhibition in Health and Disease Conditions. Cancers (Basel). 2019;11(9).

263. Barclay JL, Nelson CN, Ishikawa M, Murray LA, Kerr LM, McPhee TR, et al. GH-dependent STAT5 signaling plays an important role in hepatic lipid metabolism. Endocrinology. 2011;152(1):181-92.

264. Flores-Morales A, Fernandez L, Rico-Bautista E, Umana A, Negrin C, Zhang JG, et al. Endoplasmic reticulum stress prolongs GH-induced Janus kinase (JAK2)/signal transducer and activator of transcription (STAT5) signaling pathway. Mol Endocrinol. 2001;15(9):1471-83.

265. Ajoolabady A, Kaplowitz N, Lebeaupin C, Kroemer G, Kaufman RJ, Malhi H, et al. Endoplasmic reticulum stress in liver diseases. Hepatology. 2023;77(2):619-39.

266. Li J, Li X, Liu D, Zhang S, Tan N, Yokota H, et al. Phosphorylation of eIF2alpha signaling pathway attenuates obesity-induced non-alcoholic fatty liver disease in an ER stress and autophagy-dependent manner. Cell Death Dis. 2020;11(12):1069.

267. Wang J, He W, Tsai PJ, Chen PH, Ye M, Guo J, et al. Mutual interaction between endoplasmic reticulum and mitochondria in nonalcoholic fatty liver disease. Lipids Health Dis. 2020;19(1):72.

268. Shreya S, Grosset CF, Jain BP. Unfolded Protein Response Signaling in Liver Disorders: A 2023 Updated Review. Int J Mol Sci. 2023;24(18).

269. Ali ES, Rychkov GY, Barritt GJ. Targeting Ca(2+) Signaling in the Initiation, Promotion and Progression of Hepatocellular Carcinoma. Cancers (Basel). 2020;12(10).

270. Sinton MC, Meseguer-Ripolles J, Lucendo-Villarin B, Wernig-Zorc S, Thomson JP, Carter RN, et al. A human pluripotent stem cell model for the analysis of metabolic dysfunction in hepatic steatosis. iScience. 2021;24(1):101931.

271. Siler SQ. Applications of Quantitative Systems Pharmacology (QSP) in Drug Development for NAFLD and NASH and Its Regulatory Application. Pharm Res. 2022;39(8):1789-802.

272. Sanchez JI, Parra ER, Jiao J, Solis Soto LM, Ledesma DA, Saldarriaga OA, et al. Cellular and Molecular Mechanisms of Liver Fibrosis in Patients with NAFLD. Cancers (Basel). 2023;15(11).

273. Chen X, Zhang L, Zheng L, Tuo B. Role of Ca(2+) channels in non-alcoholic fatty liver disease and their implications for therapeutic strategies (Review). Int J Mol Med. 2022;50(3).

274. Puchalska P, Martin SE, Huang X, Lengfeld JE, Daniel B, Graham MJ, et al. Hepatocyte-Macrophage Acetoacetate Shuttle Protects against Tissue Fibrosis. Cell Metab. 2019;29(2):383-98 e7.

275. Lu Q, Tian X, Wu H, Huang J, Li M, Mei Z, et al. Metabolic Changes of Hepatocytes in NAFLD. Front Physiol. 2021;12:710420.

276. McCommis KS, Finck BN. Treating Hepatic Steatosis and Fibrosis by Modulating Mitochondrial Pyruvate Metabolism. Cell Mol Gastroenterol Hepatol. 2019;7(2):275-84.

277. Mantovani A, Dalbeni A. Treatments for NAFLD: State of Art. Int J Mol Sci. 2021;22(5).

278. Zhang J, Guo J, Yang N, Huang Y, Hu T, Rao C. Endoplasmic reticulum stress-mediated cell death in liver injury. Cell Death Dis. 2022;13(12):1051.

279. Latif MU, Schmidt GE, Mercan S, Rahman R, Gibhardt CS, Stejerean-Todoran I, et al. NFATc1 signaling drives chronic ER stress responses to promote NAFLD progression. Gut. 2022;71(12):2561-73.

280. Xu X, Poulsen KL, Wu L, Liu S, Miyata T, Song Q, et al. Targeted therapeutics and novel signaling pathways in non-alcohol-associated fatty liver/steatohepatitis (NAFL/NASH). Signal Transduct Target Ther. 2022;7(1):287.

Appendix

Appendix Table 4.1 *Predicting Pimozide Target Proteins Using Molecular Similarity Ensemble Approach*.

Target Gene	Target Protein	P-Value
Scn2a	Sodium channel protein type 2 subunit alpha	1.32E-37
OPRM1	Mu-type opioid receptor	1.02E-26
KCNK2	Potassium channel subfamily K member 2	2.40E-24
DRD2	D (2) dopamine receptor	1.71E-21
GLRA1	Glycine receptor subunit alpha 1	6.48E-21
DRD2	D (2) dopamine receptor	2.93E-20
Abcb1a	Multidrug resistance protein 1A	3.90E-11
OPRK1	Kappa-type opioid receptor	2.69E-10
Htr7	5-hydroxytryptamine receptor 7	2.56E-09
CACNA1G	Voltage-dependent T-type calcium channel subunit alpha-1G	1.01E-08
WDR48	WD repeat-containing protein 48	3.26E-08
CYP2D6	Cytochrome P450 2D6	4.12E-08
USP1	Ubiquitin carboxyl-terminal hydrolase 1	4.57E-08
OPRD1	Delta-type opioid receptor	8.79E-08
KCNH2	Potassium voltage-gated channel subfamily H member 2	7.39E-07
HTR6	5-hydroxytryptamine receptor 6	2.89E-06
XBP1	X-box-binding protein 1	0.0004112
ABCB1	Multidrug resistance protein 1	0.008744

HRH4	Histamine H4 receptor	0.07585

Appendix Table 4.2 *Predicting Paliperidone Target Proteins Using Molecular Similarity Ensemble Approach.*

Target Gene	Target Protein	P-Value
HTR2A	5-hydroxytryptamine receptor 2A	3.83E-30
DRD2	D (2) dopamine receptor	8.88E-16
KCNH2	Potassium voltage-gated channel subfamily H member 2	6.36E-06

Appendix Table 4.3 *Predicting Lurasidone Target Proteins Using Molecular Similarity Ensemble Approach.*

Target Gene	Target Protein	P-Value
Htr1a	5-hydroxytryptamine receptor 1A	3.55E-61
Drd2	D (2) dopamine receptor	1.26E-40
Drd2	D (2) dopamine receptor	1.11E-36
Htr1a	5-hydroxytryptamine receptor 1A	1.61E-36
HTR2A	5-hydroxytryptamine receptor 2A	4.86E-19
Adra1a	Alpha-1A adrenergic receptor	9.07E-19
Htr2a	5-hydroxytryptamine receptor 2A	1.11E-16

Appendix Table 4.4 *Predicting Clozapine Target Proteins Using Molecular Similarity Ensemble Approach.*

Target Gene	Target Protein	P-Value
DRD1	D (1A) dopamine receptor	5.90E-81
HRH4	Histamine H4 receptor	7.07E-70
H1F0	Histone H1.0	5.49E-64
Drd1	D (1A) dopamine receptor	2.12E-50
Htr2a	5-hydroxytryptamine receptor 2A	3.09E-37
DRD2	D (2) dopamine receptor	3.24E-32
Htr2c	5-hydroxytryptamine receptor 2C	4.26E-32
Drd2	D (2) dopamine receptor	1.46E-31
Hrh1	Histamine H1 receptor	2.58E-30
DRD5	D (1B) dopamine receptor	2.73E-26
DRD4	D (4) dopamine receptor	1.98E-23
DRD2	D (2) dopamine receptor	2.38E-22
DRD3	D (3) dopamine receptor	4.40E-22
Drd4	D (4) dopamine receptor	2.65E-21
HTR3A	5-hydroxytryptamine receptor 3A	6.05E-21
Htr3a	5-hydroxytryptamine receptor 3A	5.29E-19
DRD2	D (2) dopamine receptor	9.99E-16
Adra1b	Alpha-1B adrenergic receptor	4.89E-15
HTR7	5-hydroxytryptamine receptor 7	1.14E-12

ADRA1A	Alpha-1A adrenergic receptor	1.23E-12
ADRA2A	Alpha-2A adrenergic receptor	2.30E-12
CHRM1	Muscarinic acetylcholine receptor M1	2.33E-12
Adra2a	Alpha-2A adrenergic receptor	5.43E-12
Drd3	D (3) dopamine receptor	4.22E-11
HRH1	Histamine H1 receptor	7.19E-11
Adra1a	Alpha-1A adrenergic receptor	2.33E-10
Chrm1	Muscarinic acetylcholine receptor M1	7.03E-10
Htr1a	5-hydroxytryptamine receptor 1A	9.74E-10
ADRA2B	Alpha-2B adrenergic receptor	1.84E-09
Chrm2	Muscarinic acetylcholine receptor M2	2.99E-09
HTR1E	5-hydroxytryptamine receptor 1E	3.66E-09
HRH1	Histamine H1 receptor	4.32E-09
Htr7	5-hydroxytryptamine receptor 7	8.37E-09
Htr1b	5-hydroxytryptamine receptor 1B	1.58E-08
NET	Transporter	1.84E-08
ADRA1B	Alpha-1B adrenergic receptor	3.57E-08
Htr1a	5-hydroxytryptamine receptor 1A	3.87E-08
HTR2A	5-hydroxytryptamine receptor 2A	3.87E-08
ADRA1D	Alpha-1D adrenergic receptor	4.19E-08
HTR6	5-hydroxytryptamine receptor 6	5.56E-08
CHRM5	Muscarinic acetylcholine receptor M5	8.12E-08
ADRA2C	Alpha-2C adrenergic receptor	2.12E-07

HRH2	Histamine H2 receptor	2.33E-07
CHRM4	Muscarinic acetylcholine receptor M4	2.75E-07
DRD3	D (3) dopamine receptor	4.02E-07
DRD1	D (1A) dopamine receptor	1.66E-06
ADRA1A	Alpha-1A adrenergic receptor	2.63E-06
Drd2	D (2) dopamine receptor	5.82E-06
HTR5A	5-hydroxytryptamine receptor 5A	6.39E-06
HTR2A	5-hydroxytryptamine receptor 2A	1.06E-05
Htr2b	5-hydroxytryptamine receptor 2B	1.61E-05
HTR2C	5-hydroxytryptamine receptor 2C	2.83E-05
DRD1	D (1A) dopamine receptor	0.0001202
HTR2B	5-hydroxytryptamine receptor 2B	0.0001929
SIGMAR1	Sigma non-opioid intracellular receptor 1	0.0002183
HTR1A	5-hydroxytryptamine receptor 1A	0.0004647
CHRM2	Muscarinic acetylcholine receptor M2	0.0006675
CHRM3	Muscarinic acetylcholine receptor M3	0.001654
SLC6A2	Sodium-dependent noradrenaline transporter	0.007874
Slc6a2	Transporter	0.009226
HRH3	Histamine H3 receptor	0.0148
HTR1B	5-hydroxytryptamine receptor 1B	0.02153
KCNH2	Potassium voltage-gated channel subfamily H member 2	0.05474
SLC6A4	Sodium-dependent serotonin transporter	0.09303

ADORA3	Adenosine receptor A3	0.8684